X-ray diffraction of a gram-negative bacterial membrane mimetic.

by

Panteha Razavi

A THESIS SUBMITTED IN PARTIAL FULFILMENT OF
THE REQUIREMENTS FOR THE DEGREE OF

MASTER OF SCIENCE

in

The Faculty of Mathematics and Sciences

Department of Physics

BROCK UNIVERSITY

June 23, 2009

Abstract

This thesis applies x-ray diffraction to measure the membrane structure of lipopolysaccharides and to develop a better model of a LPS bacterial membrane that can be used for biophysical research on antibiotics that attack cell membranes. We have modified the Physics department x-ray machine for use as a thin film diffractometer, and have designed a new temperature and relative humidity controlled sample cell. We tested the sample cell by measuring the one-dimensional electron density profiles of bilayers of POPC with 0%, 1%, 10%, and 100% by weight lipo-polysaccharide from *Pseudomona aeruginosa*.

Background

We now know that traditional antibiotics are losing their effectiveness against ever-evolving bacteria. This is because traditional antibiotics work against specific targets within the bacterial cell, and with genetic mutations over time, the antibiotic no longer works.

One possible solution are antimicrobial peptides. These are short proteins that are part of the immune systems of many animals, and some of them attack bacteria directly at the membrane of the cell, causing the bacterium to rupture and die. Since the membranes of most bacteria share common structural features, and these features are unlikely to evolve very much, these peptides should effectively kill many types of bacteria without much evolved resistance.

But why do these peptides kill bacterial cells, but not the cells of the host animal? For gram-negative bacteria, the most likely reason is that their outer membrane is made of lipopolysaccharides (LPS), which is very different from an animal cell membrane. Up to now, what we know about how these peptides work was likely done with phospholipid models of animal cell membranes, and not with the more complex lipopolysaccharides. If we want to make better peptides, ones that we can use to fight all types of infection, we need a more accurate molecular picture of how they work. This will hopefully be one step forward to the design of better treatments for bacterial infections.

Contents

List of Tables

List of Figures

Acknowledgements

I would like to express my gratitude toward my supervisor Dr. Thad Harroun, whose help, advice and guidance was invaluable. I would like to thank Electronic and Machine shop at Brock University for mainlining the x-ray machine and building the sample cell. Also, I would like to show my appreciation to faculty and staff of Physics Department, especially Dr. S. Bose and Dr. F. Razavi for their advice and suggestions.

Finally, I would like to thank family and friends for their love and support: Dr. H. Yekani, Dr. H. Jalili, Parmida and Sourena Razavi and especially Shahab Jamali for always being there.

I would like to dedicate this thesis to

People in Iran for their courage to fight for freedom and change,

and

my parents, Mrs. Shohreh M. Kashani and Mr. Homayoun Razavi for their love and devotion.

Chapter 1

Introduction

The purpose of this study is to design and tes a possibly useful model of the lipopolysaccharide outer membrane of gram negative bacteria th t can, in future, be used to study the actions of antibiotics such as antimicrobial peptides. The x-ray machine in the Physics Department was used to measure the properties of the thin membra e films. However, in order to study hydrated thin films, especially biological membranes, some ha rdware and software design and testing, as well as building a sample cell was necessary. The deta ls on characteristics of the sample cell and its use with the x-ray machine is explained in Methods section. The results of the x-ray diffraction analysis of our new membrane model is given in the Res lts section. The remainder of the Introduction will be a tutorial on lipopolysaccharides (LPS) and the use of x-rays to study membrane structure.

1.1 History of lipopolysaccharides

Rietschel and Westphal recently documented the history of lipopolysaccharide [4]. The history began in the eighteen century with search for the reasons behind fever and was thought to be a putrid poison or toxin. In 1872, Klebs, a Germa bacteriologist related most of the death during war to living microorganisms that he named "Micr sporon septicum" [36]. Two years later, Panum, a Danish pathologist obtained a water-soluble an heat-resistant toxin from putrid matter. Later on, Koch developed pure-culture techniques and con luded that different diseases were caused by specific bacteria. In 1892, Pfeiffer, from the same lab ratory, reported that the agent of cholera, *Vibrio cholerae*, can produce a non-secreted toxin tha was heat-stable and he called it an "endotoxin". Later on, endotoxins were shown to be the re presentative of outer membrane of gram negative bacteria [2].

Although today we know that not all end toxins are fatally toxic, the term is still used for

lipopolysaccharide molecules. The first structural studies of the molecules were done in 1930s and 1940s. At that time, researchers noticed that the membrane consists of a lipid and protein part, and they called the lipids lipopolysaccharides. The basic structure of the lipid has been defined since 1954. By 1970 the biochemistry synthesis and structure analysis of *Escherichia coli* and *Salmonella* were well determined as the best complex LPS examples in nature. At present, x-ray diffraction, NMR and mass spectrometry have important roles in the studies of properties of LPS molecules [4].

1.2 The importance of bacterial lipopolysaccharides

Previously, the reasons behind most of the structural analysis were done on LPS molecules were medical or veterinary. In many cases, bacteria that were not considered to be human pathogens were still found in sick patients. In other cases, bacteria that were pathogenic for animals, became pathogens for humans and vice versa. The answer to these strange cases lies in the fact that the fever-inducing agent was not the bacteria itself, but LPS, which is common to all gram-negative bacteria [24].

Presently, lipopolysaccharide studies are focused on the LPS of gram negative bacteria and nitrogen fixing bacteria that are not normally pathogenic [5]. Although LPS is not released by the bacterium, cell division can pass small amount of the molecule into the host organism. Larger amounts of LPS can enter into the bloodstream when bacteria are killed by antibiotics or treatment with divalent cation [13]. Small amount of LPS in an infected patient can be protective by stimulating the immune system and can be used to shrink tumours. However large release of LPS in a cell could be fatal. It can cause high fever, increase heart rate, and lead to septic shock and death by lung and kidney failure, intravascular coagulation, and systemic inflammatory response [29, 5].

1.3 Properties of bacterial lipopolysaccharides

LPS molecules combine with other lipids and proteins to make the outer membrane of gram negative bacteria. In solution, they can form aggregates with different morphologies, however, chemical treatment such as removing the divalent metal cations or treatment with surfactants can eliminate

the aggregation [5]. LPS molecules are anionic and they can interact with cationic antimicrobial molecules. These molecules are affected by their surrounding conditions; they can go through molecular changes and produce various supramolecular structures. There is a possibility of a phase transition between gel and liquid crystalline states for LPS molecules [10].

The components of LPS molecules, going from the bacterial membrane toward the outside in order are: lipid A, linked to the core oligosaccharide, itself linked to the O chain or O-specific antigen, if any, which consists of a sequence of repetitive subunits. Figure 1.1 shows the membrane of *E. coli* bacteria.

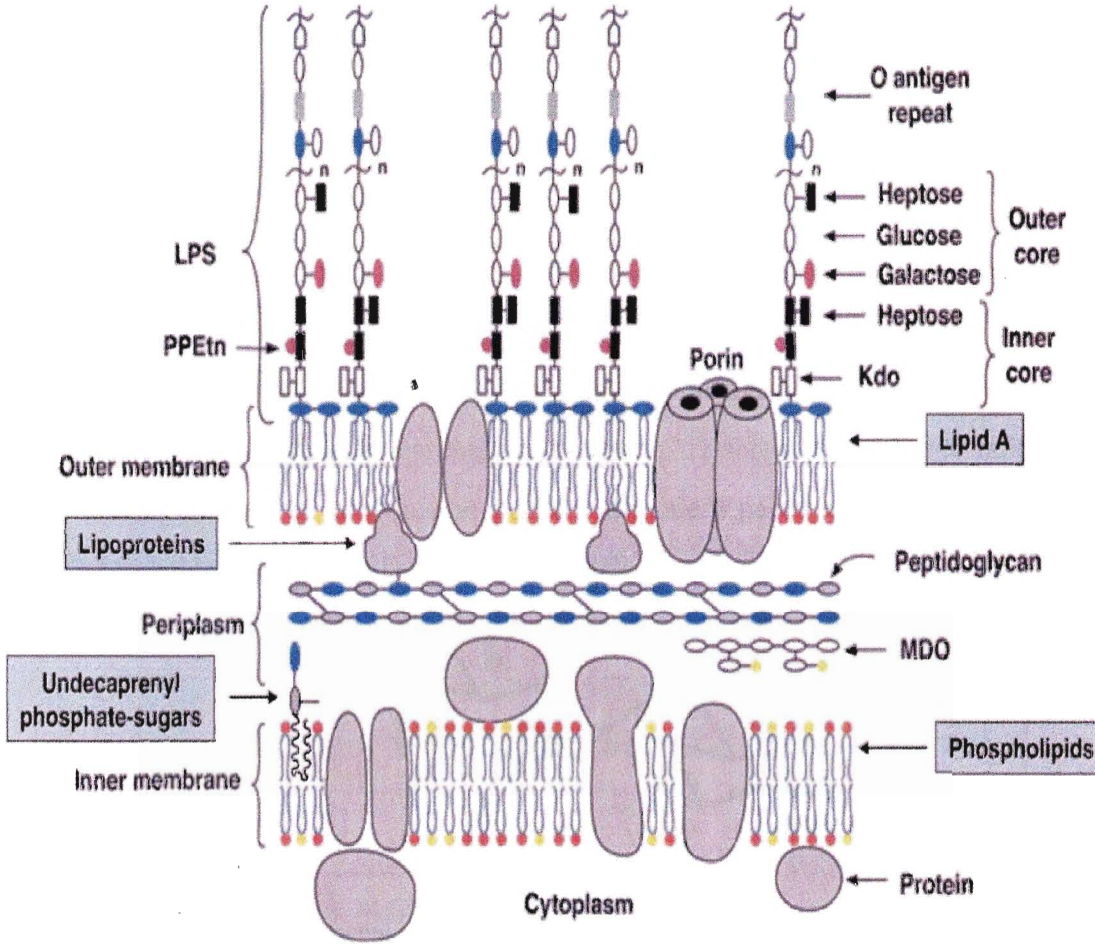

Figure 1.1: **Structure of LPS molecule.** Membranes of E. coli K-12 bacteria shows the Inner membrane, Periplasmic membrane and Outer membrane of LPS molecules [31].

1.3.1 Lipid A

Lipid A is the proximal region of bacterial membrane and connects LPS to the outer membrane. Since the 1950s there has been evidence that that lipid A is the reason for endotoxic properties of gram negative bacteria. The endotoxins were recognized as the properties of the external leaflet of the bacterial outer membrane. Lipid A is the main component by mass (45 %) and occupies ~75 % of the surface of the bacterium [5].

Lipid A is water insoluble and chloroform soluble, and can be formed as free lipid A and chemically synthesized. In 1985, it was demonstrated that both forms of lipid A from LPS of *E. coli* have identical structures and endotoxic characteristics. Free lipid A is produced by mild acid hydrolysis of lipid moiety separated from a LPS molecule [5]. Many enzymes of lipid A biosynthesis like LpxC have been validated as targets for development of new antibiotics [25].

The backbone of lipid A is mostly conserved in bacteria from various species. In classical LPS, the backbone of lipid A is a $\beta - 1$, 6-linked disaccharide of 2-amino 2-deoxy D-glucose (D-glucosamine, D-GlcN) to which fatty acids, typically 3-hydroxyalkanoic acids, are attached by ester or amide linkage. Lipid A is hydrophobic; but, it links to polar region through phosphoester. Lipid A has significant variations in its carbon chain Figure 1.2 shows a drawing of lipid A. In a large number of bacterial species, GlcN in the lipid A backbone is partly or totally replaced by its close relative 2,3-diamino-2,3-dideoxy-D-glucose (GlcN3N)

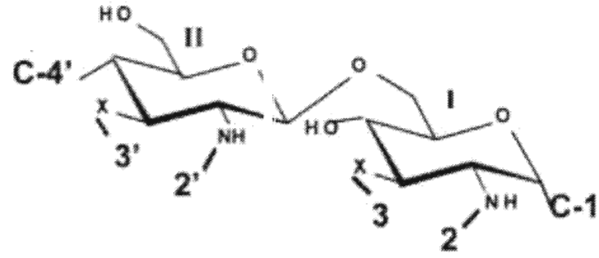

Figure 1.2: **Lipid A.**The general structure of classical lipid A. Shown are the two glucosamine groups where C-1 and C-4' are the polar parts linked to lipid A via O-P- bond. 2, 3, 2′,3′ are mostly hydrophobic C_nOH or C_nOC_m groups. The groups are varied in different species. X represent Oxygen or Nitrogen atoms [5].

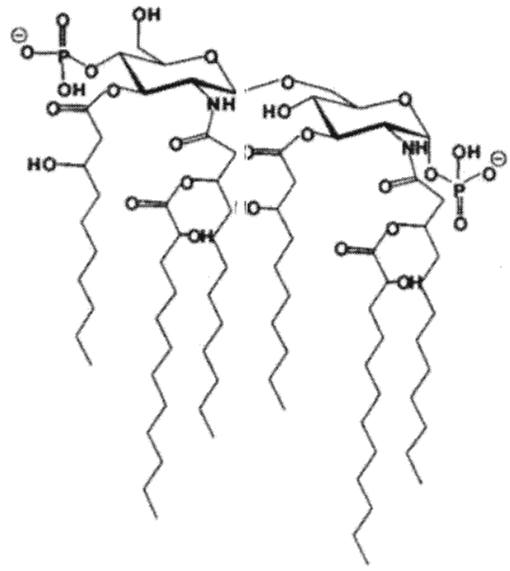

Figure 1.3: **Lipid A of Pseudomona aeruginosa.** Structure of non classical lipid A from *Pseudomona aeruginosa* with its polar headgroup [28].

1.3.2 Core Oligosaccharide

In so-called "smooth" LPS, the core oligosaccharides are divided into two regions: inner core (lipid A) and outer core. The outer core region provides a connection site for O-polysaccharide, or otherwise called the O-antigen. The role of the inner core is to maintain the structure and functions of the outer membrane.

The inner core has a conserved composition with branched structure. The core domains of LPS molecules usually contain a few repeats of 3-deoxy-Dmanno-oct-2-ulosonic acid (KDO) at their inner end, and an addition of non stoichiometric heptose which some times carry phosphorylated component. The KDO is the only component found in all the cores. In some cores D-glycero-D-talo-oct-ulosonic acid (KO), a derivative of KDO is also present [31]. Heptose is a monosaccharide with seven carbon atoms.

The inner region of the core oligosaccharide is ionized. KDO, phosphate, and other acid residues make the anionic functions of the core. LPS charged groups, like the polar groups of phospholipids, are important to the molecular structure and function of the bacterial outer membrane. In bacteria from different species, the inner core usually remains the same. In many cases, only the structure

of the carbohydrate backbone is known for a given core oligosaccharide, and the extent of phosphorylation and nonstoichiometric additions are unknown [31]. This is one of the difficulties in studies of structural analyses.

The outer core has more structural diversity because of the exposure to host responses and environmental stresses. However, the extent of structural differences in core oligosaccharides within a given species are still limited. The structural limitation for a given genus, make the core oligosaccharide an interesting target to produce therapeutic antibodies.

1.3.3 O side chain

The O-side chain consists of a single, neutral polymer of repeating oligosaccharide units that is attached to outer core of oligosaccharide through covalent bonds. The O-side chain is the hydrophilic and antigenic part of LPS.

LPS molecules are described as different types regarding to the variations of O side chain: S-type LPS or smooth LPS, consists of molecules with different degrees of polymerisation of the O-specific side chain; SR-types are LPS molecules with only a single repeating unit; R-type or rough LPS, are molecules without any side chain; and core defective R-types, or molecules with an incomplete core oligosaccharide. R-type and core defected LPS are sometimes called lipo-oligosaccharides or glycolipids, reflecting their molecular size. Some organisms have short O side chains, which allow them to have intimate interaction with host cell membrane. Some others do not even need an O side chain because their surface is covered by a thick layer of capsular polysaccharide.

There is a large structural diversity for the O side chain and biological specificity is achieved though chemical diversity. In nature there are lots of SR-LPS that contains only one unit, the abundance of LPS molecules decreases as the number of units increase to about 15 units, above that the number of molecules increases again to reach the maximum limit size which is usually from 25 to 30 O units per molecules [34]. Those maximum limits are specific for the strain and the growth temperature of the molecules. The abundance of the molecule decreases sharply after reaching the maximum limits of O units.

1.4 Pseudomonas Aeruginosa

The LPS used in the experiment was from *Pseudomonas aeruginosa* serotype O10. *P. aeruginosa* is an adaptable organism, living in moist environments and even in distilled water. It is very resistant to chemical disinfecting solutions and antibiotics [26]. This organism is one of the top three pathogens responsible for sepsis due to gram negative bacteria with mortality rate of 60 % [35]. The LPS from this organism is capable of overstimulating the immune system [8]. This organism can be isolated as opportunistic pathogen in recurrent infections patients. *P. aeruginosa* is the major cause of mortality in patients with compromised immunity, including those with cystic fibrosis CF, neutropenia, extended burs and AIDS [17, 30].

P. aeruginosa is composed of two chemically and antigenically distinct forms of LPS known as the A band and the B band [33]. The A band and LPS is made of common O antigen of short chains. These O antigens are mostly neutral homopolymers [6]. The chains are composed of 70 D-rhamnose (D-Rha) residues arranged as 23 trisaccharide repeating units [43]. The A band can be a contributing factor in the persistence of inflammatory processes and lung damage in the host with CF [6].

The B band LPS is made of O specific antigen. These antigens carry heteropolymer of negative charge. They are made of more than 50 repeating units of di- to penta-saccharide of different monosaccharides [18, 20]. The B band LPS determines the serotype of the bacterium. There are twenty serotype strains of *P. aeruginosa*, the so called International Antigenic Typing System (IATS) strains [21, 22], although it seems likely that additional serogroups are present in the natural environment [35]. Similar unlinked elements are responsible for serotype differences between strains in a given sequence group [32]. Different strains may have similar resistance patterns, however, sequential clinical isolates of the same strain may produce different antibiotic susceptibility forms [3]. The serotype O10 that was used in the experiments is made of the following repeating units: O10 : [-3)-a-L-Rha-(1-4)-a-L-GalNAcA-(1-3)-a-D-QuiNAc-(1-] [27]. Table 1.1 shows more information on these abbreviations.

Abbreviation	IUPAC Name	Formula	Weight ($\frac{g}{mol}$)
Rha	R-6-metyloxane-2,3,4,5-tetrol	$C_6H_{12}O_5$	164.16
GalNAcA	N-acetylglucosamine	$C_8H_{15}NO_6$	221.208
QuiNAc	6-deoxy-N-acetylglucosamine	$C_8H_{15}NO_{12}$	317.204

Table 1.1: **Molecular formula.** Molecular identification of rhamnose (Rha) of A band and serotype O10 of B band in Pseudomonas Aeruginosa

1.5 Membrane diffraction

X-ray and neutron diffraction has been used since the early 1960s to study the structural and phase properties of lipid systems [23]. A large amount of structural detail has been determined from diffraction and scattering experiments. For example, some early, important papers are listed in the references [44, 41, 42]. A typical method of 1-dimensional diffraction is shown in Figure 1.4, where the structural profile is measured only in the direction of the perpendicular to the membrane plane. The sample consists of aligned membrane stacks, with water in the in-between membrane spaces.

Structure determination of lipid bilayers is complicated by the disorder of the bilayers, which is because of the high mobility of molecules in all directions, as well as fluctuations of the membrane itself. Consequently, the measured structural profile of the bilayer in the direction normal to the plane of the bilayer, be it from X-rays (electron density) or neutrons (scattering length density, SLD), is of lower resolution. Higher resolution profiles can be gained through partial dehydration and alignment of the bilayers on a flat substrate such as shown in Fig. 1.4. However, the commonly understood crystallographic definition of resolution is $d/h_{\max}$, where d is the size of the unit cell stacks of lipid bilayers, and $h_{\max}$ is the maximum order of the crystallographic Bragg peaks. This value is typically on the order of 6-11 Å, which means that two objects closer than this cannot be resolved. Although we cannot have atomic resolution, it will be shown in the results section that many structural features can be identified with high precision.

X-ray and neutron diffraction have been used to determine the structure of LPS before [7, 10, 15, 16], however no experiment of *P. aeruginosa* could be found in the literature. Also, nearly all experiments were done with "deep-rough" LPS, where most of the core saccharide region was removed. This makes the LPS in these experiments little different from just lipid A. In these LPS, for example that from *Salmonella minnesota*, it was found to have a bilayer structure much like most

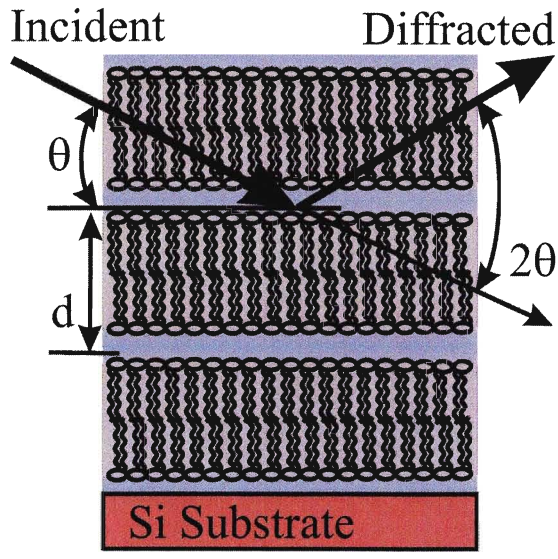

Figure 1.4: Drawing of 1-dimensional diffraction from aligned stacks of lipid bilayers.

other bilayer forming phospholipids such as the phosphatidylcholines, as well as a hydrocarbon gel phase, and it is easy to determine the head-to-head distance and thus the bilayer thickness [7, 10]. These lipids may give good structural detail by diffraction experiments, but they do not really make a good model of a bacterial membrane, because antimicrobial peptides are not really encountering a polysaccharide domain, just lipid A.

An important early study that made the comparison of LPS from *Salmonella minnesota*, *Salmonella typhimurium* and *Escherichia coli* shows that it is difficult to see much structural detail with LPS that has more of the core saccharide region [16]. Even though the lipid A hydrocarbon region is the same, for LPS with more of the core region still attached, there is much less detail in the electron density profiles in all parts of the bilayer. First the headgroup position, normally located by the phosphate high electron density peak becomes less distinct, to the point where it is too hard to say what the bilayer thickness is. Second, there is much less order in the hydrocarbon region.

Therefore, in order to build a good structural model that has more of the core saccharide region, and still gives good structral detail in diffraction experiment, we add small amounts of rough LPS with most of the core region in place, to a phospholipid that is known to form high resolution bilayers.

Chapter 2

Methods

Much of my research time was spent adapting the use of the Physics Department x-ray single crystal machine for use in diffraction of thin films and biological materials. The challenge of measuring biological samples with x-ray diffraction is maintaining the sample in a correct equilibrium conditions. The biological samples used in these series of experiments were made of lipids that can be found inside a living organism. To be able to run the experiments under the conditions close to those *in vivo*, the samples have to be in an aqueous environment. A new sample cell was designed and constructer to overcome this challenge. X-ray diffraction can give reasonable measurements only if the environmental factors affecting the sample are under control. In the case of membranes these factors are primarily temperature and humidity. In these sets of experiments the change in the temperature was monitored using a temperature controller made in the electronic shop at Brock university, specifically for the purpose of our experiments. The level of humidity is controlled by using saturated salt solutions. The next challenge was the positioning the thin film sample and the sample cell in the direction of the x-ray and recording the diffraction data. These challenges were resolved by introducing a stage controller that moves the sample cell and aligning the sample inside the cell.

More details on sample cell properties, sample preparation, and alignment of the sample is described in this chapter. Also in this chapter, specifications of the x-ray diffractometer, and various steps in running the experiment and data analysis are explained.

2.1 Sample cell

The sample cell was designed according to experimental needs and then was made in the mechanical shop at Brock University. Figure 2.1 shows various part of the sample cell.

The main part of the sample cell is the sample box. The sample box provides a closed environment to control humidity and temperature of the sample. The sample box is a hollow $(4 \times 3 \times 4)$ cm^3 with 0.2 cm wall thickness. It has a removable fitted lid and a removable tray so that it holds the saturated salt solutions. The box is made of aluminum which is light weight and easy to machine. The sample box has two 1×1 cm^2 windows parallel on its side walls, covered with Kapton tape. Kapton tape is a good shield because when the x-ray beam passes through, there would be only a very small loss in intensity. The x-ray beam can pass the windows at angles of a minimum 0 degrees to a maximum of 38.66 degrees.

There is a hole on the rear wall of the sample box. This hole is tightly fitted with a copper plate, on which the sample lies flat. The copper plate also links the sample box to the rest of the cell. A thermocouple with platinum probe is connected to the copper plate and to a peltier temperature controller device to measure the accurate temperature of the sample. The benefit of using a copper plate instead of aluminum is the higher thermal conductivity of copper: 401 $Wm^{-1}K^{-1}$ at 25°C [38].

The copper plate is attached to a peltier, or thermoelectric cooler (TEC). A TEC is a heat pump made of numerous junctions of two different metals. Most TEC are made from alternating p-type and n-type semiconductor elements [1]. When DC current passes through the junctions, to maintain a uniform temperature, it is necessary that heat is emitted at one junction and absorbed at the other junction, creating hot and cold sides. The direction of heat transfer depends of the direction of applied current. The TEC used to build the sample cell is "Thermoelectric Cooler CP2-31-10" and was purchased from Melcore. Table 2.1 shows the specifications of the TEC. The TEC is connected to a heat sink, which absorbs the heat and provides the cold side of TEC with a low temperature. The heat sink is a $(5 \times 1.2 \times 5)$ cm^3 copper box with a U shape hole through it. The holes are connected to a flowing cold water source. The heat sink and the copper plate make a sandwich that holds the TEC in place by long plastic screws, so that heat can not diffuse through screws.

The heat sink is joined to two linear positioning stages. The positioning stage is manually operated and oriented at right angles to each other. Assuming that the x-ray beam points in the X direction and the normal to the sample plane lies in the Y direction, then according to the right

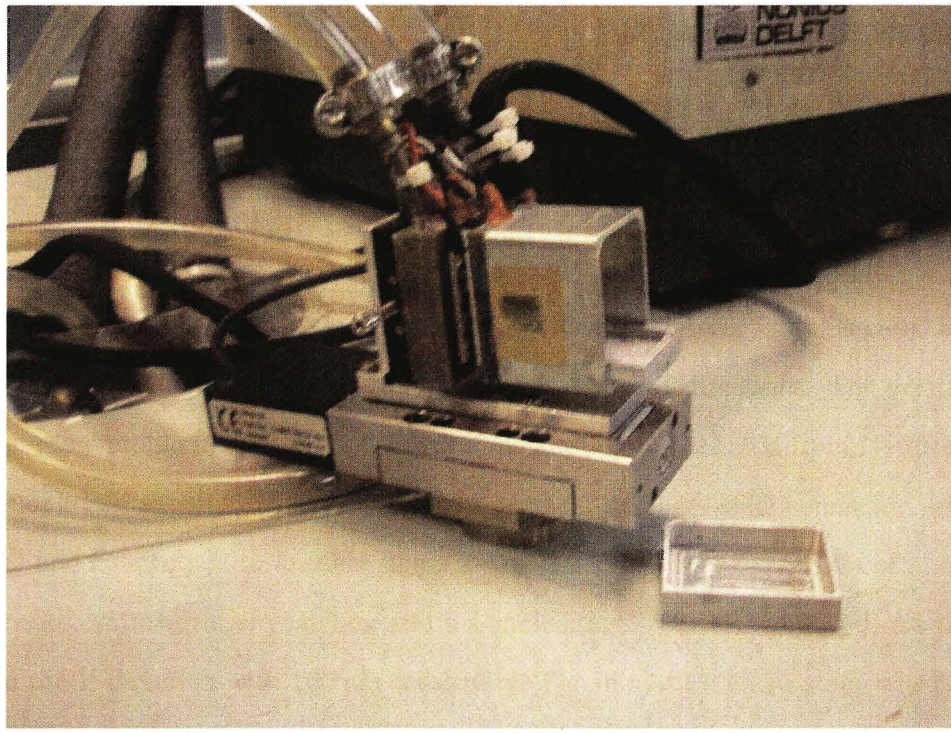

Figure 2.1: **Sample Cell.** All parts of the sample cell are shown in this picture. Sample box, sample holder, peltier and heat sink are connected to a travel stage which is attached to linear stage though a L shape holder.

Hot Side Temperature ($°C$)	$25°C$	$50°C$
Q_{max} (Watts)	18.8	21.4
Delta T_{max} ($°C$)	67	77
I_{max} (Amps)	9.0	9.0
V_{max} (Volts)	3.75	4.00
Module Resistance (Ohms)	0.35	0.40

Ceramic Material:	Alumina (Al_2O_3)
Solder Construction:	138°C, Bismuth Tin (BiSn)
Max Operating Temperature:	80°C

Table 2.1: **Peltier performance specifications** [39].

Travel Range:	25 mm
Minimum Incremental Motion:	0.1 μm
Load Capacity:	50 N
Motor:	DC servo motor UE1724SR
Guaranteed Uni-directional Repeatability:	0.3μm
Guaranteed Accuracy:	8 μm
Resolution:	0.0175 μm
Maximum Speed:	2.5 mm/s

Table 2.2: **Linear stage specification** [40].

hand rule, the Z vector would be pointed to the laboratory ceiling. In this case, the positioning stage can move the sample box up to 13 mm in both X and Z directions. The positioning stage is "460A series low-profile integrated ball bearing linear stage" purchased from Newport Inc.

The sample cell assembly is attached to a I -shaped, stainless steel connector, which holds the sample cell and connects it to another linear stage. This linear stage consists of a motor-mounted rotary encoder, an integrated gear box and a sample stage. The DC motor allows the sample cell to move in the Y direction with 100 nm sensitivity. The miniature linear stage was purchased from Newport company and belongs to MFA-CC series. The properties of the linear stage are explained in Table 2.2. The control of the motorized positioning stage was added to the x-ray control software by the Brock electronics shop.

Finally, an attachment mechanism based on the design of a standard goniometer head was connected to the bottom of the motorized stage so the whole sample cell device could be mounted on a goniometer. The attachment mechanism is made of brass and adds 1 cm to the sample cell hight.

2.2 Sample preparation

Several pieces of a single crystal wafer of silicon were cut into 1×1 cm^2 pieces to be used as sample substrates. The pieces were washed with water, methanol and chloroform and then air dried to erase fingerprints.

1-palmitol-2-oleoyl-sn-glycero-3-phosphocholine (POPC) and

1,2-dimyristoyl-sn-glycero-3-phosphocholine (DMPC) were bought from Avanti Polar Lipids (Al-

abaster, Alabama). POPC is hygroscopic as lyophilized powder. Cholesterol and lipopolysaccharides (LPS) were purchased from Sigma (St. Louis, Missouri). LPS were from species of the *Pseudomonas aeruginosa* serotype O10, purified by phenol extraction with less than 3% protein by weight as possible impurities. All materials were used as supplied, without further purification.

In the experiments different samples were used; 20% by molar cholesterol in DMPC; pure POPC; mixtures of 1%, 10% and pure LPS in POPC. The desired amounts of samples were measured and dissolved in a 3:1 mixture of methanol:chloroform solvent. A few drops of water were added to 10% and 100% LPS samples solution to make a smooth homogeneous sample and prevent aggregation of the solution. Droplets of solution were put evenly on the substrate until the substrate was covered with all the sample solution. Samples were air dried and then vacuum dried for an hour, so that all the solvent would be evaporated.

Before putting the sample on the sample holder, a saturated salt solution was made inside the sample tray by filling the tray with salt and adding few drops of water. Saturated salt solutions were used to control the humidity level inside the sample box. In the experiments potassium nitrate, potassium sulfate and potassium chloride were used. Salts were ACS Grade, with 99% purity and were purchased from VWR International (Mississauga, Ont). One of the experimental difficulties arise from dealing with saturated salt solutions. The salts tend to crystallize at the edge of the sample box and the crystal allows solution to rise by capillarity and crystallize further up. This caused problems in moving and washing out the sample tray during replacement with a new saturated salt solution. If the capillary crystals fall out of the sample cell box, they may even make problems in rotation of the axes gears in the x-ray diffractometer.

Lipid samples should adjust themselves and reach the equilibrium with temperature and humidity before any measurements can be run. At equilibrium, measurements should be reproducible. The equilibria was obtained within a few hours of keeping the sample in the sample cell.

2.3 X-rays

2.3.1 X-ray production

X-rays are electromagnetic radiation that is produced by accelerating electrons in order to collide with a metal target. In the lab, a Picker high voltage generator with an Enraf-Nonius CAD4 goniometer and Siemens sealed copper anode x-ray tube was used to produce the x-ray beam. In the x-ray tube, the electron falls through a potential difference of V and obtains energy of eV electron volts. When the electron slows down into the anode, this energy converted to photons, producing a spectrum of x-rays known as Bremsstrahlung radiation, with a minimum wavelength of λ:

$$\lambda = \frac{hc}{eV} \tag{2.1}$$

The electron collisions in copper, generally increases atomic vibrations and so generates heat in the copper. About 0.1% of the incident electron energy is usefully converted into x-ray radiation and the rest appears as heat. The heat is removed from the system by flow of water passing thorough the x-ray tube. If the voltage applied to an x-ray tube is large enough, then the accelerating electron can have sufficient energy to remove an electron from inner shell of the copper atoms. As a result other electron from higher energy level fills up the vacancy. If the energy difference between the two electrons in different shell levels is ΔE then the wavelength of x-ray emission would be:

$$\lambda = \frac{hc}{\Delta E} \tag{2.2}$$

In the case of copper, the spectrum consists of two pronounced wavelengths of K_α with $\lambda = 1.542$ Å and K_β with $\lambda = 1.392$ Å [19].

A graphite crystal monochrometer is used to remove the Bremsstrahlung and K_β line by Bragg diffraction, which is explained below.

2.3.2 Crystallography

In a crystal structure, atoms repeat with symmetric units. These units are made of evenly spaced parallel planes which set the position and orientation of the atoms. When the x-ray beam is incident on these planes some beams reflect from the atoms and the rest penetrate through crystal and hit the atoms of the adjacent plane and then reflect. The beams that reflect from different planes travel different path lengths, and will then interfere with one another. The interference is at least partially destructive unless the path difference is an integer multiple of their wavelengths. Bragg's law simply explains the path difference for constructive reflected beams.

$$\lambda/d = 2\sin(\theta) \tag{2.3}$$

where d is the distance between the atom planes, and θ is the angle the x-ray beam makes with the atom planes.

The constructive beams that have the highest intensity produce diffraction patterns. If the Bragg equation is satisfied, x-ray beams scattered by adjacent unit cells will be in phase.

The geometrical description of scattering and diffraction is based on the idea of reciprocal space. An incident beam of photons scatters from atoms within the sample. The spatial correlation of atoms from each other gives rise to constructive and destructive interference in the direction of the detector. All scattering instruments create beams with well defined direction of incidence $\vec{k_i}$, a vector in the laboratory frame of reference whose length is $|\vec{k_i}| = 2\pi/\lambda$, where λ is the wavelength of the x-ray. The x-ray detector measures the intensity of the interaction with matter at well defined directions $\vec{k_f}$.

The change in momentum of the scattered photons due to their interaction with the sample can be defined as $\vec{q} = \vec{k_f} - \vec{k_i}$. In this case, all scattering is mapped into reciprocal space by the scattering function $I_m = I_0|F(\vec{q})|^2$. In here, I_m is the measured intensity of radiation in a direction $\vec{k_f}$, and I_0 is the incident intensity. When the detector is in the direction where the reciprocal space vector $\vec{q}$ is made parallel with spatially correlated atoms, constructive interference results and a higher intensity is recorded as symmetry allows

The form factor $F(\vec{q})$ is given by

$$F(\vec{q}) = \frac{1}{N}\left|\sum_i f_i e^{i\vec{q}\cdot\vec{r_i}}\right|^2, \tag{2.4}$$

where the sum is over all N atoms in the sample located at positions $\vec{r_i}$. The strength of the interaction between atom and probe is expressed via the term f_i, which for x-rays is the Thomson scattering factor whereby the atom's electrons are considered to be moving freely in clouds of electron density.

The location of scattering atoms $\vec{r_i}$ from Equation 2.4 can be rewritten in terms of the atom layers representing a repeating structural unit. For example, if a one-dimensional fundamental structural motif has a repeating size d, the total sample may have N repeating layers of this motif, for a total thickness of $N \cdot d$. An atom located at position R_i in the first unit is repeated in all units, and it is found at the location within layer h at

$$r_i = l \cdot d + R_i. \tag{2.5}$$

In this case, the sum of Eqn. 2.4 becomes

$$\sum_i f_i e^{i\vec{q}\cdot\vec{r_i}} = \sum_n f_n e^{i\vec{q}\cdot\vec{R_i}} \sum_h e^{ih\vec{q}\cdot\vec{d}}, \tag{2.6}$$

where the first sum is over all atoms in just one structural motif. This term modulates the second sum which now takes in to account the total number of repeating units making up the sample. The second term can have a very strong maximum when $q \cdot d = h2\pi$, which is Bragg's law when $|\vec{q}| = |\vec{k_f} - \vec{k_i}| = 4\pi \sin\theta/\lambda$. Therefore, structural motifs in lipid dispersions that repeat with well defined correlation lengths give rise to extremely strong constructive interference.

The incident waves have the same wavelength and frequency but with different amplitude and phase as the resultant scattered beam. The phase and amplitude of the reflected beam has the information to determine the structure of unit cell. The important part of the x-ray measurement would be determining these values. The intensity of a scattered beam is proportional to the square of the amplitude of the beam and it is expressed in terms of the intensity of the beam reflected

from unit cell. This intensity also depends on geometrical factors of the crystal and experimental conditions. The experimental measurements for the phase of the reflected beam is not possible because after taking the square root of the measured intensity to get the values of Equation 2.4, any phase information $e^{i\vec{q}\cdot\vec{r_i}}$ is lost [19].

Luckily for the case of lipid membranes, the central symmetry of the unit cell means that the phase of F_h will be either 0 or π. Therefore after taking the square root of the measured intensity, and correcting for experimental factors, the only unknown would be the sign of F_h.

2.4 Correction Factors

When a x-ray beam hits the electron in the sample its energy can be transferred in various ways. The loss of energy can be measured as the ratio of intensity of the incident to intensity of the scattered beam. This ratio depends on the polarization, Lorentz and absorption factors.

2.4.1 Lorentz Factor

When a sample crystal is rotating at a constant angular velocity, reciprocal lattice points can pass through the conditions of reflection at different rates and so they would have different times of when they are in the condition of Bragg's law [19]. When x-ray beam is normal to the rotation axis of the four circle diffractometer, Lorentz factor can be derived as $L = 1/\sin(2\theta)$.

2.4.2 Polarization Factor

Originally, the beam is unpolarized from the x-ray tube. The x-ray beam is an electromagnetic wave and has both electric and magnetic vector components. When the x-ray beam is emitted, its electric vectors have random direction. Each of these electric vector can be recognized by two components perpendicular to each other. The intensity of the unpolarized x-ray beam depends on the sum of all these random vectors.

When the beam reflects from any plane surface, the electric field vector perpendicular to the surface is absorbed more than when it is parallel. Therefore, after reflection, the beam becomes

partially polarized parallel to the surface. This loss of intensity must be taken into account.

For the CAD4 goniometer, the beam becomes partially polarized in the vertical direction because of the horizontal graphite monitor. Then this beam is partially polarized in the horizontal direction after hitting the vertical sample. The polarization factor depends on Bragg angle for the monochromator and the geometry of the apparatus.

2.4.3 Perfect and Imperfect Crystals

Samples can be perfect or imperfect crystals. In perfect crystals atoms lie on parallel planes inside the unit cell. In this case there is a $\pi/2$ phase shift at each reflection and the intensity of reflected beam from all the layers are the same.

In imperfect crystals instead of parallel planes, atoms lie on the mosaic of misaligned blocks. In this case when the x-ray beam hit the first layer of atoms, there may not be another atom in the proper position in the lower layer. In this case most of the incident intensity would be reflected from the first layer and just small amount of the x-ray penetrate inside the crystal and reflect from the lower layer so intensity of the incident and reflected beam for each layer are different. In an imperfect crystal because of large size of the mosaic blocks there would be multiple scattering inside each block. Multiple scattering would cause interferences between the incident and all the other scattered beam. In the case of double reflected beam the phase difference between incident and reflected beam is π. The biological samples that were used in the sets of experiments, were all considered as imperfect crystals [19].

2.4.4 Absorption Factor

Absorption of x-ray in a sample can happen in two different ways [19, 37]: The energy of the x-ray photon, δE absorbed completely to remove an electron from the atom of the crystal. This is a strong absorption and is called Photoelectric absorption. The x-ray beam scatters from the plane of atoms inside the crystal. Scattering processes can happen in two different ways: Compton modified scattering, or scattering with loss of energy and so with an increase in the wavelength of the reflected beam. The other scattering process is Rayleigh, or unmodified scattering. In this scattering the

energy and wavelength of incident and reflected beam stays the same. Bragg reflection is the basis for the Rayleigh scattering.

However, according to characteristics of the imperfect crystal, there is a small reduction in the intensity of reflected beam in unmodified scattering.

2.5 CAD 4 Geometry

The x-ray diffractometer is an Enraf-Nonious CAD4 goniometer, mounted to a Picker x-ray generator, with a copper anode. The x-ray generator was typically run at 600 W power. A new copper tube was purchased from Bruker AXS (Madison, WI, U.S.A) and aligned carefully.

Figure 2.2 shows the geometry of goniometer. The CAD4 is a four-circle, single crystal goniometer in the Kappa-orientation. The Kappa goniometer holds the goniometer head which keeps the samples in the center of diffractometer. The Kappa goniometer consists of three axes of rotation, as seen in Figure 2.2. All the axes meet together in the center of diffractometer. A standard sample goniometer head (or the sample cell described above) is placed on Phi axes which is supported by Kappa block. Kappa block rotates the Kappa axis, which is at a fixed angle to the Phi axis. When Kappa is at zero degrees, the Phi axis runs vertically in the laboratory frame of reference. The Kappa axis is mounted on Omega block. The Omega block rotates Omega axis which is carried by base plate of diffractometer. This plate is mounted on detector and supports the detector rotation through the 2Theta angle. As a result, the 2Theta axis coincides with the Omega axis.

The plane that is perpendicular to all the axes and passes though the center of diffractometer is called horizontal scattering plane. The primary x-ray beam is in this plane and points toward the center of diffractometer, where the sample cell is located. The detector also measures the intensity and position of diffracted beam in the same plane. X Y and Z component of Cartesian rotation are assumed to be in and perpendicular to this plane respectively.

An analyzer or motion controller controls all the axes of the goniometer and was built by the Brock electronics shop. There was some difficulty in the reliability of the control software and many revisions and repairs were made. One important revision involved the zero reference point of the angles. The zero angle is determined by the direct beam, although there are mechanical angle

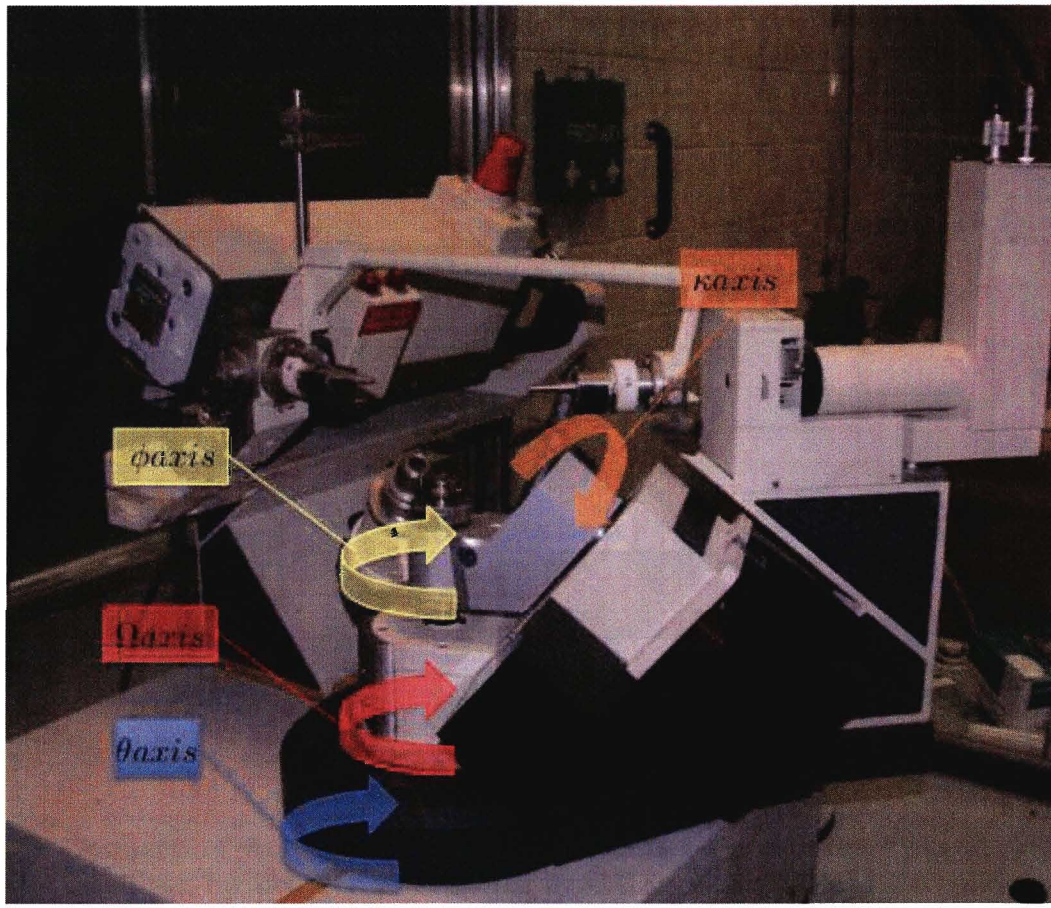

Figure 2.2: **Diagram of the four axis of the CAD4 goniometer.** Data collection were usually taken with the fixed angles of Phi=90, Kappa=0. This orientation keeps the axis of Phi, Omega, and 2Theta coincident.

counters attached to the CAD4 goniometer. Working with the electronics shop, the software was changed to allow offset values to be applied to the motion of the angles so that arbitrary zero points could be used in the alignment. Figure 2.3 shows the connection between the sample cell, goniometer and computer. The devices colored in orange, were built and modified specifically for purpose of our experiments. As it can be seen from the picture, detector is connected directly to goniometer and the analyzer while the sample cell is connected to goniometer, stage and temperature controller. The count controller monitors the intensity at a given time frame and record them through computer.

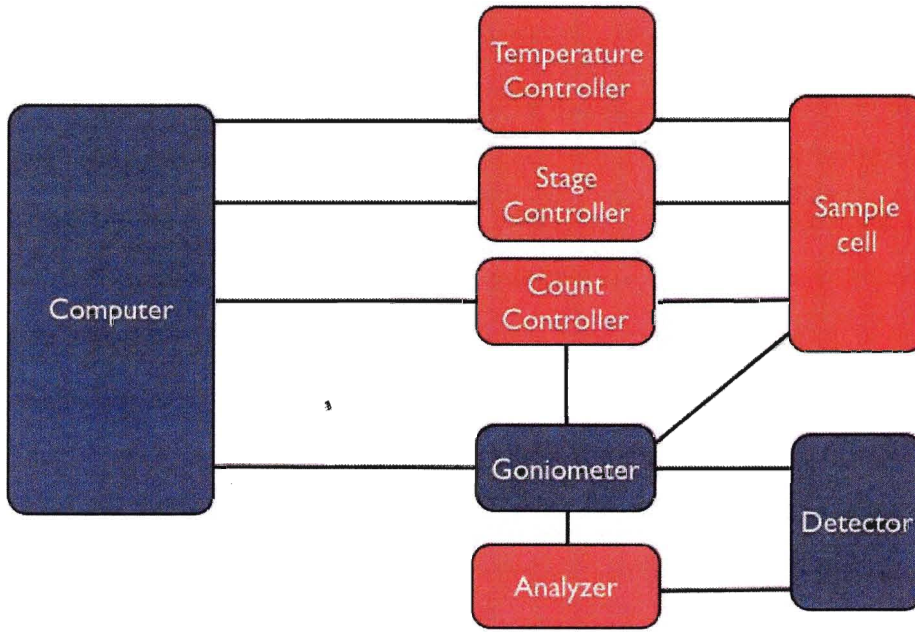

Figure 2.3: **Connection from sample cell and CAD4 to computer.** The diagram shows that the x-ray detector is monitored by CAD4 goniometer and the analyzer through computer. The sample cell is under the control of temperature and stage controller while is connected to goniometer.

2.6 Aligning the sample

Alignment is one of the major steps to achieve a reasonable data, which consists of two main steps in these sets of experiments: 1- Alignment after replacing the x-ray tube, which includes the alignment of position of focal spot and center of the detector. 2- Alignment of the center of the primary x-ray

beam with respect to axes of diffractometer and the receiving aperture. This alignment should be done before running each set of experiments. The Phi angle was adjusted to a constant value of 90° for all sets of experiments. According to experimental setting, at this value of Phi, x-ray beam is perpendicular to the sample cell window. There are six other adjustments to find the best alignments for rotating axes: aligning 2Theta, adjusting sample position, adjusting Omega, aligning Kappa, aligning sample stage position and final aligning of Omega value.

The key to aligning the Theta value is to adjust the zero degree point. At this point x-ray beam was passed through the Kapton tape window without hitting the sample. The detector collects data by moving the Theta axis from a positive to a negative number while Omega and Kappa were kept at zero. Theta adjustment can be measured by fitting the data on a gaussian graph with center at zero degree. The important point at this stage is when the reflected beam is very small, e.g $2\theta < 0.8°$, the main beam will have a very high intensity. To prevent damaging the detector, the intensity absorbed by detector should be almost less than 10,000 counts per second. As a result, if an x-ray beam is passing straight through the Kapton tape or when the beam is hitting the sample with a low angle, the beam intensity should be decreased experimentally. The low counts per second can be obtained by keeping attenuator on and adding Aluminum sheets in front of detector.

The next step in alignment is to adjust position of the sample. In this step all angles were kept at zero and experiment runs by changing the sample stage position. The position that detector measures half the intensity of straight beam, is considered to be the position to keep the sample. In this step attenuator and aluminum sheets should still shield the detector.

The first act in adjusting the Omega value is to find the first 2Theta peak. This can be done by measuring intensity verses change in 2Theta and keeping Omega and Kappa constant. Then fitting the data into a gaussian curve and finding the center of 2Theta peak. The second part is keeping 2Theta constant at the measured value with Kappa at zero and changing the Omega. Offset of Omega value is measured when center of Omega curve is assigned to be half of the 2Theta value. Next step is aligning Kappa. Data were collected by changing Kappa versus intensity and keeping 2Theta and Omega at the peak values. Data were then gaussian fitted.

After measuring the peak values for all the axes, the sample stage was then aligned with the measured values. A curve of intensity versus sample stage position were measured and final position

of sample stage were obtained. Moving the sample stage can have effects on Omega adjustments, so there would be need for a final alignment of Omega. At this point 2Theta, Kappa and stage position were kept at their peak value and center peak for Omega were measured.

Now that sample is aligned with all the axes, the experiments can be run. Detector starts moving 2Theta axis from 0.8° to 14° and Omega follows the change in Theta values starting from 0.4° to 7°, while Kappa stays constant at the measured value. The collimator used in measurements is a fine focus collimator with beam diameter of 1.3 mm. Depending on the samples and strength of its peaks, the experiment can be divide into 2 or 3 parts. Usually the first peak or the first order reflection is much more intense than the higher reflection peaks, in this case attenuator were kept on and 1 second would be consider as time constant between each taken data. Then for the next two or three peaks time constant were change to 10 second. For the rest of the peaks 100 second would be consider as time constant. Each sample were run at set of various temperatures.

2.7 Calculations

The goal of calculation is to obtain the electron density profile. To do so, the corrected intensity for each peak should be calculated. This value can be measured form the experimental intensity I_{exp}, and correction factors such as Polarization P, Absorption A and Lorentz L factors.

$$I_{cor} = I_{exp} \times \frac{L}{P \times A} \tag{2.7}$$

Data collected by x-ray diffractometer at each specific temperature is intensity versus change in 2Theta and Omega. Each data set consists of different number of peaks, depending on sample properties. Each peak was analyzed by a Gaussian curve and a linear back ground to determine the parameters such as area, center of the peak and peak width. Background subtraction of the area underneath each peak gives the experimental intensity of that peak. Correction factor formulas are as follow:

The polarization correction for partially polarized beam and a perfect monochromator material

is:

$$P = \frac{cos(2\theta_m) + (cos(2\theta))^2}{1 + cos(2\theta_m)} \tag{2.8}$$

where $\theta_m = 13.3075$ is the Bragg angle for monochromator.

The absorption correction is

$$A = \frac{sin\theta}{2\mu d}[1 - exp(\frac{-2\mu d}{sin\theta})] \tag{2.9}$$

where d is the path length of x-ray through the material or the thickness of the sample which is 0.0009 cm and μ is the linear absorption coefficient. This value is calculated by summing over μ of each element(cm^2/g) multiplied by the mass density of that element(g/cm^3). Mass absorption coefficients for each element at K_α Cu wavelength of 1.5418 Å are obtained from International tables for x-ray crystallography.

The inverse of the Lorentz factor $1/L$ is:

$$\frac{1}{L} = \frac{1}{\sin(2\theta)} \tag{2.10}$$

Structure factor graphs can be calculated as a function of F_h vs. q;

$$q = \frac{h}{d} = \frac{2sin\theta}{\lambda} \tag{2.11}$$

where λ is the wavelength of copper K_α spectrum and h is the number of the peak order and d is the size of the unit cell in Z direction, also called the lamellar spacing.

$$F_h = \pm 1 \times \sqrt{I_{cor}} \tag{2.12}$$

The coefficient value of ± 1 depends on the phase and the order of the peak.

This uncertainty of the sign of the coefficient, is called the phase problem, because the sign of the phase can not be measured experimentally. This value can be assumed theoretically by comparing the shape of the structure factor profile and the electron density profile of the sample with previously known phospholipid bilayers. The coefficient used in this experiment were typically

(-1,-1,1,-1) starting with -1 value for the first reflection. There are similar sets of coefficient used in measurements of lipopolysaccharide of Salmonella Minnesota [10].

The error for each order of structural factor can be measured through polynomial of order three as a function of q. After measuring the structural factor for each sample, the Fourier transform can be calculated for each and every environmental change in the sample by using:

$$F(q') = \Sigma_{h=-h_{min}}^{h_{max}} F_h \frac{sin[\pi(q'D-h)]}{\pi(q'D-h)} \tag{2.13}$$

here q' is an arbitrary value between 0 to 50 (A^{-1}).

Graphs of $F(q')$ and graph of F_h v.s q were plotted. Errors of Fourier transform can be measured using variant and co variant matrix and least square multiple regression and equation:

$$var(F_h) = \Sigma_{i=1}^{N} \Sigma_{j=1}^{N} v_{ij} q^{i+j-2} \tag{2.14}$$

$$\delta F_h = t(var(F_h))^{1/2} \tag{2.15}$$

$$\delta F(q') = [\Sigma_{h=-h_{min}}^{h_{max}} \delta(F_h)^2 \frac{sin^2[\pi(q'D-h)]}{(\pi(q'D-h))^2}]^{0.5} \tag{2.16}$$

where v_{ij} is the element in the i-th row and j-th column of variant covariant matrix. t is the student factor value, in these experiments the confidence limit were measured for 95% confidence limit. In these experiments the values were fitted into polynomial of order three so the value of N used is $N = 3 + 1$

Finally the electron density profile is calculated through:

$$\rho(x) = 2\Sigma_{h=}^{h_{max}} F_h cos\left(\frac{2\pi hx}{D}\right) \tag{2.17}$$

where ρ(x) is the scattering density, x is the distance from origin of unit cell. Again 95% confidence limit were measured using:

$$\delta[\rho(x)] = 2[\Sigma_{h=1}^{h_{max}} [\delta(F_h)]^2 cos^2(\frac{2\pi hx}{D})]^{0.5} \tag{2.18}$$

Chapter 3

Results

X-ray diffraction patterns of $\theta - 2\theta$ scans was recorded for every sample at different temperatures and hydration level. In each sample, the first peaks have the highest number of the counts. The number of the counts for these peaks were measured using an attenuator so that the count numbers decreases under 10,000 cps. The time base for the diffraction pattern for each sample was divided into three sections to produce clear peaks and save time during the experiments: first peak has time constant of 1 sec. The second, third and forth peak have time constant of 10 sec and the rest of the peaks were measured using time constant of 100 sec. Figure 3.1 shows an example of raw data on a logarithmic scale. The sample is POPC using saturated salt solution of KNO_3 at 40°C corresponding to relative humidity of 89%. This sample has 8 Bragg peaks. The number of order values are different for each sample, they also can be varied by changing the temperature within a sample. After analyzing the data, the structure factor and the electron density profile for each sample are measured and graphed. This chapter explains the graphs and what was learned about the structures of the samples.

3.1 DMPC with 20% cholesterol

3.1.1 Structure factors

Initially DMPC samples were made in a solution of 40% molar cholesterol concentration which is similar to the molar concentration of the cholesterol inside many plasma membranes in the body, including the nerves [9]. The graphs of diffraction patterns of this sample includes the peaks belonging to the cholesterol in crystalline phase, that were produced through a too high concentration of the cholesterol in the solutions [14]. Therefore for the further set of experiments the

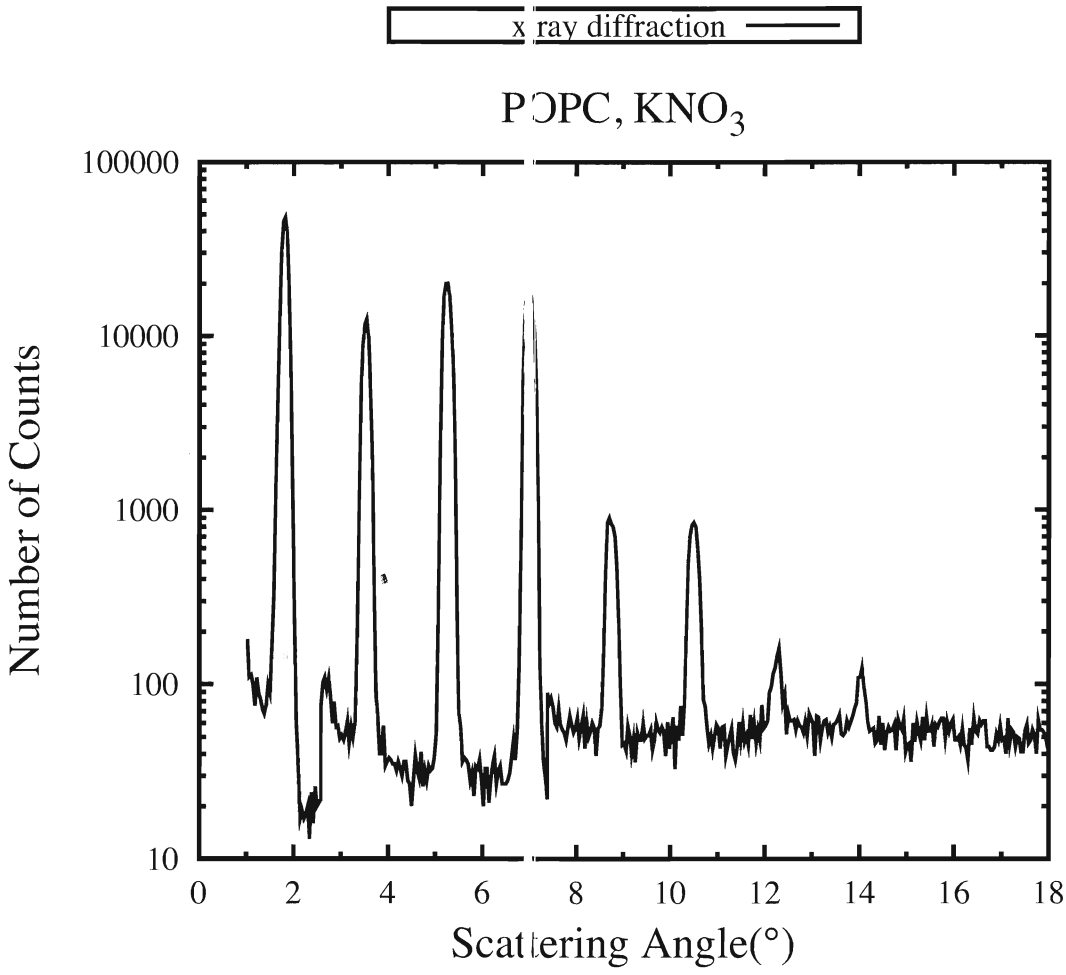

Figure 3.1: **X-ray Membrane Diffraction** X-ray diffraction pattern of POPC multilayer at 40°C. The pattern is a function of counts versus scattering angle of $\theta - 2\theta$. The position of the 8 peaks are clearly shown in logarithmic scale within three different time base at an angle of 2.42 Å and 7.44 Å.

concentration of cholesterol was decreased to 20 % inside the sample solution. The x-ray diffraction peaks in this solution are positioned at the expected angle and lamellar spacing. The data were collected in six sets at different temperature within the range of 18 °C to 28 °C with the lamellar spacing in the range of 56.45 Å to 58.02 Å using KNO_3 as saturated salt solution.

Amplitudes, obtained by taking the square root of the corrected intensities, are plotted in figure 3.2 as a function of the $q = 4\pi sin\theta/\lambda$ for each order of h. Each value represents a peak in the raw-data graph of counts versus scattering angle of 2θ. Nine order values of DMPC, 20% cholesterol can be seen in this graph. The research done by Hung et al [14] also shows the same number of order values for the solution of DMPC with 17% cholesterol at temperature of 30°C with the relative humidity of 91.8%. This research shows that the DMPC solutions with more than 17% cholesterol concentration are in gel phase at various temperatures and humidity levels. Referring to this research and the x-ray diffraction plots of DMPC with 20% cholesterol concentration at the temperature range of 18 °C to 28 °C, it can be conclude that the sample was in the gel phase during the experiments at all the temperatures.

In the figure 3.2, the line of the best fit for each sets of order value were measured by least squares third order polynomial curve. The shape of the structure factors can be clarified by graphing the Fourier transform at minimum temperature of 18° C and maximum temperature of 28° C in blue and yellow lines respectively. These Fourier transforms were measured by giving q a set of 50 values between 0 to 1 and calculating F_q as described in equation 2.13. These graphs show that the orders fall on a single Fourier transform curve. The data points for each single order also fall on a smooth curve of a third order polynomial and are shown with black.

To find out whether changes in the temperature would cause a significant change in the structure factor, the 95% confidence limit of Fourier transform at minimum temperature of 18° C and maximum temperature of 28° C were calculated. The confidence limit were measured using the variance-covariance matrix and equation 2.14. These graphs were plotted in the top panel at figure 3.3. A comparison between this plot and the structure factor graph 3.2, shows that a change in the structure factor appears at fourth order values.

The shape of these graphs were compared with a single curve of Fourier transform at Frank and Lieb study [9] in the bottom panel of figure 3.3. In their study, the effect of change of hydration

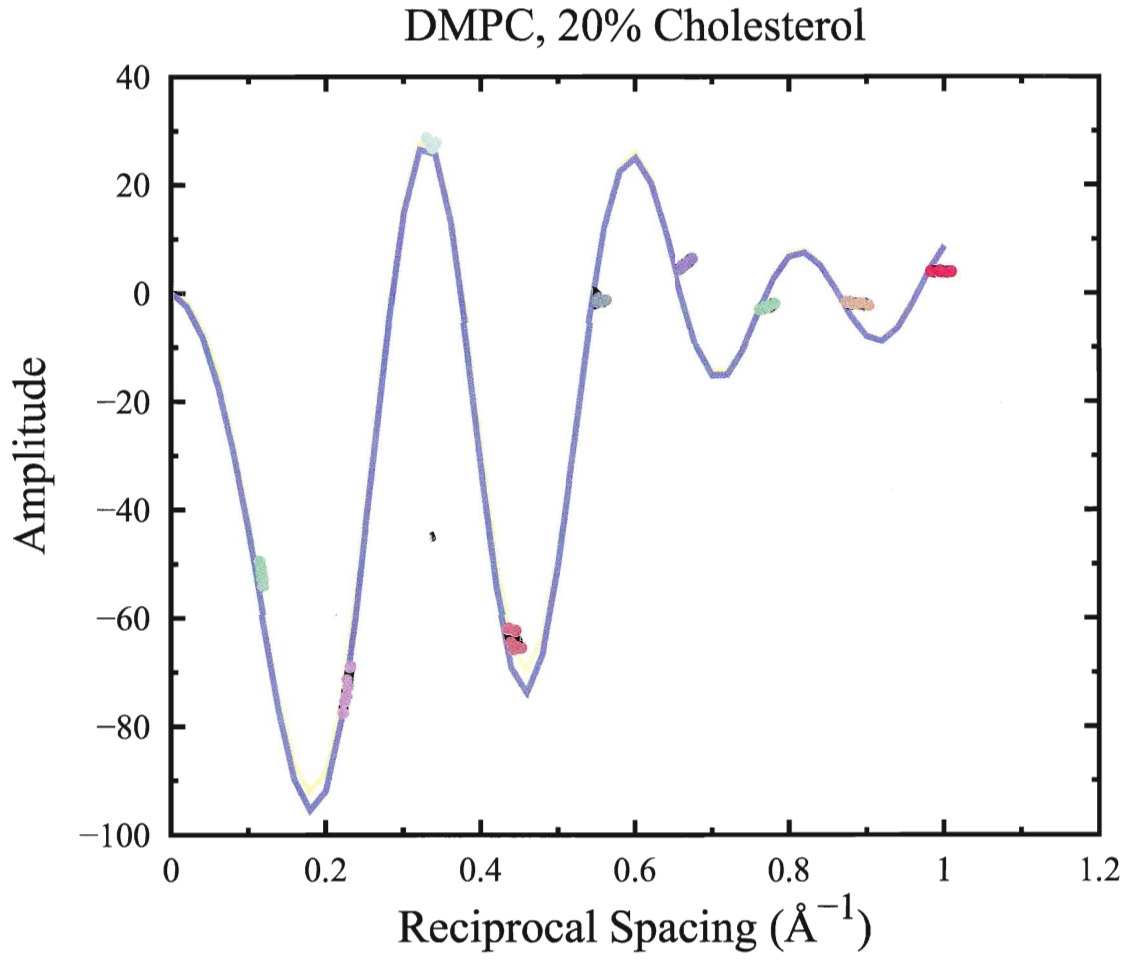

Figure 3.2: **Structure factors of DMPC with 20% cholesterol.** Each of the nine sets colorful dots, are the indication of the structure factor at a specific order value of h, starting with lime color dots as $h = 1$. The line of the best fit for each set is shown in black. The blue and yellow curves represent the Fourier transform at 18°C and 28°C degree.

level on structure factor of dimyristoyl lecithin in 40% cholesterol solution with confidence limit of 95% were measured. To be able to plot the graph, the data were fitted in to the $F(q')$ formula and the error equation. The hydration graph has a lamellar spacing of 51.79 Å and a temperature of 23° C. Our Fourier transform graph at 18 °C and 28 °C have lamellar spacing of 57.749 Å and 56.472 Å respectively.

The shape of the structure factor graph can be compared with figure 3.4: The x-ray structure factor as a function of reciprocal lattice spacing of dimyristoyl lecithin in 40% cholesterol solution from Frank and Lieb paper [9]. This graph was obtained by changing the humidity level between 32% and 100% while the lamellar spacing were changed between 47.90 Å and 57.51 Å. The data for each set of order number fall on a smooth polynomial curve, as does our data, and this indicates that structural change of the sample is continuous [9].

A three dimensional Fourier transform graph were plotted in the appendix in Fig. A.8 for easier visualization of the structure factor. The plot is a function of $F(q)$ versus q and temperature. The q values are 50 numbers in the range of 0 to 1 and temperature are in the range of 18° C to 28° C degree. The changes in Fourier transform graph are very smooth.

3.1.2 Electron density profile

Electron density profiles are shown in figure 3.4 for the 6 temperatures within the range of 18 °C to 28 °C. The profiles have offsets in the vertical direction for clarity of presentation. The major peaks in the electron density graph at about ± 20 Å correspond to the phosphate group of the DMPC molecule and the trough at the middle of the graph corresponds to the center of bilayer and the methyl group. By comparing the plots for each temperature, it can be seen that by increasing the temperature the peak position become close to each other. Also by increasing the temperature the lattice spacing decreases and the plots become more condensed which means the lipids order increases at the higher temperature. At the lower temperature the electron density profile are smoother which is another indication of increasing the order of the hydrocarbon chains at higher temperatures.

The 95% confidence limit for the minimum and maximum temperature electron density profile

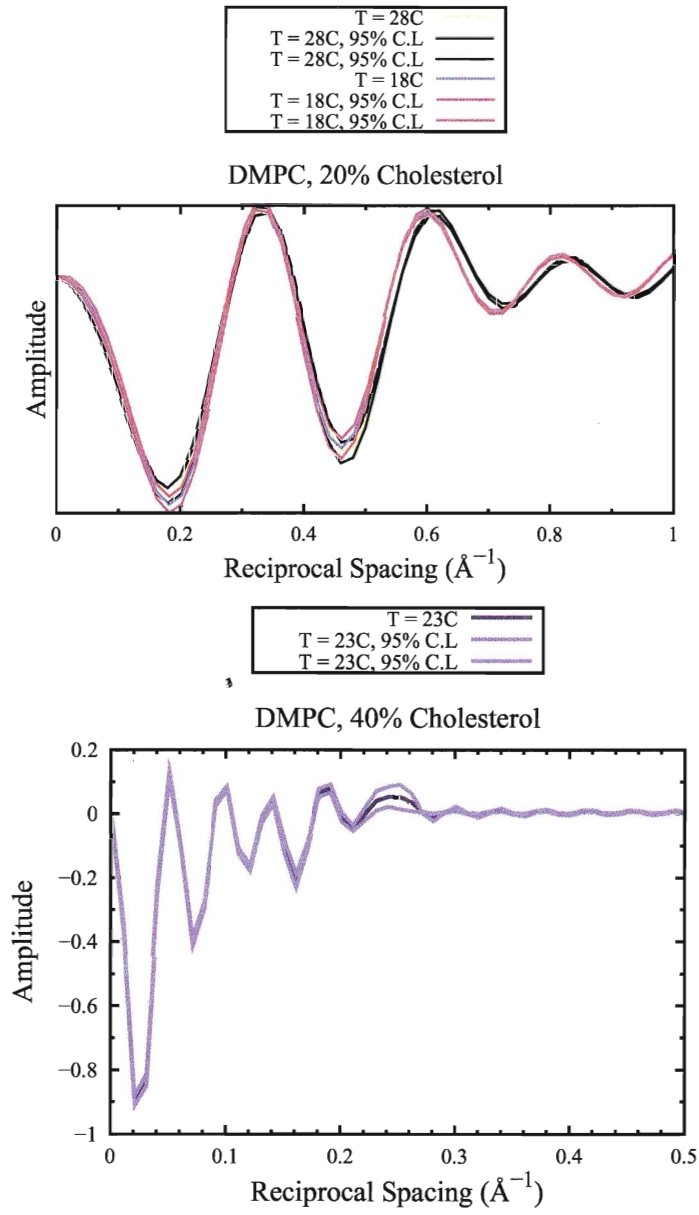

Figure 3.3: **Fourier transform of DMPC with 20% cholesterol.** The top panel shows the 95% confidence limit of Fourier transform at minimum and maximum temperature measured in the experiment. The bottom panel describes the Fourier transform of hydration graph at 23 °C. The data was taken from Frank and Lieb paper [9].

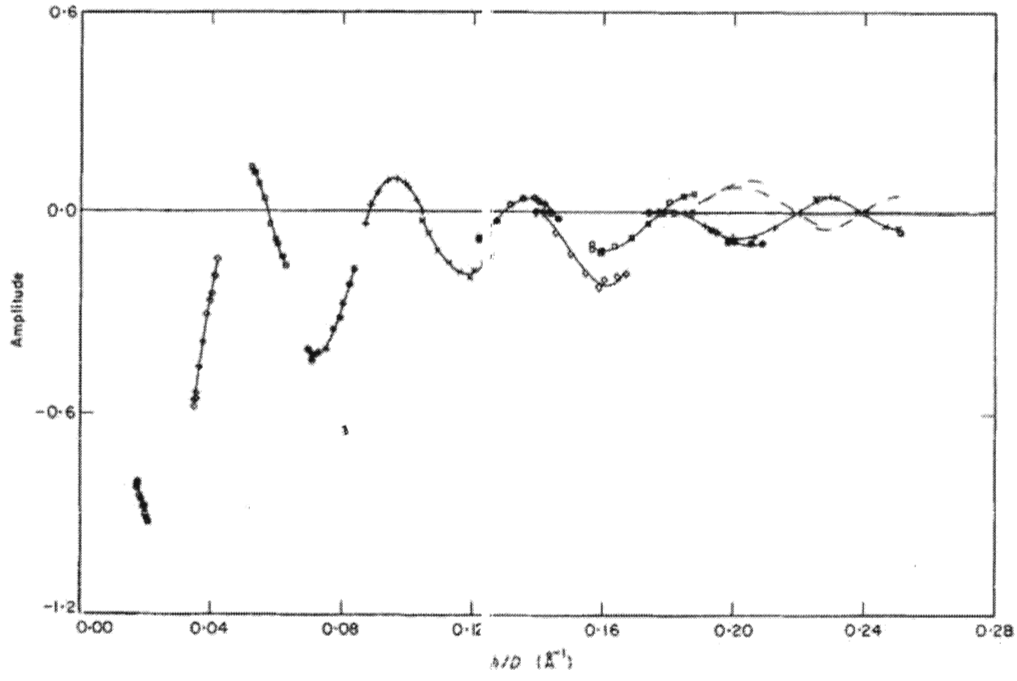

Figure 3.4: **Structure factor of lecithin with 40% cholesterol.** The structure factor of dimyristoyl lecithin in 40% cholesterol solution from Frank and Lieb paper [9] as a function of reciprocal lattice spacing. This graph indicates a continues change in the sample structure.

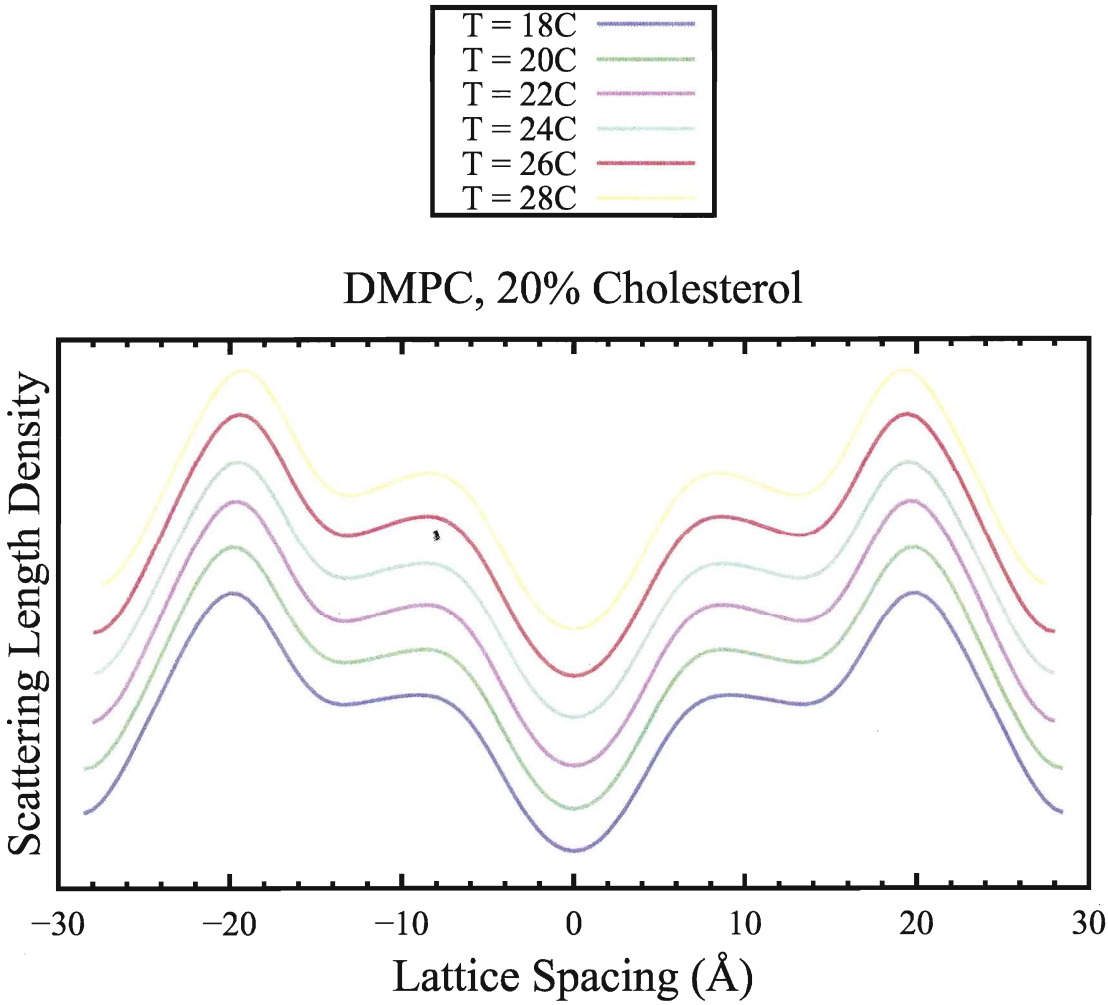

Figure 3.5: **Electron density profile of DMPC with 20% cholesterol.** The electron density is a function of temperature and has equal offset in vertical direction.

were plotted in figure 3.6. The confidence limit profiles prove that the change in electron density for 18 °C and 28 °C is minor. The effect of temperature change is more significant with respect to 95% confidence limit in the electron density profile compared to the Fourier transform graph, meanwhile, both results confirm each other. This effect shows that there is a some structural change within the temperature range: the bilayer thickness decreases as seen in the decrease in the distance between the phosphate peaks at ~19 Å. The structure at the center of the membrane changes very little.

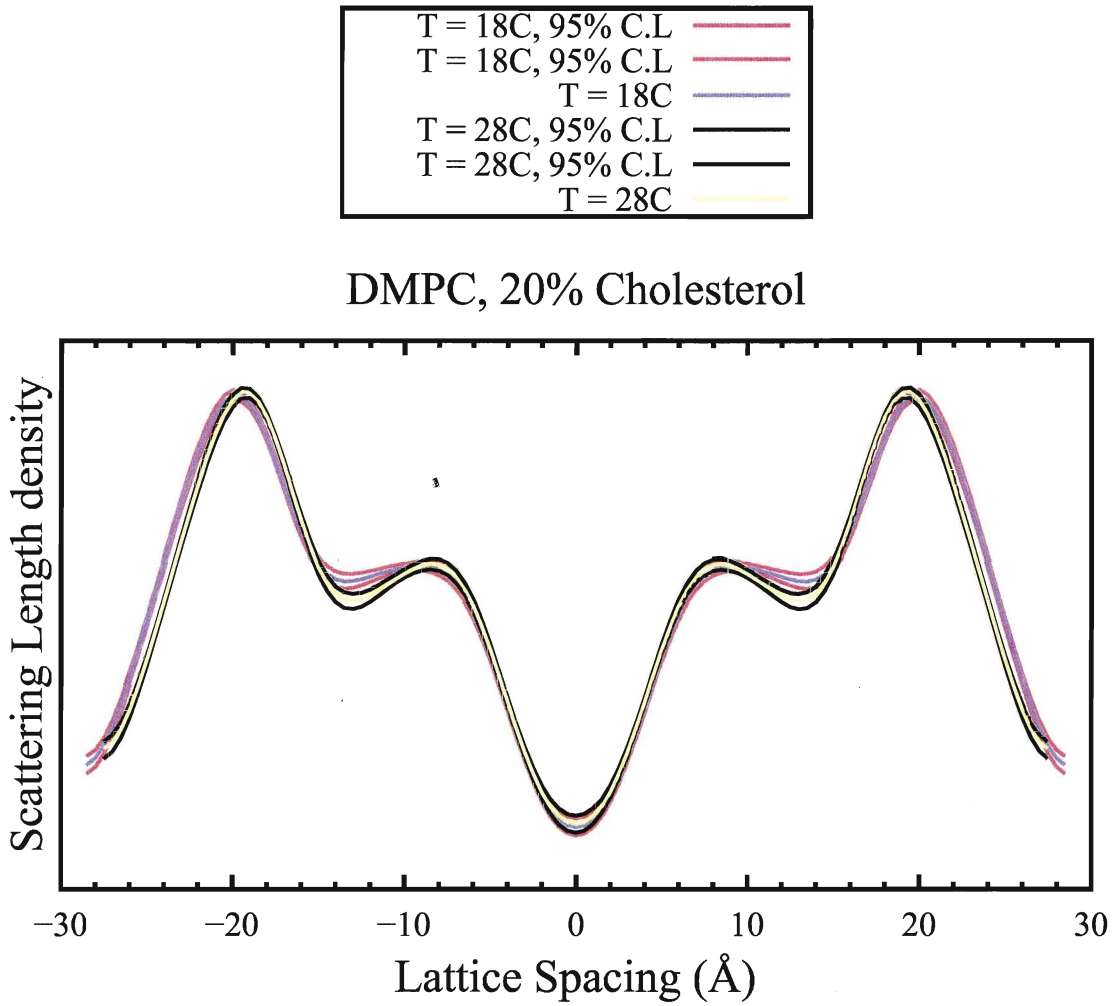

Figure 3.6: **C.L of electron density profile at DMPC with 20% cholesterol.** The electron density profile with 95% confidence limit for the minimum and maximum temperature plots of DMPC 20% cholesterol.

A comparison between the electron density profile of DMPC with 20% cholesterol at temperature 22 °C and 40% cholesterol in lecithin solution at temperature 23 °C are shown in the figure 3.7. The 40% cholesterol in lecithin graph were plotted using the data from Frank and Lieb's paper [9] with

95% confidence limit. In the lecithin hydration plot, the lamellar spacing is at $D = 51.79$ Å and there are 13 h values, while DMPC graph has 9 order values at lamellar spacing of $D = 57.43$ Å. The plot and its 95% confidence limit of electron density profile of lecithin with 40% cholesterol are multiplied by a factor 100, to put onthe same scale as our data.

The dominant component of one sample is DMPC and the other is lecithin. This variant cause a structural difference in the two sample, however because the molecular formula of both components are similar to each other, the profiles can be comparable. A comparison between these two profiles show that the electron density plots of DMPC 20% cholesterol solution sample are smoother than lecithin 40% cholesterol solution. There are few reasons explaining the smoothness of the plot: The graph shows that by increasing the concentration of cholesterol, there would be more details in the electron density profile [14]. Which is because at higher concentration of cholesterol, the structure of cholesterol molecule also appears in the electron density profile. Another reason is that the higher order number in x-ray diffraction pattern would cause a better resolution in electron density profile. In the 20% cholesterol sample the order number is 9, while the 40% cholesterol solution has order value of up to 13.

To keep the analysis as simple as possible regarding the change in bilayer thickness, Figure 3.8 is graphed as a function of temperature. Where d is half of the distance across the bilayer, d_{pp} is the distance from bilayer center to the phosphate groups, which is half of the distance between the highest peaks in the bilayer and d_w is half of the water layer thickness $d_w = d - d_{pp}$. d and d_{pp} indicate the measure of lamellar spacing and the thickness of the bilayer [10].

The figure 3.8 agrees with previous results that with increasing the temperature, the order decreases in the bilayer. However the decrease in order does not effect the molecular distance between the lipid linearly. The lamellar spacing and the bilayer thickness decreases with increasing temperature while the water thickness inside the lipids only fluctuates. The graph indicates that at this temperature range, the disorder between the lipid molecules occurs mostly in hydrocarbon region of DMPC and cholesterol rather than hydrophilic region of the molecule.

Table 3.1.2 shows the lamellar spacing for a bilayer DMPC sample with 20% Cholesterol concentration. In the table, the lamellar spacing d' is the distance across the bilayer $d' = 2d$.

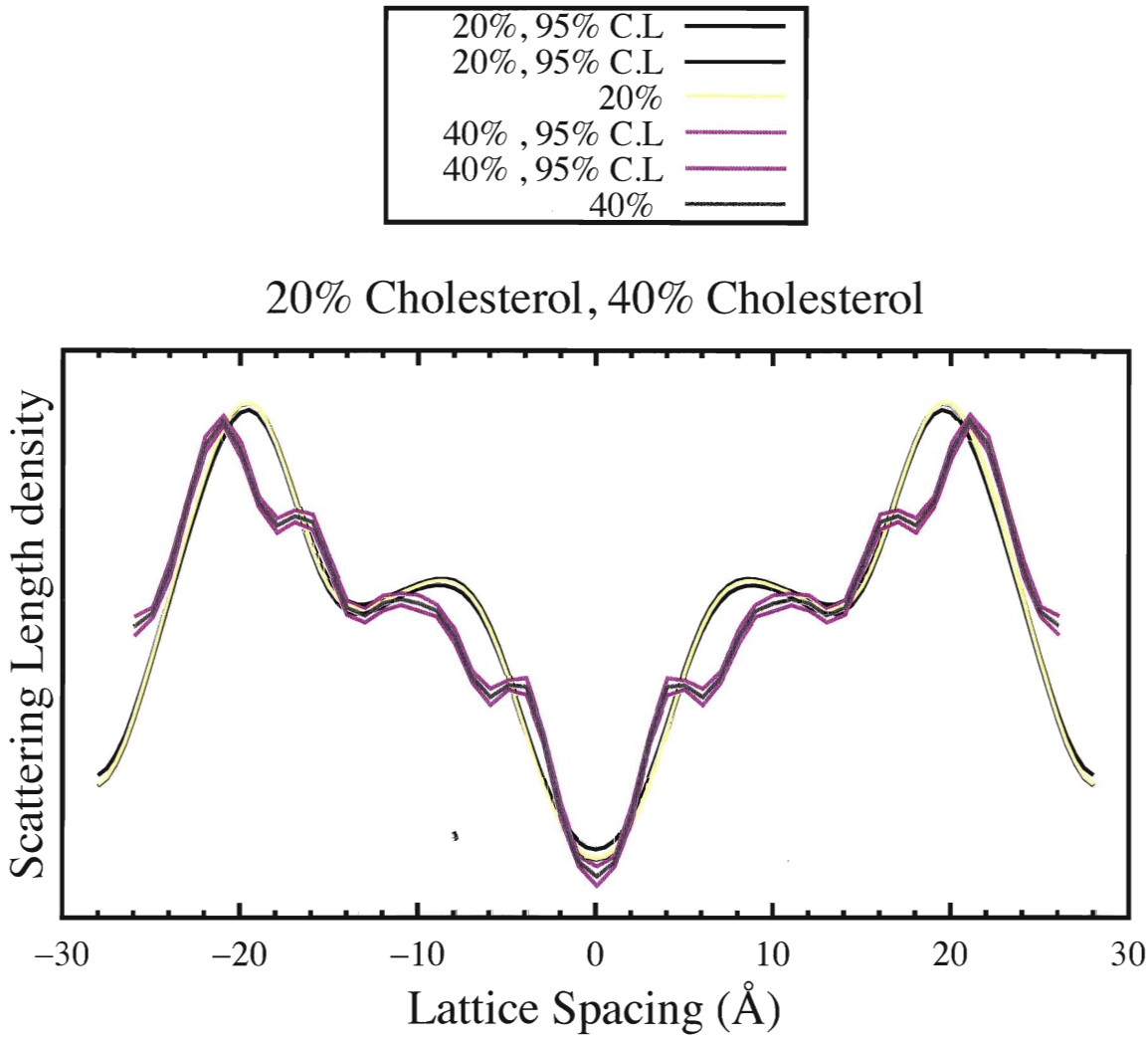

Figure 3.7: **Electron density profile comparison.** Comparison between electron density profile of DMPC 20% cholesterol at 22° C and 40% cholesterol in lecithin solution at 23° C, both with 95% confidence limits.

Temp (°C)/ Sample	DMPC, 20% Cholesterol (Å)
18	57.75
20	57.38
22	56.91
24	56.71
26	56.40
28	55.85

Table 3.1: **Lamellar spacing of bilayer DMPC.** The lamellar spacing of DMPC sample with 20% Cholesterol concentration using saturated salt solution of KNO_3. The units of lamellar spacing are Angstrom.

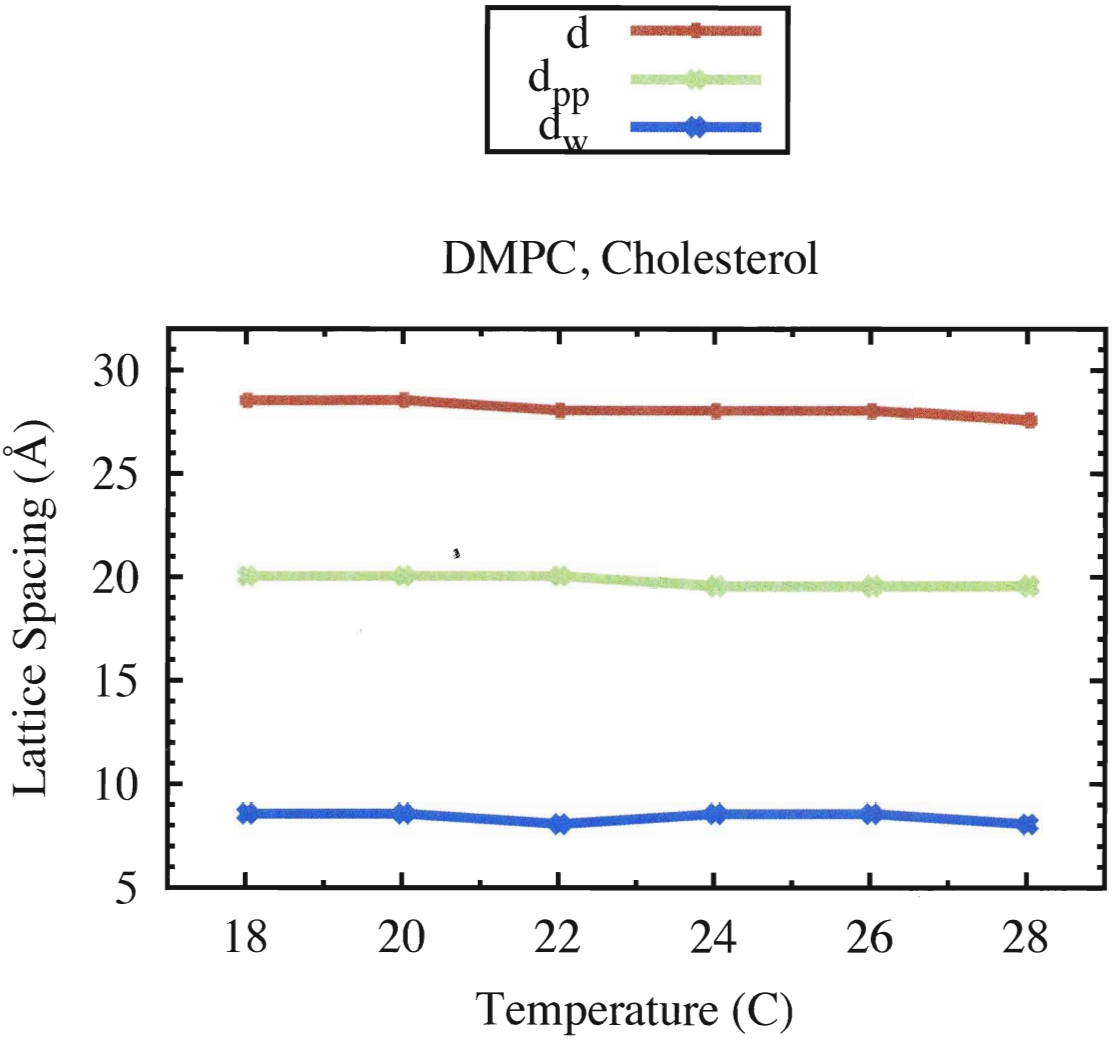

Figure 3.8: **Lattice spacing of DMPC with 20% cholesterol.** The change in lamellar spacing d, bilayer thickness d_{pp} and water thickness d_w as function of temperature.

Temp/ Sample	POPC, K_2SO_4	POPC, KNO_3	POPC, KCl
15°C		95.41 ± 0.96	
20°C	97.59 ± 0.53	94.62 ± 0.66	85.11 ± 0.29
25°C	97.30 ± 0.45	93.58 ± 0.55	84.34 ± 0.26
30°C	97.00 ± 0.4	92.31 ± 0.60	83.62± 0.25
40°C		89.03 ± 1.2	

Table 3.2: **Relative humidity of saturated salt** Relative humidity of the saturated salt solutions with respect to the temperature range used in the experiments [12].

3.2 POPC

In this section the effect of temperature and hydration on POPC samples are determined. POPC is 1-palmitoyl-2-oleoyl-sn-glycero-3-phosphocholine bilayers. The effect of the temperature can be measured by keeping the hydration constant. However change in the temperature has direct effect on hydration level. Minimizing this effect, specific salts were chosen to provide the least humidity change within the experimental temperature range. The saturated salt solutions of Potassium Sulfate, Potassium Nitrate and Potassium Chloride were used to control the hydration in the range of 83.6% to 97.6% relative humidity. Table 3.2 shows the relative humidity of these saturated salts at temperatures used in the experimental sets. In the hydration experiments, the temperature range used are within the range of 22 °C to 32 °C. The change in the relative humidity of the three saturated salt solution within the range are about 2% and is negligible.

3.2.1 Structure factors

POPC with K_2SO_4

Structure factors for five orders of POPC with saturated salt solution of K_2SO_4 is shown in figure 3.9. In the figure, blue and yellow lines represent the Fourier transform at the minimum and maximum temperature of 22° C and 32° C respectively. The structure factors are indicated with separate sets of colored dots and the black lines show the third order polynomial fit of each set of structure factor. The graph shows that four out of five structure factors are lined between Fourier transform of the minimum and maximum temperature and the change in the structure factors are smooth.

The significant change of the Fourier transform profile for the POPC sample with K_2SO_4 satu-

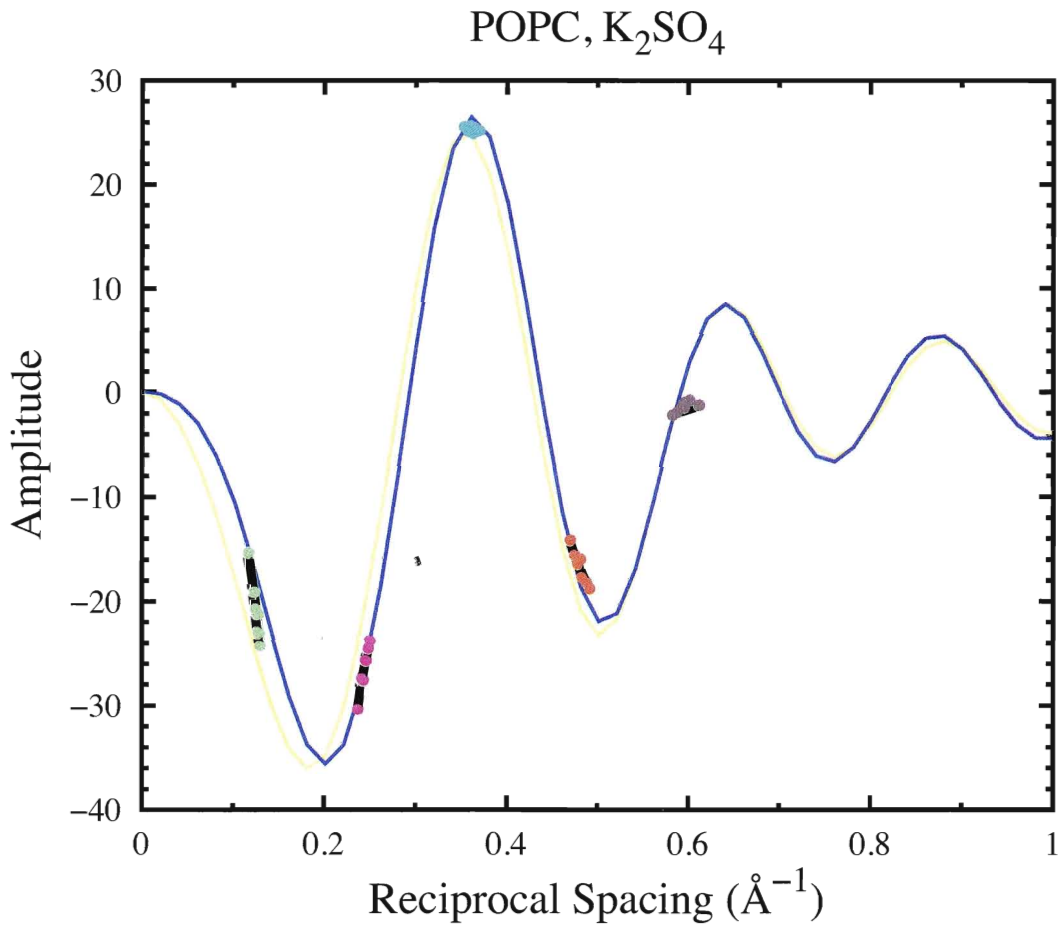

Figure 3.9: **Structure factors of POPC with K_2SO_4.** Each sets of colorful dots show the structure factor for a specific order value. The black lines are the polynomial fit for the structure factors. The blue and yellow line are the plots of Fourier transform at minimum and maximum temperature range.

rated salt is shown in figure 3.10. The graph shows the minimum and maximum temperature with blue and yellow lines and their 95% confidence limit with red and black lines respectively. The 95% confidence limit of the two temperature are separated from each other mostly in the first order, which means the change in the molecular structure of POPC sample within the temperature range are significant.

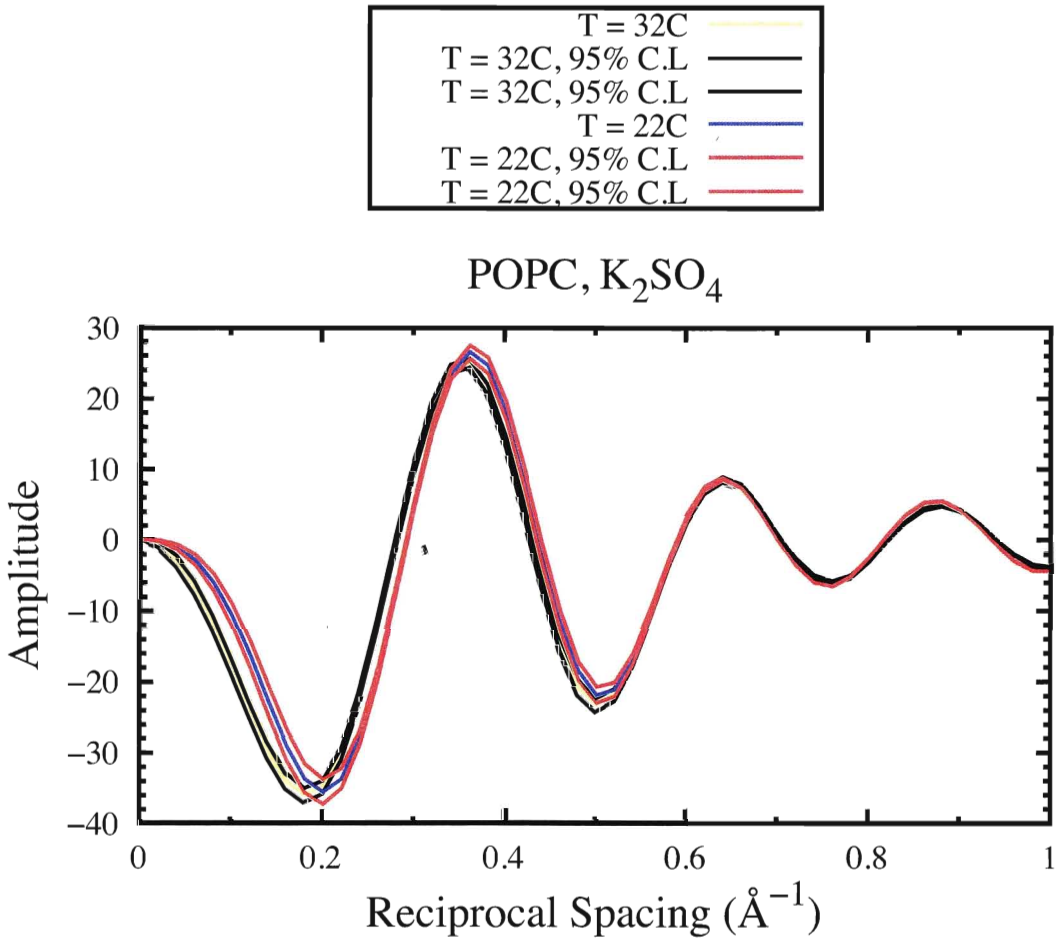

Figure 3.10: **Fourier transform of POPC with K_2SO_4.** Fourier transform graph of 22° C and 32° C of POPC sample with K_2SO_4 saturated salt at 95% confidence limit

Fourier transform in three dimensions for POPC is shown in the appendix in Fig. A.9 as a function of temperature in the range of 22° C to 32° C, reciprocal lattice and amplitude. The change in the Fourier transform profile is smooth, however a structural change around temperature of 28° C can be verified.

POPC with KCl

The x-ray diffraction profile of POPC sample with saturated salt solution of KCl has 6 order values. The structure factor of these 6 orders, their polynomial fit and the Fourier transform of minimum and maximum temperature of 22° C and 32° C can be seen in figure 3.11.

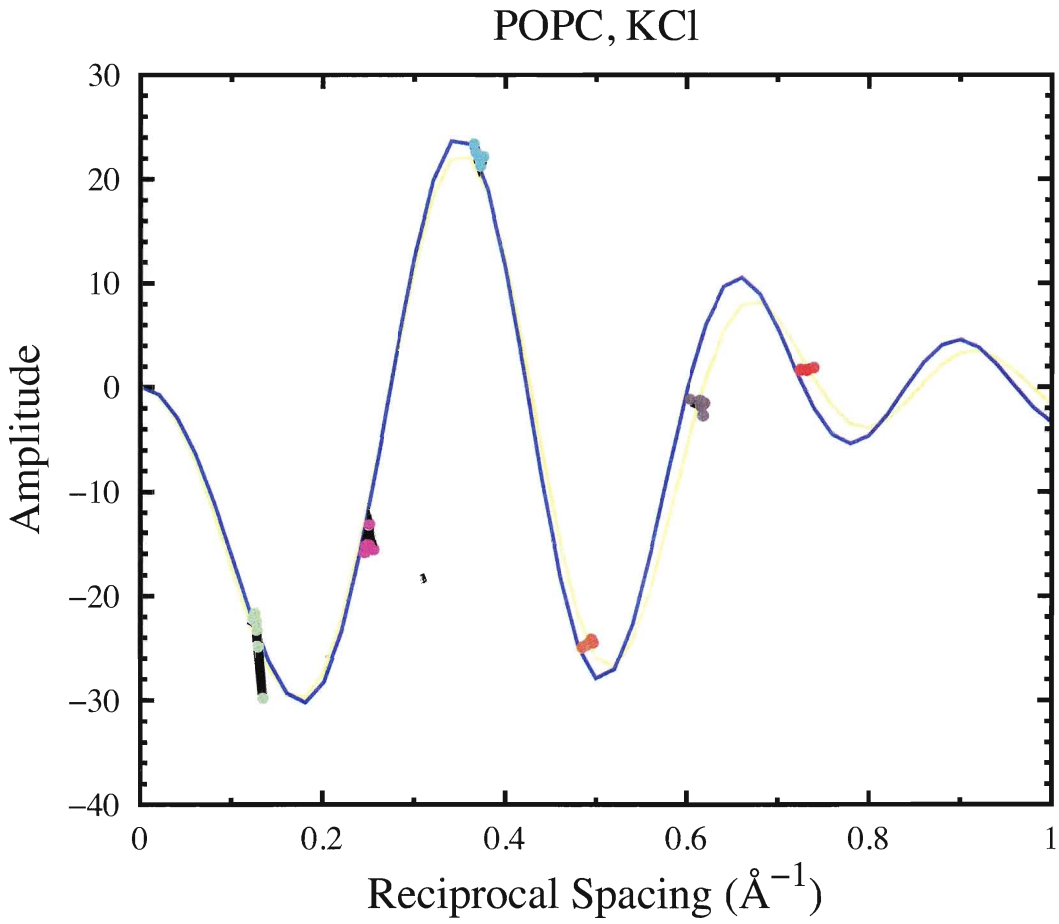

Figure 3.11: **Structure factors of POPC with KCl.** The structure factors of six order value of POPC with KCl saturated salt are shown in different colors, while the best fit for each order value is shown with black line. The Fourier transform line of minimum and maximum temperature at 22° C and 32° C are shown with blue and yellow line respectively.

Fourier transforms for the minimum and maximum temperature with their 95% confidence limit is plotted in the figure 3.12. Yellow and blue lines are the maximum and minimum temperatures and black and red lines are the 95% confidence limit respectively. A comparison between this graph and the structure factor graph shows that for the first and second order values, the change

in the temperature is not significant, however, by increasing the lamellar peaks the change in the temperature become more significant.

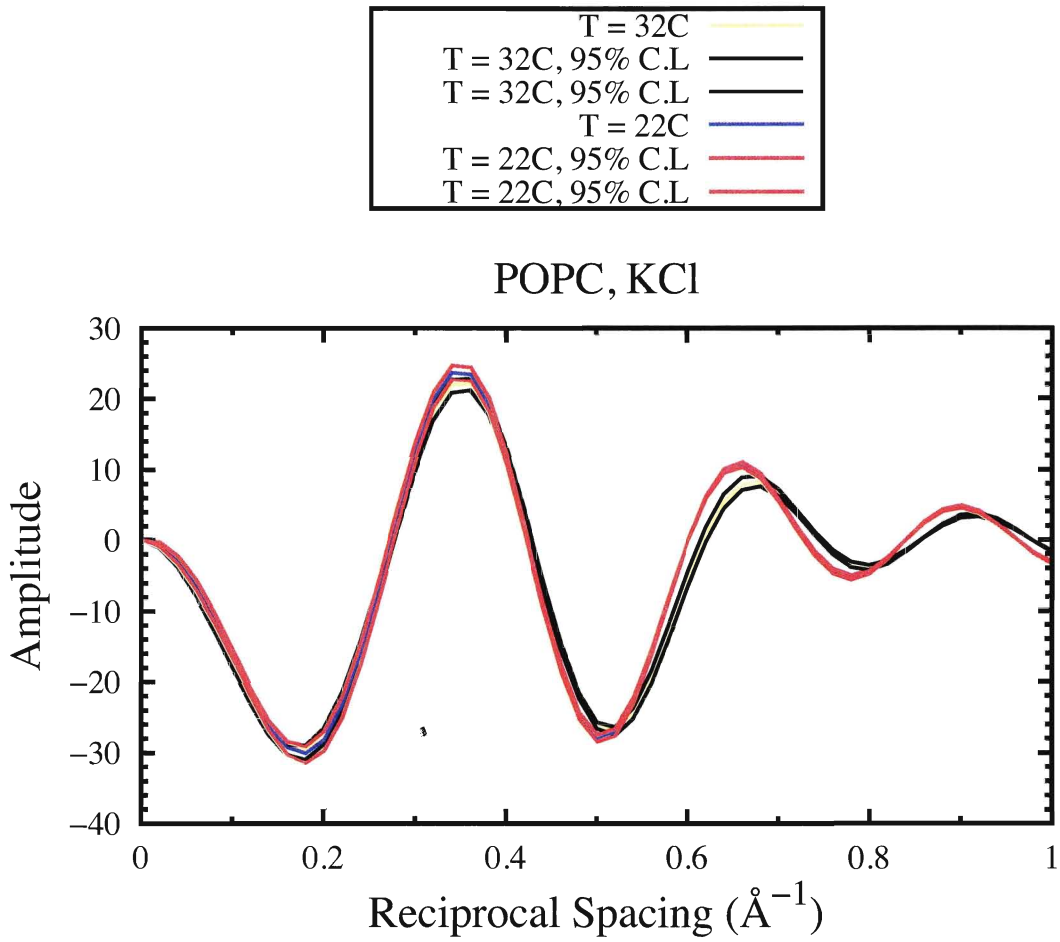

Figure 3.12: **Fourier transform of POPC with KCl.** Fourier transform plots at minimum and maximum temperature of 22° C and 32° C with 95% confidence limit for POPC sample with KCL salt solution.

The three dimensional plots of Fourier transform for POPC sample with KCl saturated salt at the temperature range of 22° C to 32° C is graphed in the figure A.10 in appendix. The plot is very smooth which shows that all the changes happen during the temperature range are steady and continuous.

POPC with KNO_3

The POPC sample with KNO_3 salt solution were measured at temperature range of 16° C to 40° C so that it can also be used for further experiments. Eight order values for salt solution of KNO_3 can be seen in the figure 3.13. The figure shows that most of the structure factor values are lie on the plot of Fourier transform at 40° C.

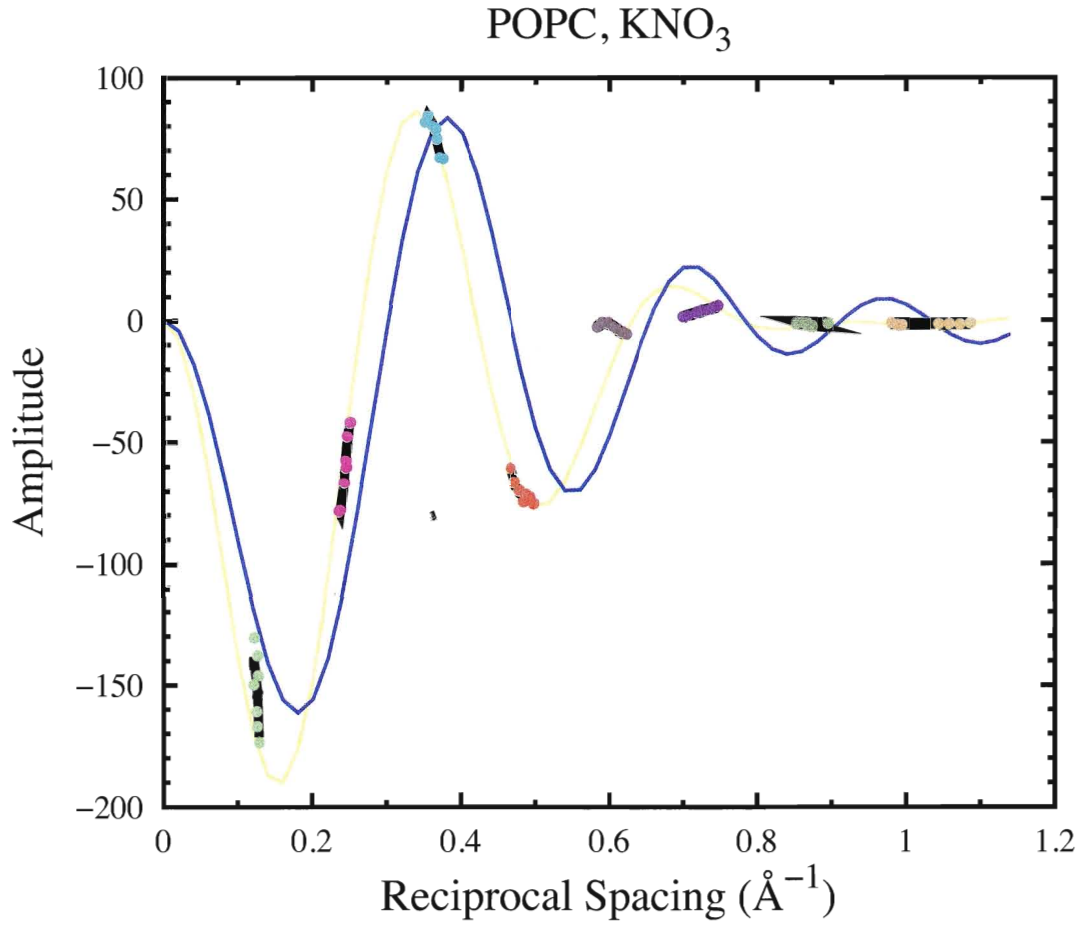

Figure 3.13: **Structure factors of POPC with KNO_3.** Fourier Transform at 16° C and 40° C is seen with blue and yellow line respectively. There are eight order values for structure factors of this salt, starting with h=1 for lime color and end with tan color for h=8. Line of best fit for each structure factor value is graphed with black.

Fourier transform functions of POPC sample with salt solution of KNO_3 at temperature of 16 °C and 40 °C with their 95% confidence limit is graphed in figured 3.14. The graph shows that the change in the temperature range is significant, especially in the first three orders.

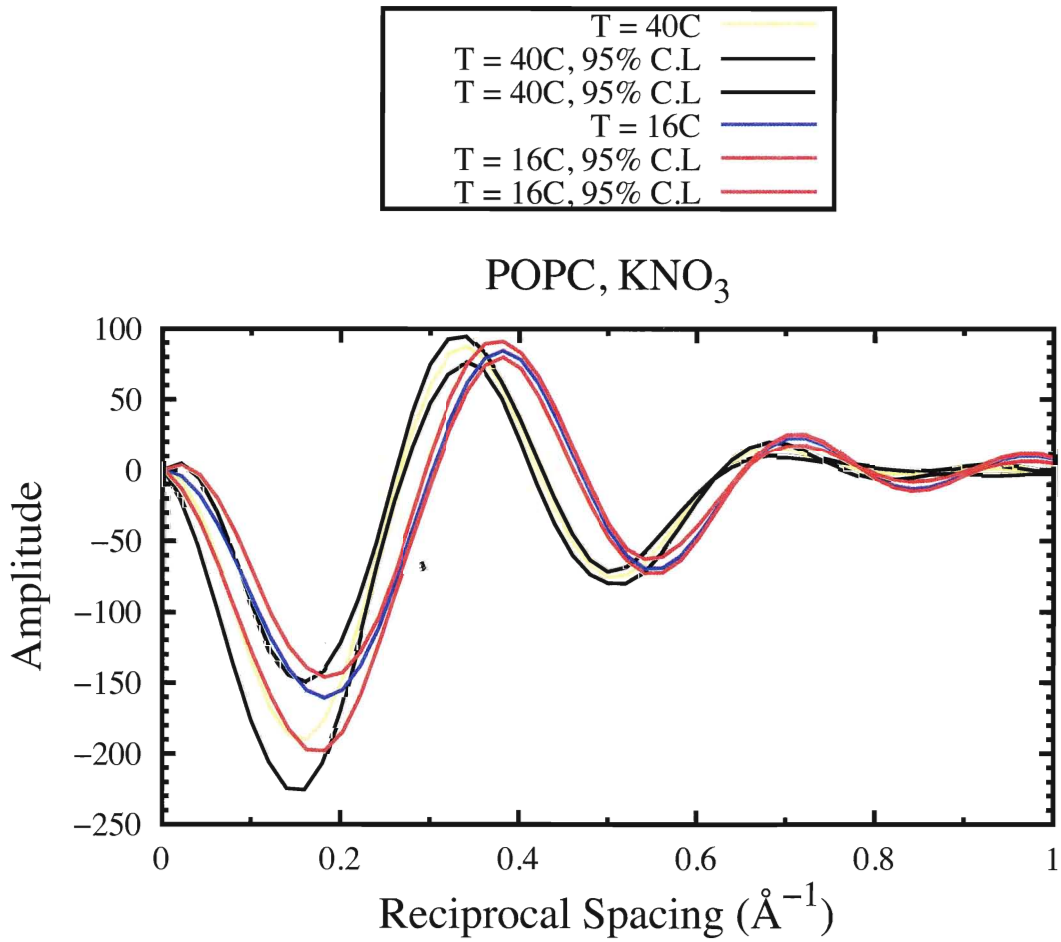

Figure 3.14: **Fourier transform of POPC with KNO_3.** Fourier transform and 95% confidence limit at the minimum and maximum temperature of POPC sample with KNO_3 salt solution show the significant change within the temperature range.

The three dimensional profile A.11 of POPC with KNO_3 salt shows that beside a sudden change in structure factor at temperature 24°C the Fourier transform changes are smooth and continuous.

3.2.2 Electron density profiles

POPC with K_2SO_4

Scattering length density profile of POPC sample with K_2SO_4 saturated solution is shown in the figure 3.15. The panel is at temperature range of 22 °C to 32 °C, with lamellar spacing of 53.748 Å to 52.099 Å. The panel has an equal offset in the y direction for temperatures higher than 22 °C to achieve a better visibility. The graph represents the humidity level of 97%. The panel shows that by increasing the temperature the lamellar spacing is decreasing.

To find out if there is any change in electron density profile within the temperature range, the 95% confidence limit for the minimum and maximum temperature were plotted in figure 3.16. The figure shows that the 95% confidence limit of the two temperature are completely different from each other, which means there is a significant change within the temperature range. The electron density profile is broader in the center of the bilayer at higher temperature.

Figure 3.17 shows the effect of temperature on the lattice spacing. As it showed in the figure 3.16 and 3.15 at higher temperature, the lamellar spacing between the bilayer decreases. In the POPC sample with K_2SO_4 saturated salt by increasing the temperature in the range of 22 °C to 32 °C the spacing between the phosphates d_{pp} did not change, while the spacing between water molecules decreased. This means the sample had a structural change within the interbilayer water area. The decrease in lamellar spacing is caused by decreases in the molecule disorder with increasing the temperature at a constant humidity level of 97%. This also explains the large change in the first order values seen in figure 3.13.

POPC with KCl

Electron density figure of the POPC sample with saturated salt solution of KCl is graphed in figure 3.18. The panel shows the electron densities profile for temperature of 22° C to 32°C with arbitraty values in y directions. The panel shows that the POPC sample at the lowest temperature

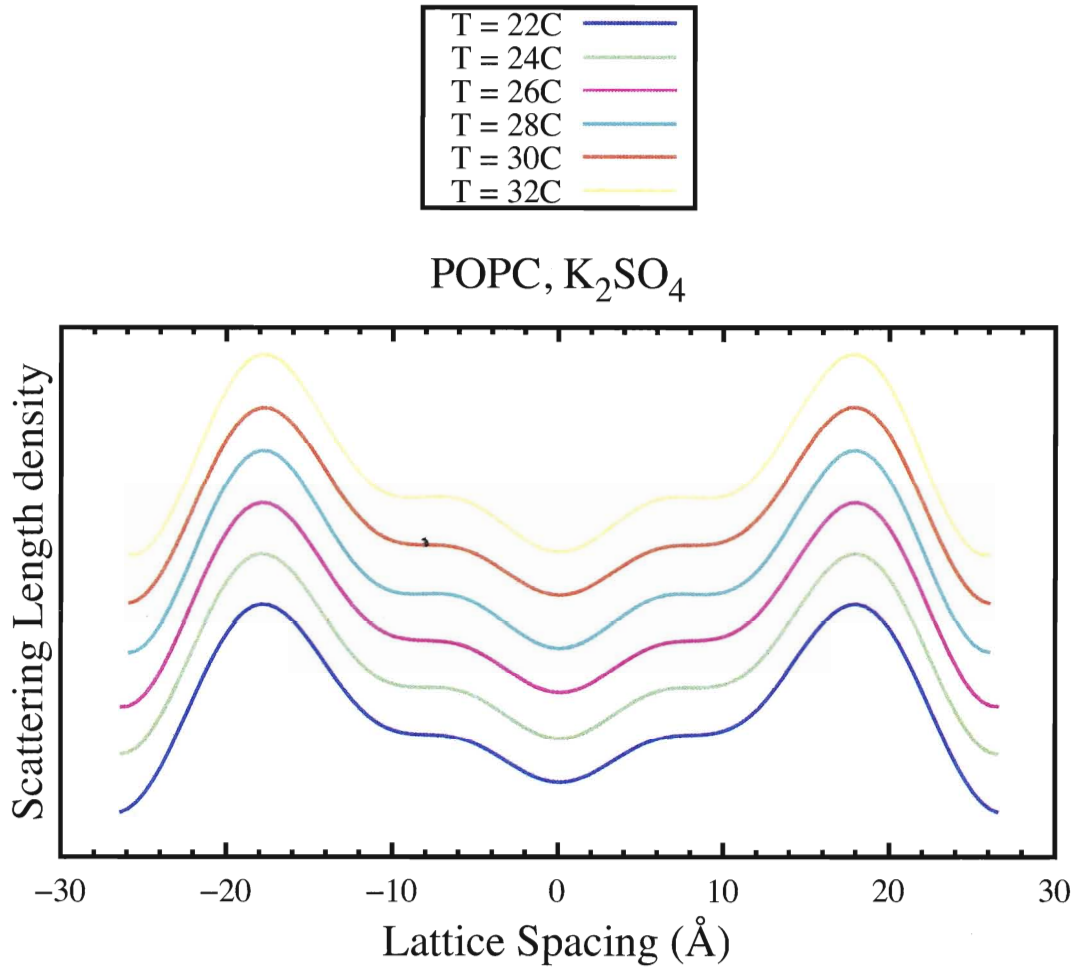

Figure 3.15: **Electron density profile of POPC with K_2SO_4** The electron density profile is at temperature range of 22° C to 32° C.

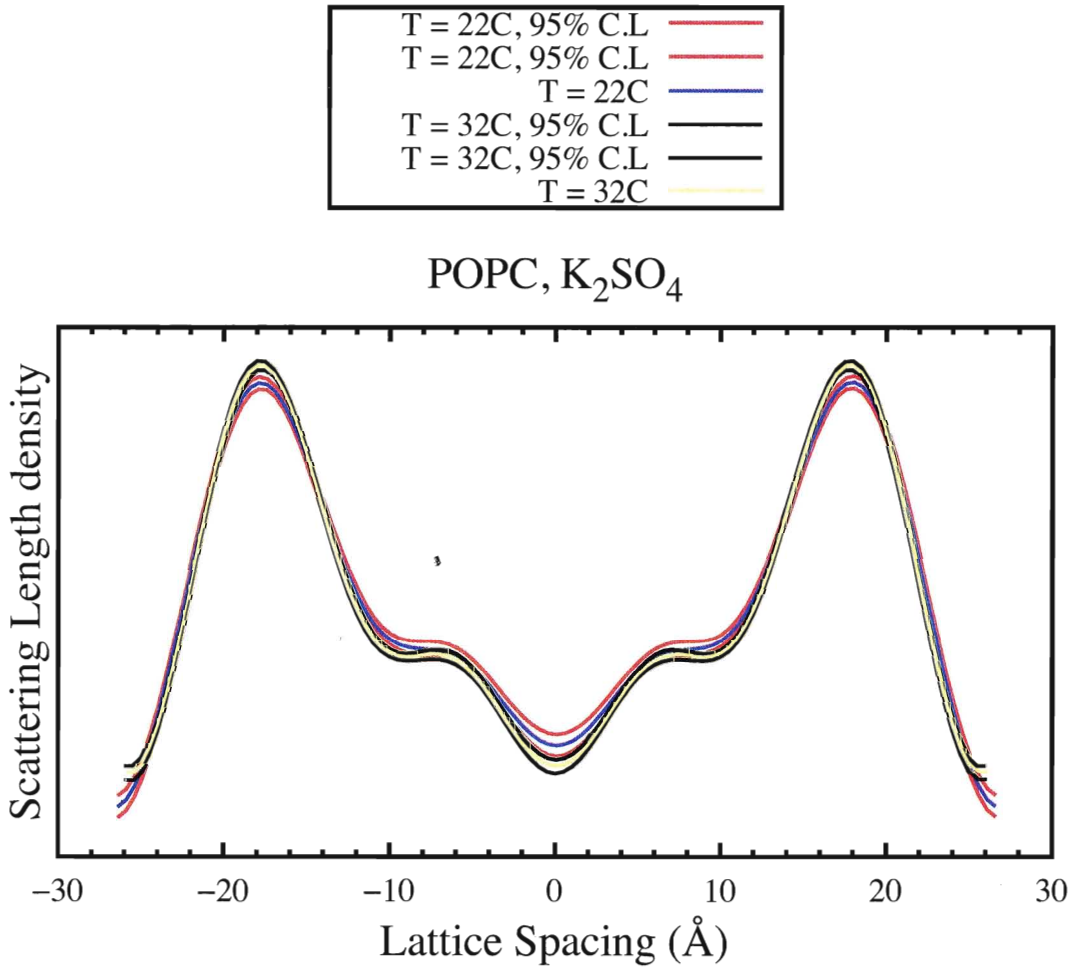

Figure 3.16: **C.L of electron density profile of POPC with K_2SO_4.** Electron density profile at temperature of 22 °C C and 32 °C for POPC sample with K_2SO_4 saturated salt at with 95% confidence limit.

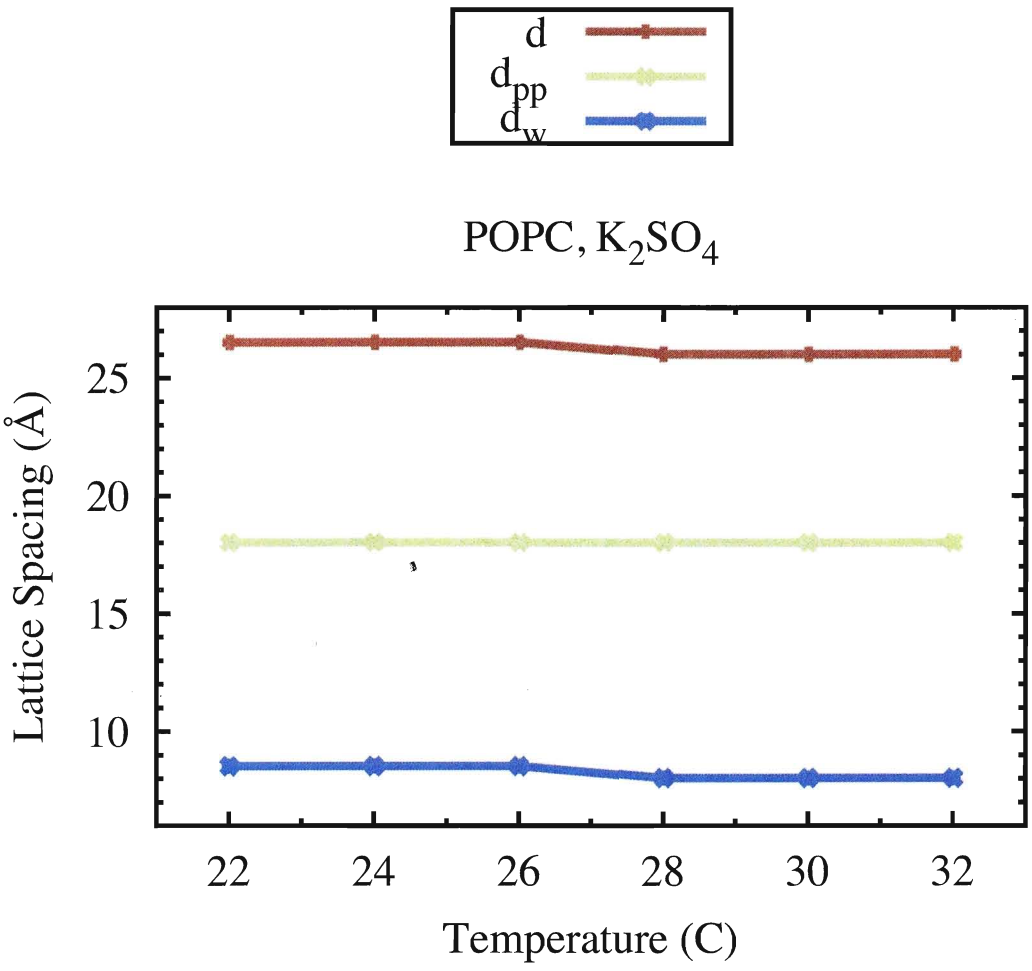

Figure 3.17: **Lattice spacing of POPC with K_2SO_4.** Change in lamellar spacing with increasing the temperature. d is bilayer spacing from center, d_{pp} is the lamellar spacing from center of bilayer to the phosphate group and d_w is the half of the water thickness.

of 22° C has the longest lamellar spacing.

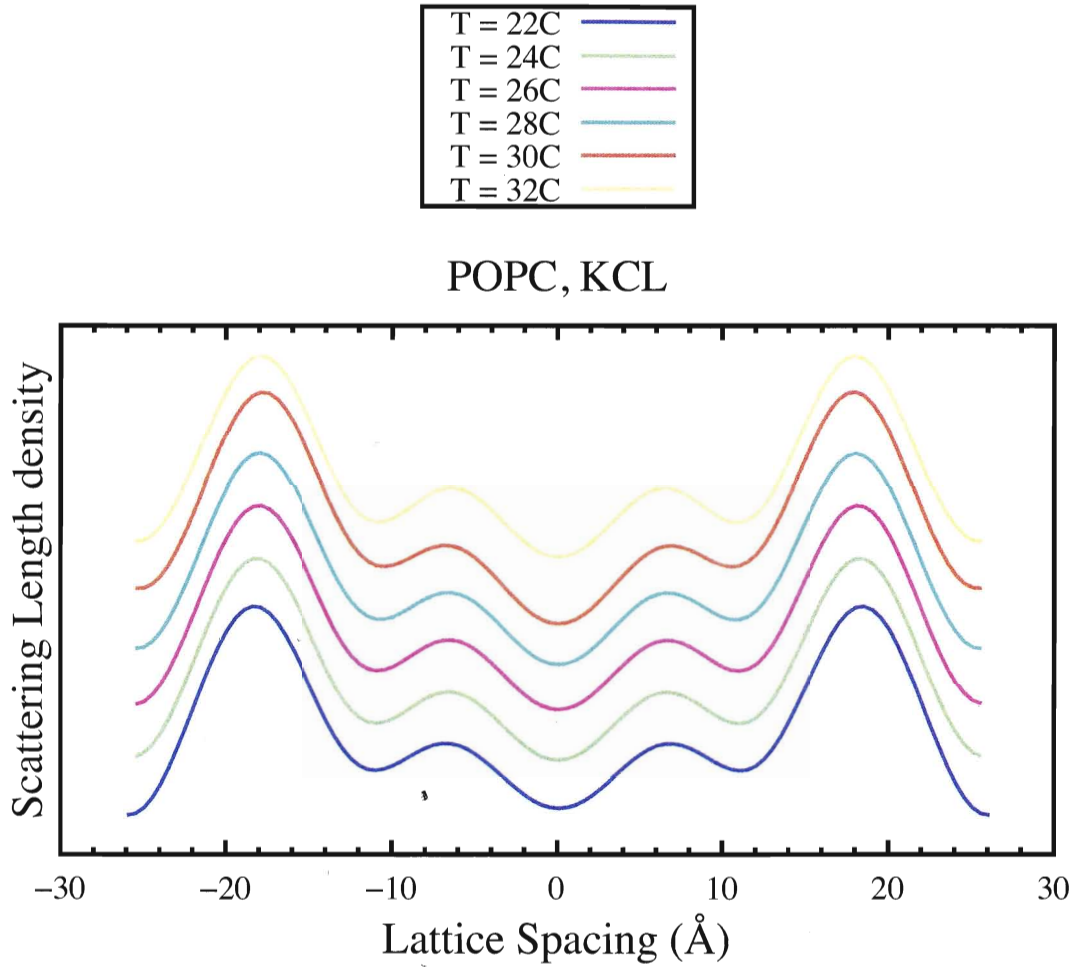

Figure 3.18: **Electron density profile of POPC with KCl.** Electron density panel of POPC sample with KCl saturated salt solution within the temperature range of 22° C and 32°. Beside the plot for the lowest temperature of 22° C, the profile has equal offsets in Y direction for all other temperatures.

Figure 3.19 shows the electron density and 95% confidence limits for the minimum and maximum temperatures of the POPC sample with KCl solution. The graph shows that the confidence limits of the two temperatures are separated from each other, although the significance of the change is not always very clear.

Changes in the lamellar spacing of the POPC samples at temperature range of 22 °C and 32 °C is graphed in figure 3.20. The temperature range with saturated salt solution of KCl correspond to humidity levels of 85 to 83 %. The graph shows that the change happens only in the temperature of 24 °C, which include the change in lamellar spacing of the bilayer and the bilayer thickness or

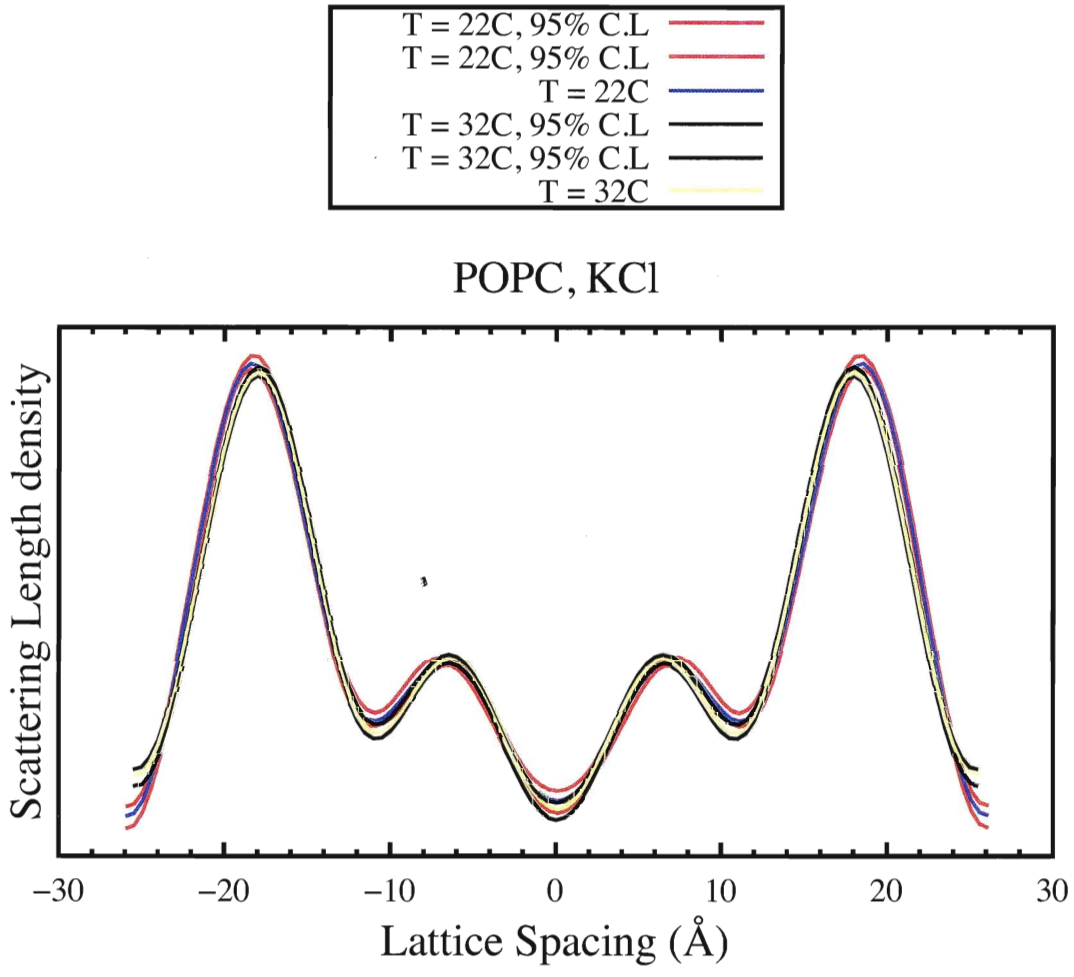

Figure 3.19: **C.L of electron density profile at POPC with KCl.** The change in the electron density profile with respect to the lamellar spacing of the POPC sample with KCl salt solution at temperature 22 °C and 32 °C. The change in the profile is represented with 95% confidence limit lines for the two temperatures.

the distance between the center of the bilayer to phosphate groups.

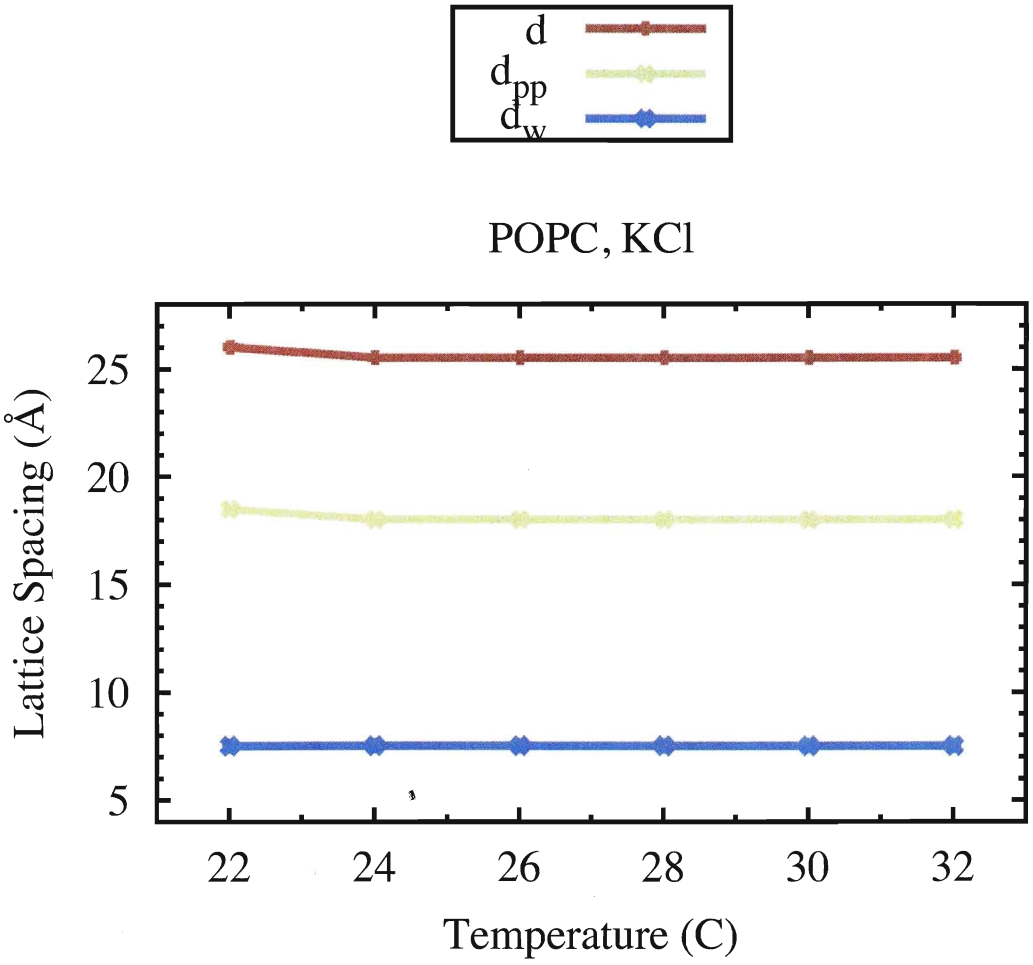

Figure 3.20: **Lattice spacing of POPC with KCl.** The graph shows the relation between lamellar spacing and increasing the temperature of POPC sample with KCl salt solution. Where d is half of the lamellar spacing, d_{pp} is the bilayer thickness and d_w is the half of the water thickness.

POPC with KNO_3

A graph of the scattering length density of the POPC sample with saturated salt of KNO_3 is plotted in figure 3.21. The temperature range for the plot is between 16 °C to 40 °C, corresponding to humidity level of 95.41 ± 0.96 to 89.03 ± 1.2. The graph shows that with increasing temperature, the lattice spacing is decreasing from 54 Å to 51 Å.

In panel 3.22 the graph of electron density of POPC sample with KNO_3 salt solution at 95% confidence limit is plotted. The top panel shows the confidence limit between the temperature of

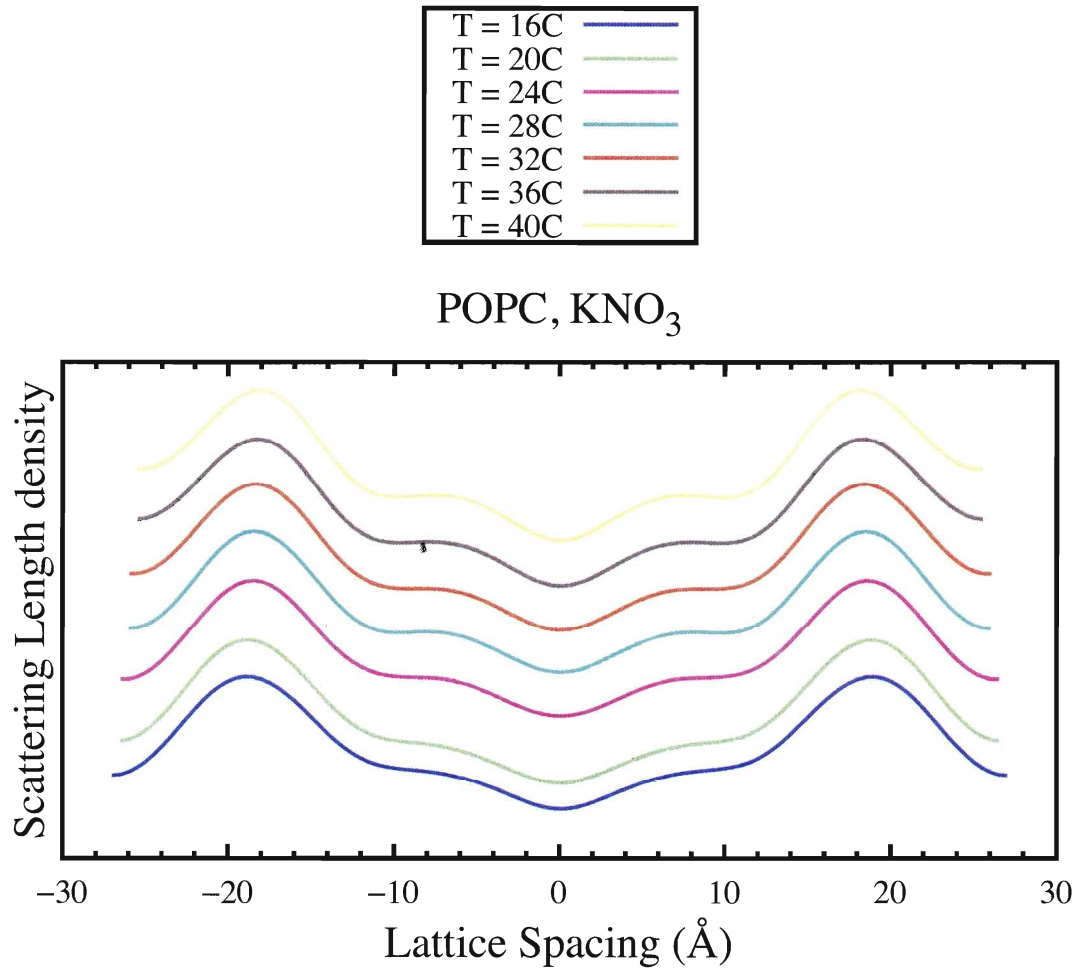

Figure 3.21: **Electron density profile of POPC with KNO_3.** Electron density profile is within the temperature range of 16° C to 40° C, with equal offsets in y direction.

20 °C and 32 °C corresponding to humidity level of 94.62 ± 0.66 to 92.31 ± 0.60 %, thus it can be compared with POPC sample of other saturated salt profile. In the bottom panel, the comparison is between the temperature at 16 °C and 40 °C. This panel includes a higher temperature range so the changes are more distinguishable. The panel confirms that with increasing the temperature the lattice spacing is decreasing. The plot also has more details at higher temperatures which is a reason for decrease in disorder of bilayer.

Figure 3.23 shows the relation between lattice spacing and temperature of POPC sample with KNO_3 salt solution. Although the temperature range is between 16 °C and 40 °C, it is easy to see that even within temperature range of 20 °C and 32 °C, with increasing the temperature the lattice spacing from center of bilayer to the edge of bilayer and also from center to the phosphate group in the bilayer is decreasing. As a result the lamellar spacing and bilayer thickness is decreasing with increase the temperature however, the water thickness is only fluctuating within the temperature range.

Figure 3.24 shows the electron density profile of POPC sample at three different hydration levels at constant temperature. POPC sample with saturated salt solution of K_2SO_4, KNO_3 and KCl at temperature of 32° C have relative humidity level of about 97%, 91% and 83% respectively. The K_2SO_4 and KCl profile were multiplied by a factor of 4.5 for a better clarity in comparison. The plot shows that the electron density profile of POPC sample at the lowest hydration level has the most details and has the smallest lamellar spacing. The peak in the hydrocarbon region is due to the fixed configuration of the double-bond on the oleoyl chain, which has been seen before in two-chain oleoyl PC lipids [41, 42]. At higher hydrations, increased disorder in the hydrocarbon chains smooths this part of the electron density profiles. Also note that the headgroup and inter-bilayer water is thicker at the less hydrated condition. There is much less difference in the strucutre of POPC between from hydratoin of 91% relative humidty and higher.

Table 3.2.2 shows the lamellar spacing of POPC sample with saturated salt solutions that were measured. Where lamellar spacing is the distance between the edge of the bilayer and is equal to $2d$.

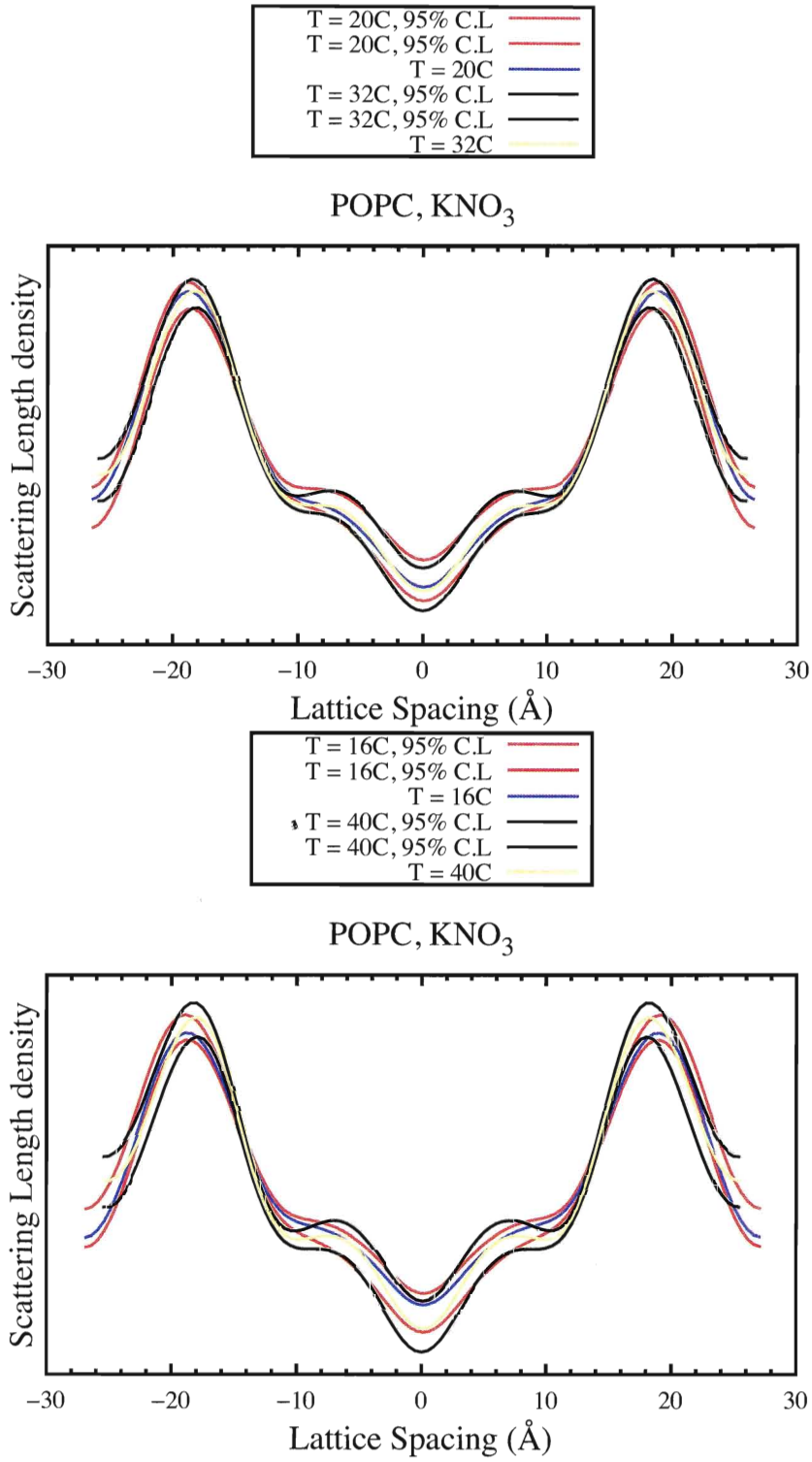

Figure 3.22: **C.L of electron density profile at POPC with KNO_3.** The top panel shows the electron density profile and the 95% confidence limit for temperature of 20°C and 32°C, while the bottom panel is the electron density profile comparison at the temperature of 16°C and 40°C.

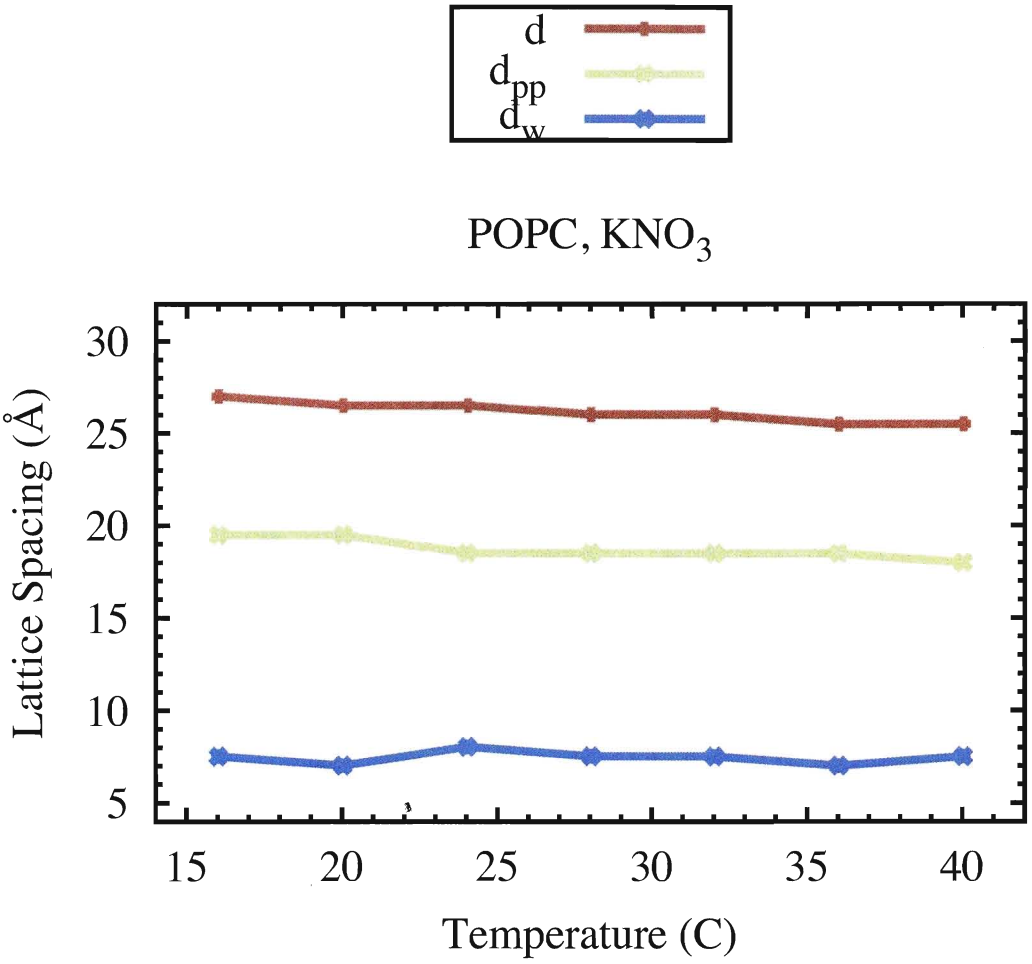

Figure 3.23: **Lattice spacing of POPC with KNO_3.** The relation between lamellar spacing and increasing the temperature of POPC sample with KNO_3 salt solution. While, d is half of the lamellar spacing, d_{pp} is the bilayer thickness and d_w is the half of the water thickness.

Temp (°C)/ Sample	POPC, K_2SO_4 (Å)	POPC, KNO_3(Å)	POPC, KCl (Å)
22°C	53.75		51.84
24°C	53.20	50.18	51.76
26°C	53.06		51.54
28°C	53.46	49.91	51.12
30°C	52.45		50.67
32°C	52.10	51.46	50.92

Table 3.3: **Lamellar spacing of POPC bilayer.** Lamellar spacing of POPC samples with different salt solution within the temperature range of 22°C to 32°C.

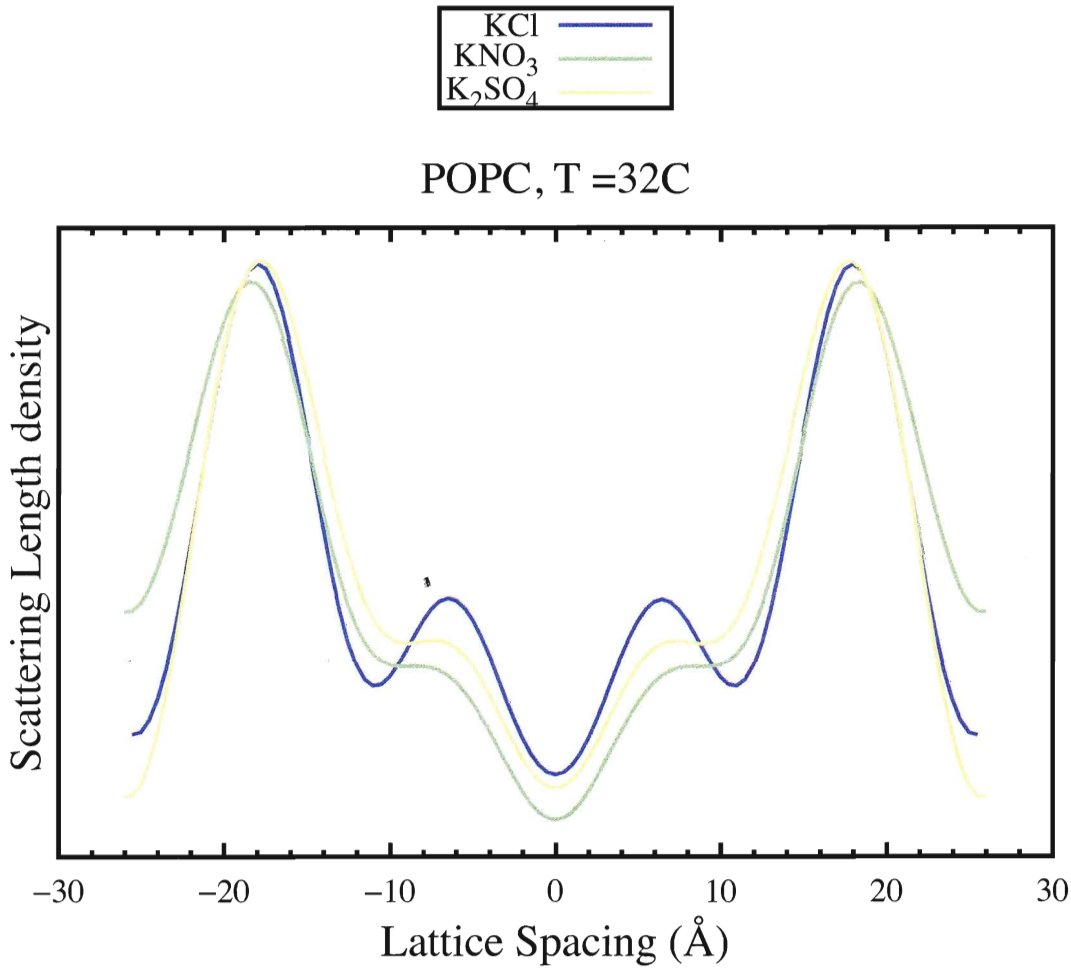

Figure 3.24: **Comparison of electron density profile of POPC at different hydration.** The electron density profile of POPC sample at three different hydration level K_2SO_4: 97%, KNO_3:91% and KCl at 83%. The plots for saturated salt solution of K_2SO_4 and KCl were multiplied by a factor of 4.5

3.3 LPS profile

Lipopolysaccharide samples extracted from *Pseudomonas aeruginosa* were made at three different concentrations of 1%, 10% and 100% w/w with POPC.

In order to obtain the best alignment for samples, rocking curves were measured. In the rocking curve the detector or the 2θ value were fixed at the first Bragg position while the sample, or the omega value, is changing. Figure 3.25 shows the rocking curve for POPC with 1%, 10% LPS and pure LPS solution. The figure shows that in all three samples, a large number of LPS molecules are well aligned into a multilayer form. The broadness of the peaks that are produced by low intensity bands extended on both sides of the main peaks represents the misaligned, or powdered, part of the sample. The 10% LPS solution has the broadest peak and thus the highest mosaic spread in alignment.

Structural factors and electron density profiles of these samples were measured using KNO_3 saturated salt solution within the temperature range of 16° C to 40° C.

3.3.1 Structure Factor profile

1% LPS

Structure factor profiles of the POPC sample with 1% LPS concentration is graphed in figure 3.26. The graph shows that the six structure factors are placed between the profiles of the Fourier transform at the minimum and maximum temperature ranges of the experiment.

The 95% confidence limit of the Fourier transform profile for the minimum and the maximum temperature range are plotted in figure 3.27. The graph shows that only at higher values of order number the changes are significant.

Three dimensional Fourier transform as a function of amplitude, reciprocal lattice spacing and temperature are plotted in appendix. The change in Fourier transform with respect to temperature for 1% LPS concentration are smooth and continuous. A comparison between the plots at low and high temperature shows that with increasing the temperature the plot becomes much smoother.

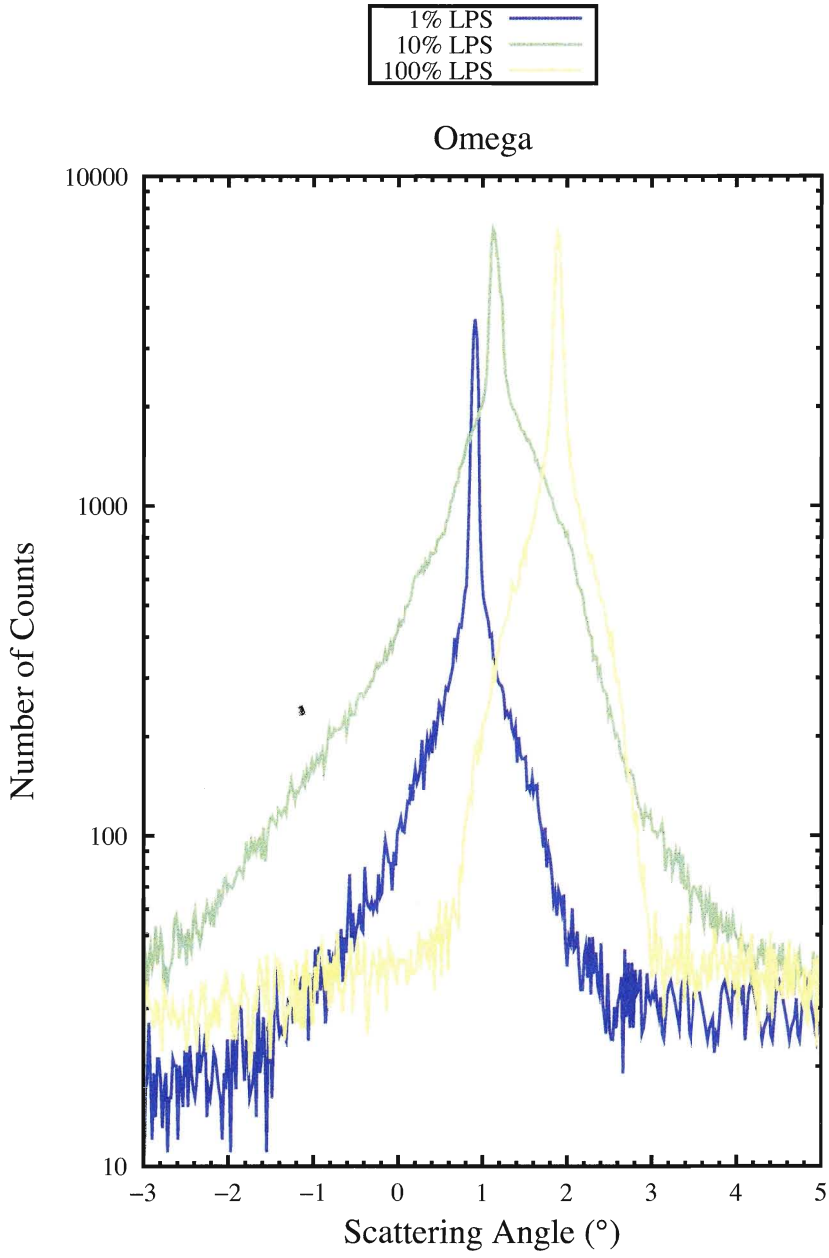

Figure 3.25: **LPS Rocking curve.** Rocking curve for three different concentration of LPS is shown in logarithmic bases, Here the detector is fixed at Bragg position while sample is rotating.

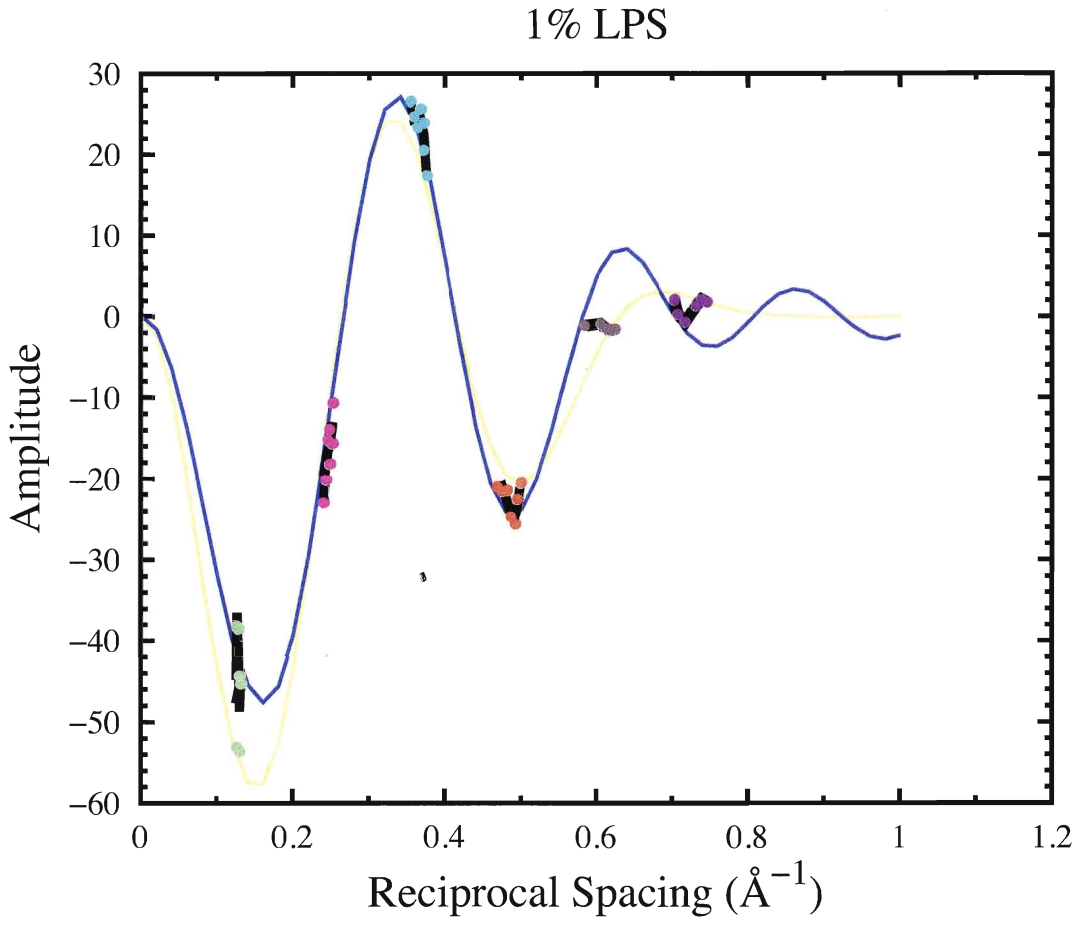

Figure 3.26: **Structure factors of POPC with 1% LPS.** Structure factor profile as a function of reciprocal lattice spacing for POPC and 1% LPS concentration sample. Fourier transform at temperature 16° C and 40° C is graphed with blue and yellow line respectively. The graph shows the six structure factors with colorful dots starting with h=1 in lime color. The black lines are the line of the best fit for each structure factors.

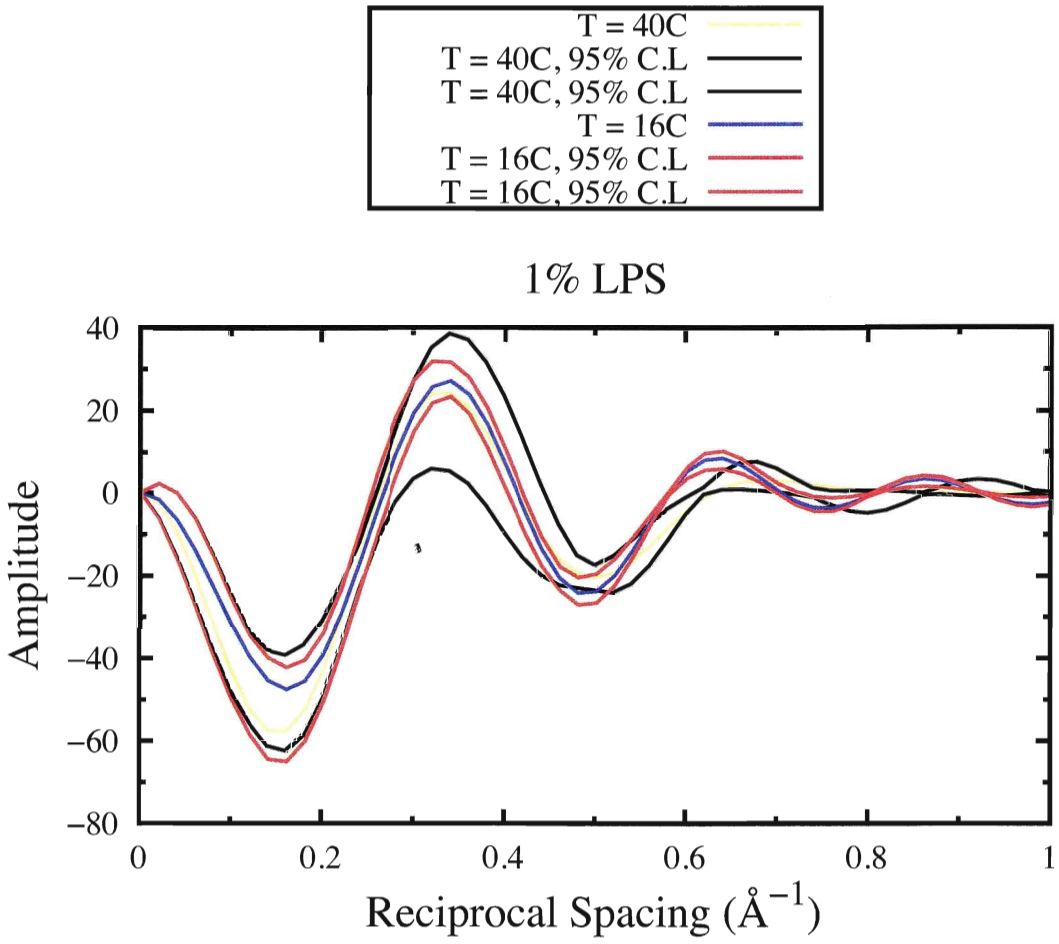

Figure 3.27: **Fourier transform of POPC with 1% LPS.** Fourier transform graph at 16° C and 40° C with 95% confidence limit for concentration of 1% LPS in POPC sample.

10% LPS

Structure factor profile of 10% LPS for four order values with Fourier transform at 16 °C and 40 °C C is graphed in figure 3.28. Structure factors of order value of 2, 3, and 4 are placed between the Fourier transform plots. At $h = 1$, the order values for temperature 16 °C and 40 °C C are positioned on their Fourier transform, however, the structure factors for the rest of the temperatures are located in wider range.

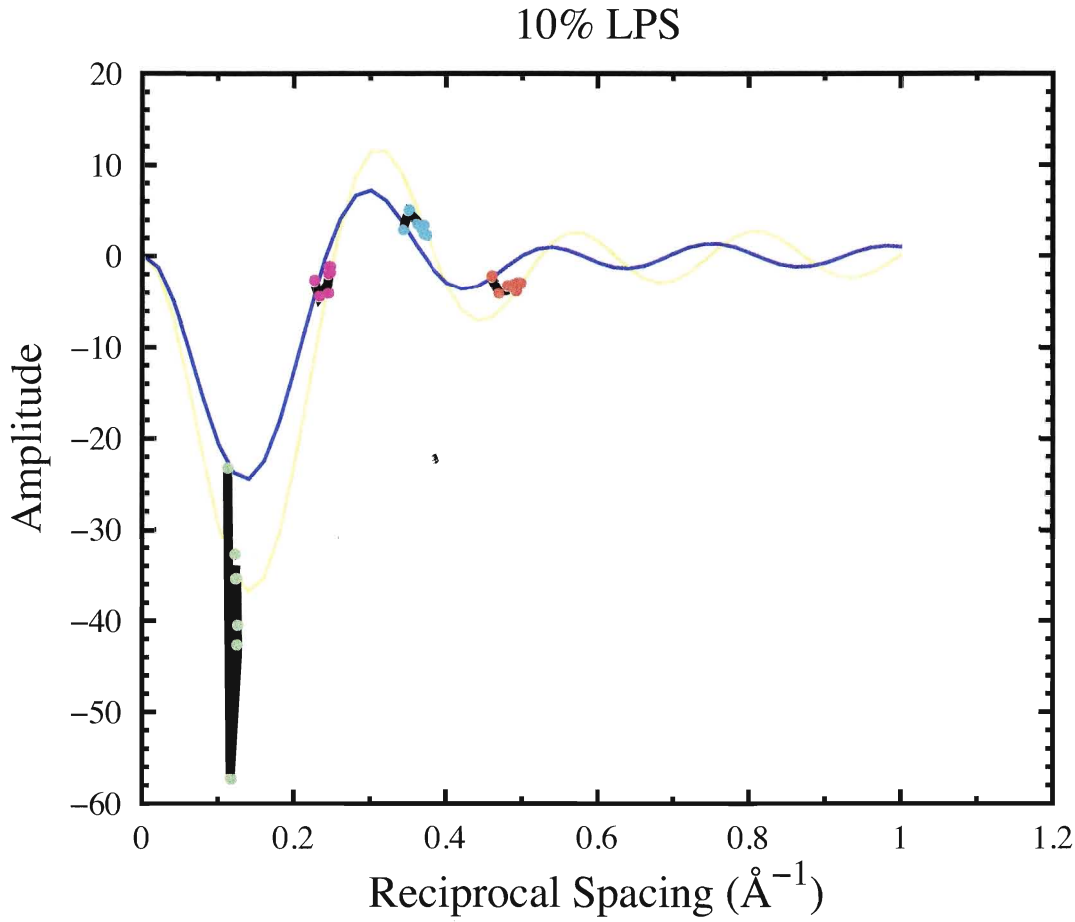

Figure 3.28: **Structure factors of POPC with 10% LPS.** Fourier transform graph of POPC sample with 10% LPS concentration, at 16 °C and 40 °C are plotted with blue and yellow line respectively. The structure factors of order 1, 2, 3 and 4 are positioned with colorful dots of lime, pink, aqua and orange with black line as their line of best fits.

Fourier transform and 95% confidence limits at minimum and maximum temperature of POPC sample with 10% LPS concentration are plotted in figure 3.29. The plot shows a clear change in

structure factor at these two temperatures. Comparing this graph with figure 3.28, shows that the change in amplitude is significant for all orders, which means that the structure is changing significantly with temperature.

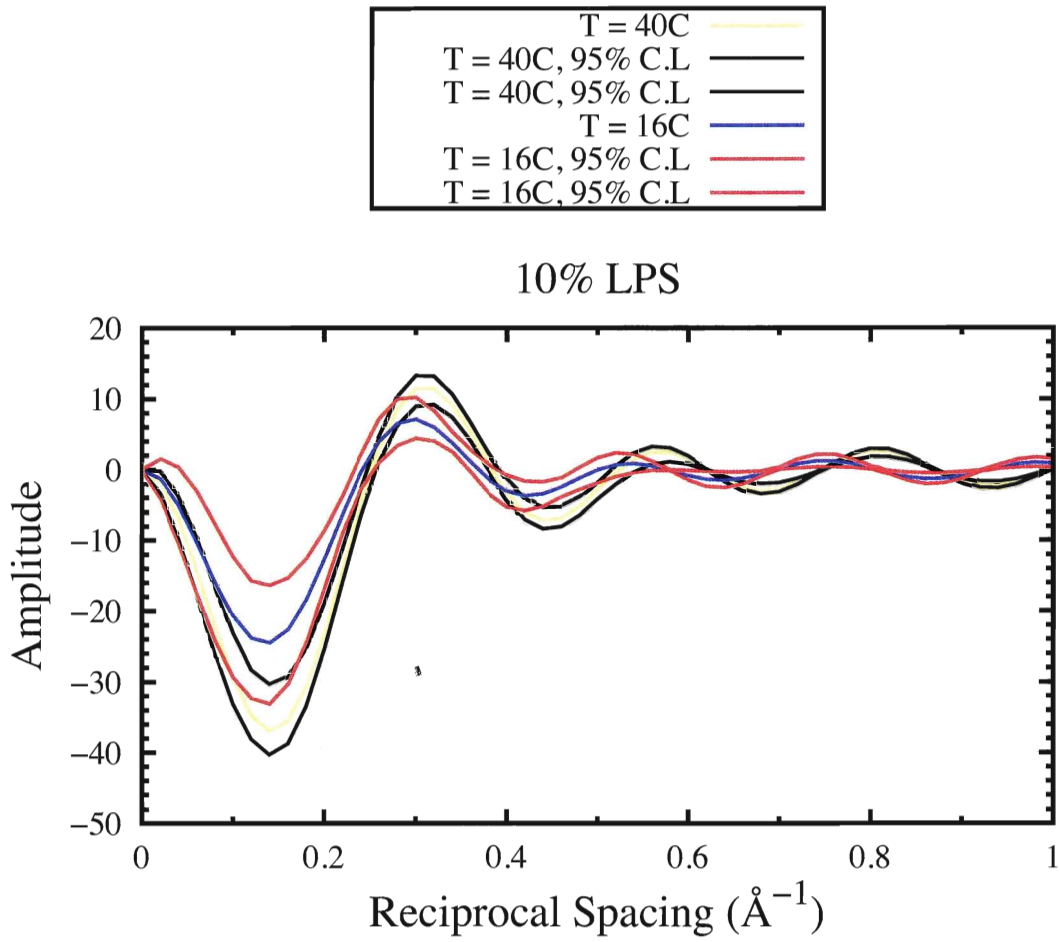

Figure 3.29: **Fourier transform of POPC with 10% LPS.** Fourier transform graph at 16 °C and 40 °C and their 95% confidence limit for 10% LPS concentration.

The three dimensions Fourier transform shows that beside the Fourier functions at temperature 16° C and 20° C, the rest of the plots have smooth and continues changes in their structures.

100% LPS

Structure factors of pure LPS sample for three orders of h is graphed in figure 3.30. At $h = 1$ order value, the structure factors for different temperature do not fit between the Fourier transform of 16 °C and 40 °C, same as the structure factors in 10% LPS concentration, which indicates a structral

change between these temperatures. Comparing the structure factors of the three concentration of LPS sample, it is clear that by increasing the concentration of LPS, the h order value, or the number of the intensity peaks in x-ray diffraction pattern, are decreasing. Also, by increasing the LPS concentration the strength of the intensity of these peaks, or the amplitude of the structure factor, are decreasing. These changes represents a significant molecular structure change within the sample.

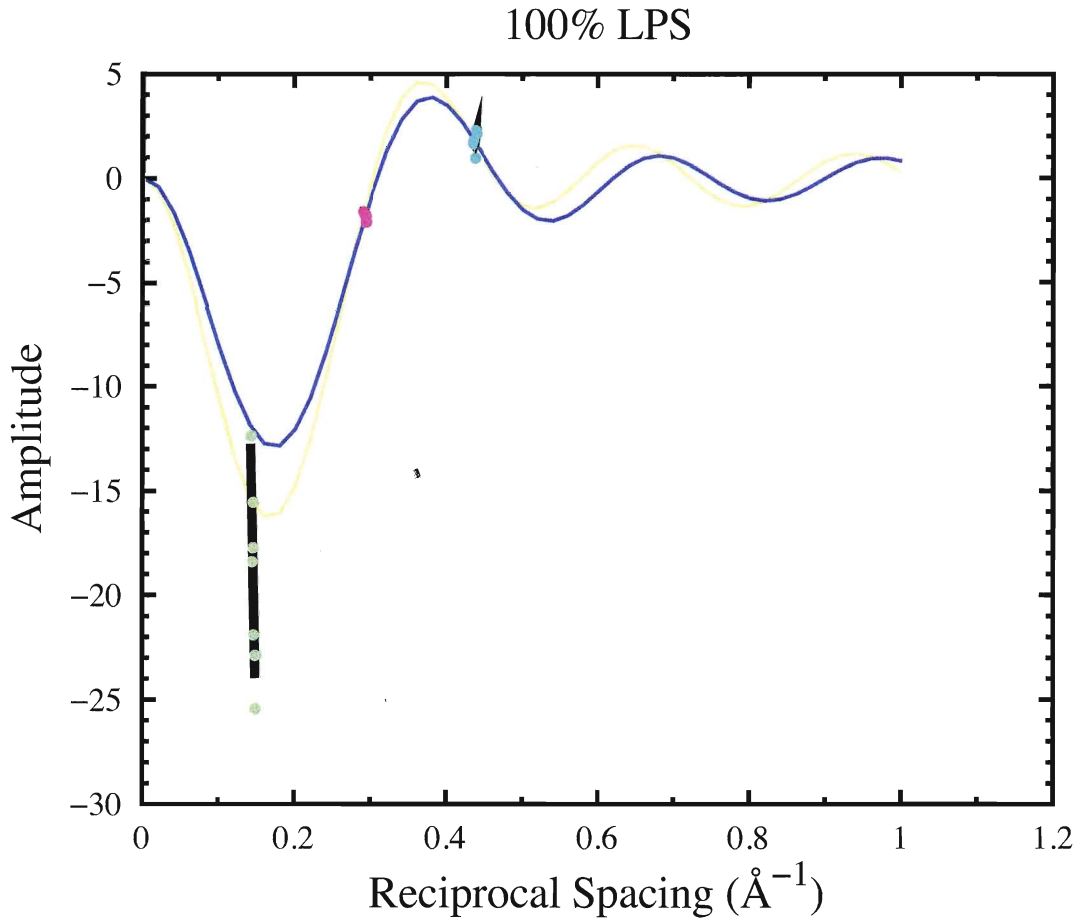

Figure 3.30: **Structure factors of pure LPS.** Fourier transform graph for pure LPS sample at 16 °C and 40 °C are plotted in blue and yellow line respectively. Three orders of structural factors are plotted with lime, pink and aqua colors. The line of best fit for each structural factors are plotted with black color.

The Fourier transform of pure LPS sample at their 95% confidence limit for temperature 16 °C and 40 °C are plotted in figure 3.31. The fourier transform of the confidence limit at temperature of 16° C has a different structure specially at higher order values. The three dimensional Fourier

transform for pure LPS sample indicates smooth and continuous changes within the temperature range, however the Fourier plot at 16° C has different structure compared to the rest of the plots.

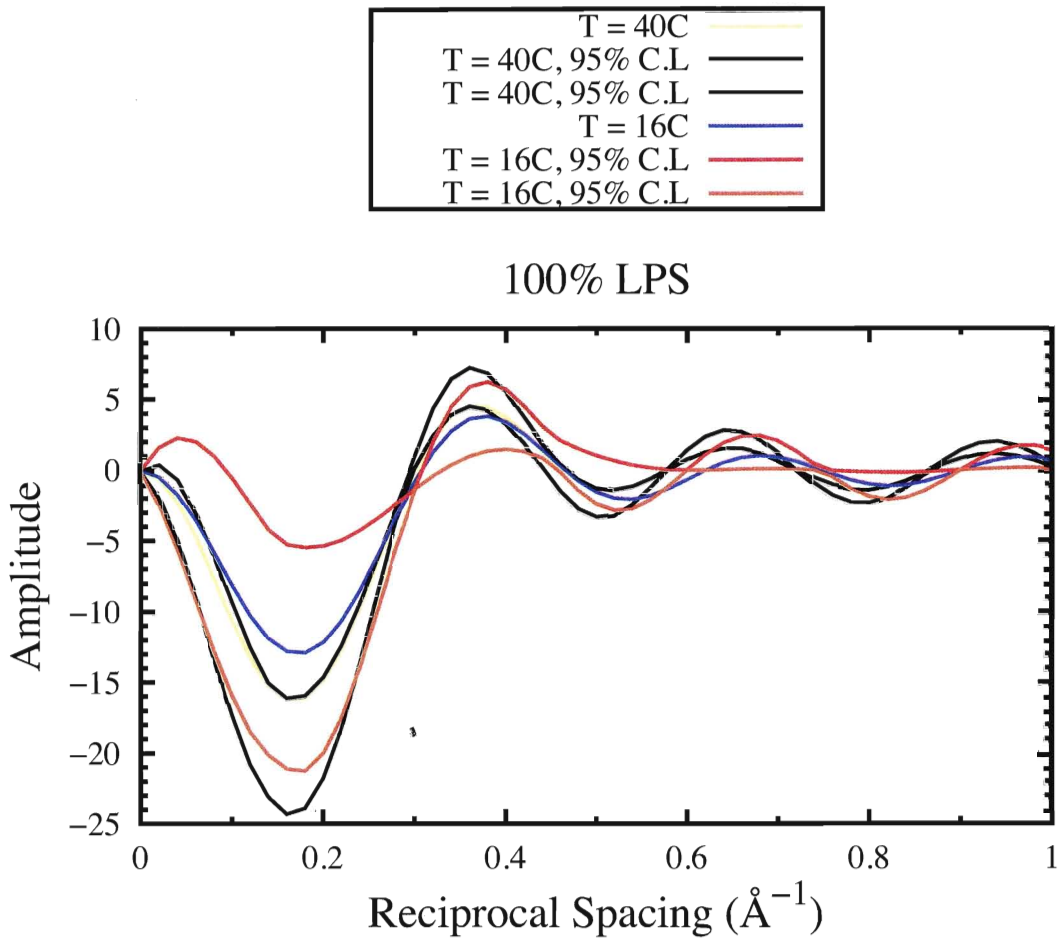

Figure 3.31: **Fourier transform of pure LPS.** Fourier transform and 95% confidence limit at 16° C and 40° C of pure LPS sample.

3.3.2 Electron density profiles

1% LPS

Electron density profiles of 1% LPS sample for six temperatures in the range of 16 °C to 40 °C is graphed in figure 3.32. The graph has equal offset in y direction for the temperatures higher than 16 °C. The profile shows that with increasing the temperature the lamellar spacing is decreasing.

Figure 3.33 shows that the change in the scattering length density of minimum and maximum

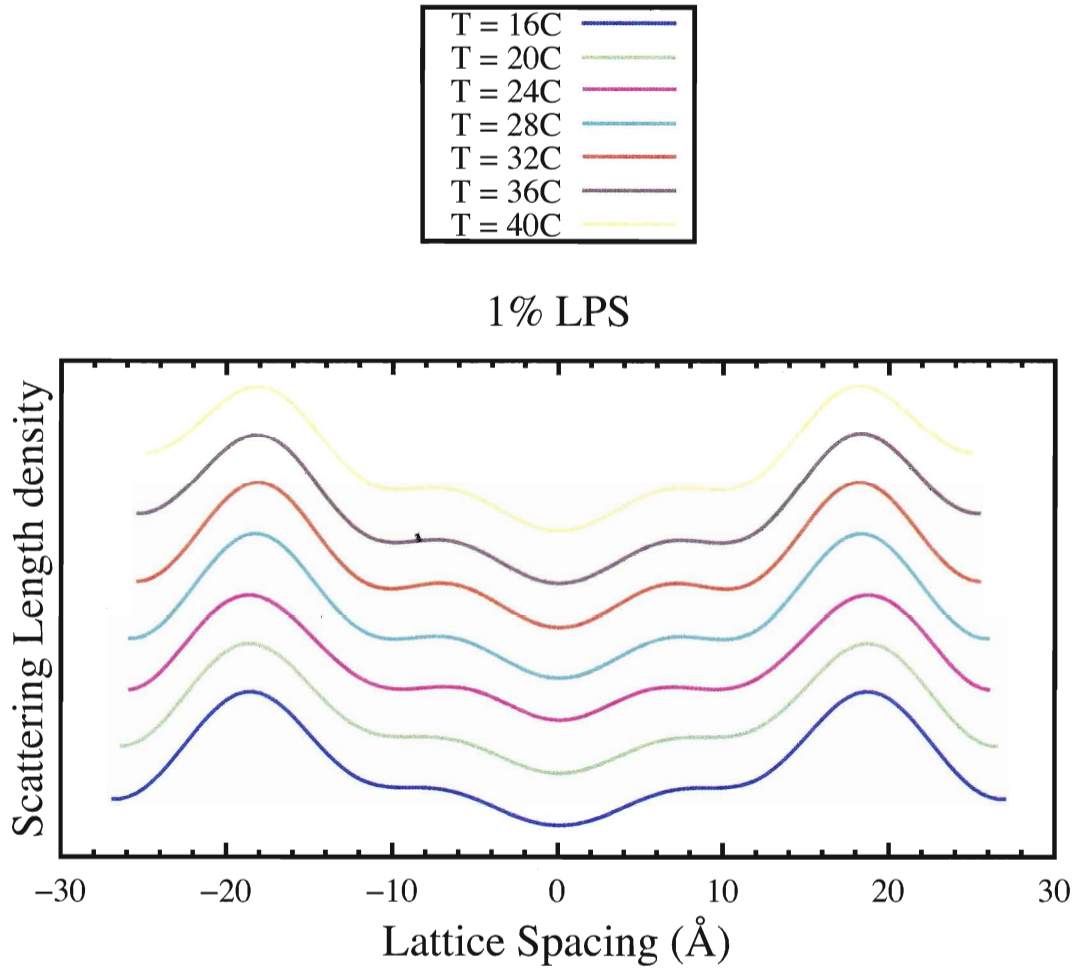

Figure 3.32: **Electron density profile of POPC with 1% LPS.** Electron density profile of POPC sample at 1% LPS concentration with saturated salt solution of KNO_3.

temperature for 1% LPS concentration is not significant in the center of the bilayer. However, it is very clear that lattice spacing is changed and also there are more details in the 40 °C electron density profile, including a peak in the hydrocarbon region, similar to the double bond peak seen in pure POPC.

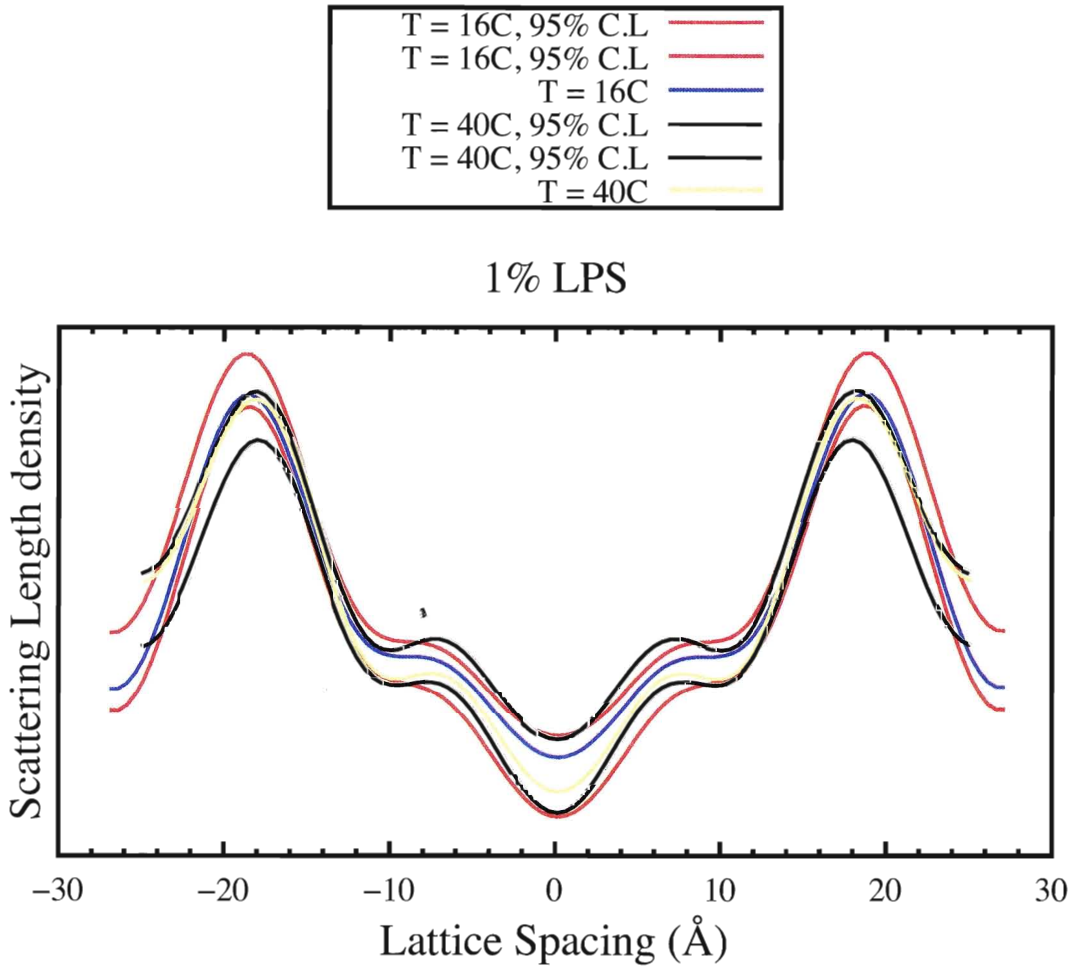

Figure 3.33: **C.L of electron density profile of POPC with 1% LPS.** Scattering length density at minimum and maximum temperature of 16° C to 40° C with their 95% confidence limit for 1% LPS concentration.

The change in lattice spacing of POPC sample at 1% LPS concentration with respect to temperature is graphed in figure 3.34 with KNO_3 as saturated salt solution. The graph confirms the electron density profile, which is with increasing the temperature the lamellar spacing is decreasing. The graph also shows that water thickness decreases with increasing the temperature while there is no significant change within the bilayer thickness.

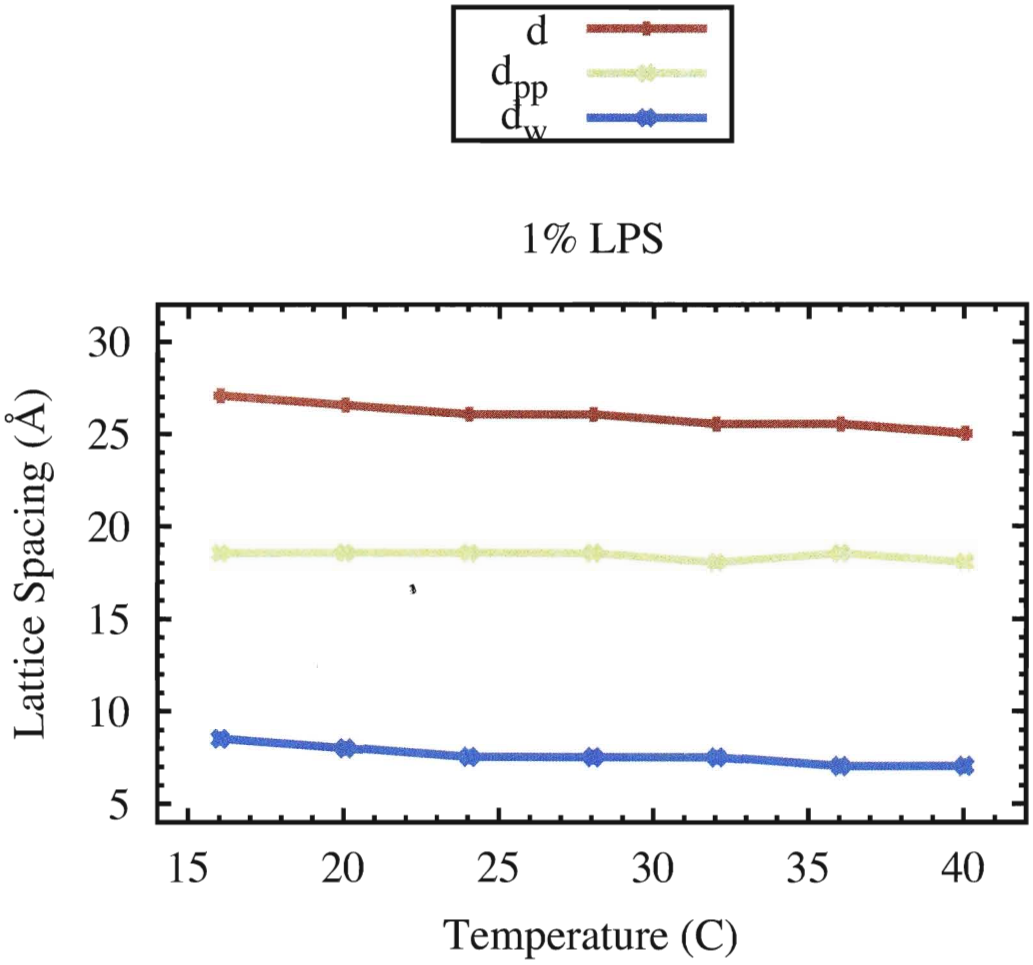

Figure 3.34: **Lattice spacing of POPC with 1% LPS.** Change in lattice spacing as a function of temperature for 1% concentration of LPS within POPC sample. Distance between center of bilayer to the edge of bilayer is represented with d, while bilayer thickness or d_{pp} is the distance from center to the phosphate group and d_w is the thickness of water molecule.

10% LPS

The scattering length density of POPC sample with 10% LPS concentration for temperature range of 16° C to 40° C, is graphed in figure 3.35 with equal offset in the y direction. Although, the electron density profiles do not follow a continuous smooth change within the temperature range but the decrease in lamellar spacing of the sample with respect to temperature is very clear from the graph.

Importantly, the phophate peak is become less distinct, and is shifted to the outside of the unit cell. We may even question if this peak is still due to the phosphate region, or more to the electron density of the core region. The similarity in shape to the previous electron density profiles means that we can still define a bilayer thickness using these two peaks. This is important for looking for structure changes when other moleculaes or proteins are included in the membrane.

The electron density profile for minimum and maximum temperature with 95% confidence limit is graphed in figure 3.36. The profile verifies the change in scattering length density of POPC sample with 10% LPS concentration. The graph clearly shows that lamellar spacing is smaller at 40 °C.

Figure 3.37 shows the change in the lattice spacing with respect to increase the temperature for POPC sample with 10% LPS concentration. The temperature range of 16 °C and 40 °C with KNO_3 saturated salt solution corresponds to humidity level of 95.41 ± 0.96 to 89.03 ± 1.2. The graph confirms that the lamellar spacing is decreasing with increasing the temperature. The graph also shows that the bilayer thickness does not change significantly and it just fluctuates, while the water thickness in 10% LPS sample decreases with increasing the temperature.

100% LPS

The electron density profile of pure LPS sample is graphed in figure 3.38 for the temperature range of 16° C to 40° C with equal offset in the y direction. The graphs are very broad, the broadness of the graphs are in the way that even the phosphate peaks are smoothed out and the details on the plots can not easily be recognized. At temperature of 24° C the smoothness of the peak was in the way that the edge of the bilayer was not distinct.

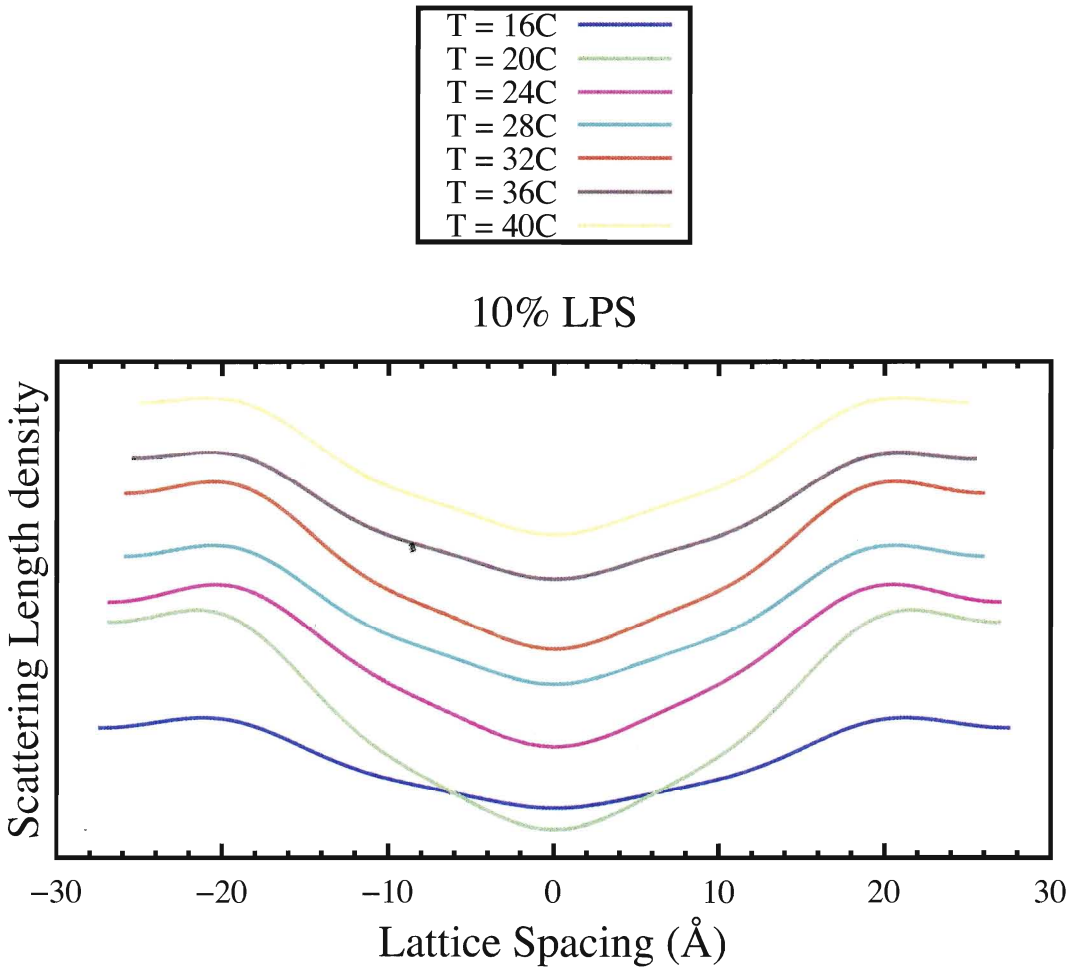

Figure 3.35: **Electron density profile of POPC with 10% LPS.** Change in electron density profile as a function of lamellar spacing within the temperature range of 16°C to 40°C.

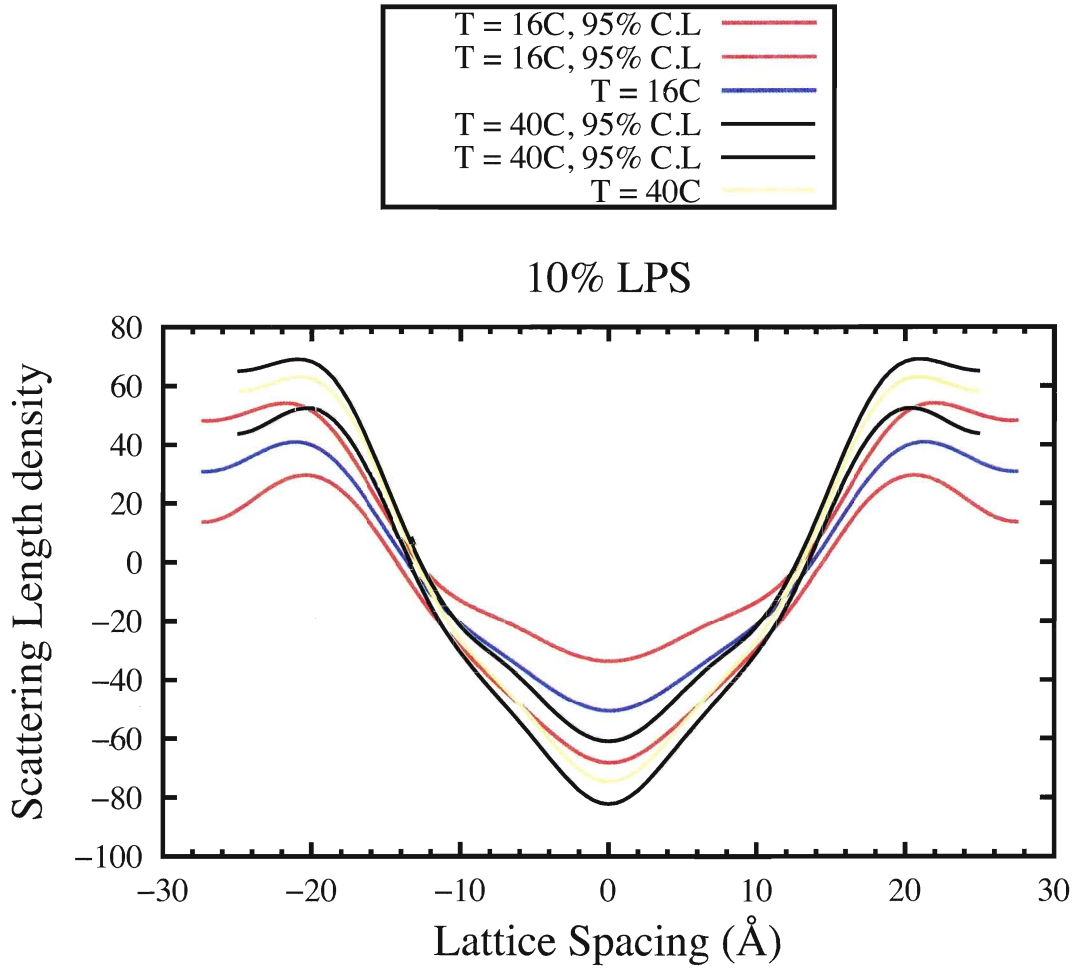

Figure 3.36: **C.L of electron density profile at POPC with 10% LPS.** Electron density profile for POPC sample at temperature 16 °C and 40 °C with their 95% confidence limit.

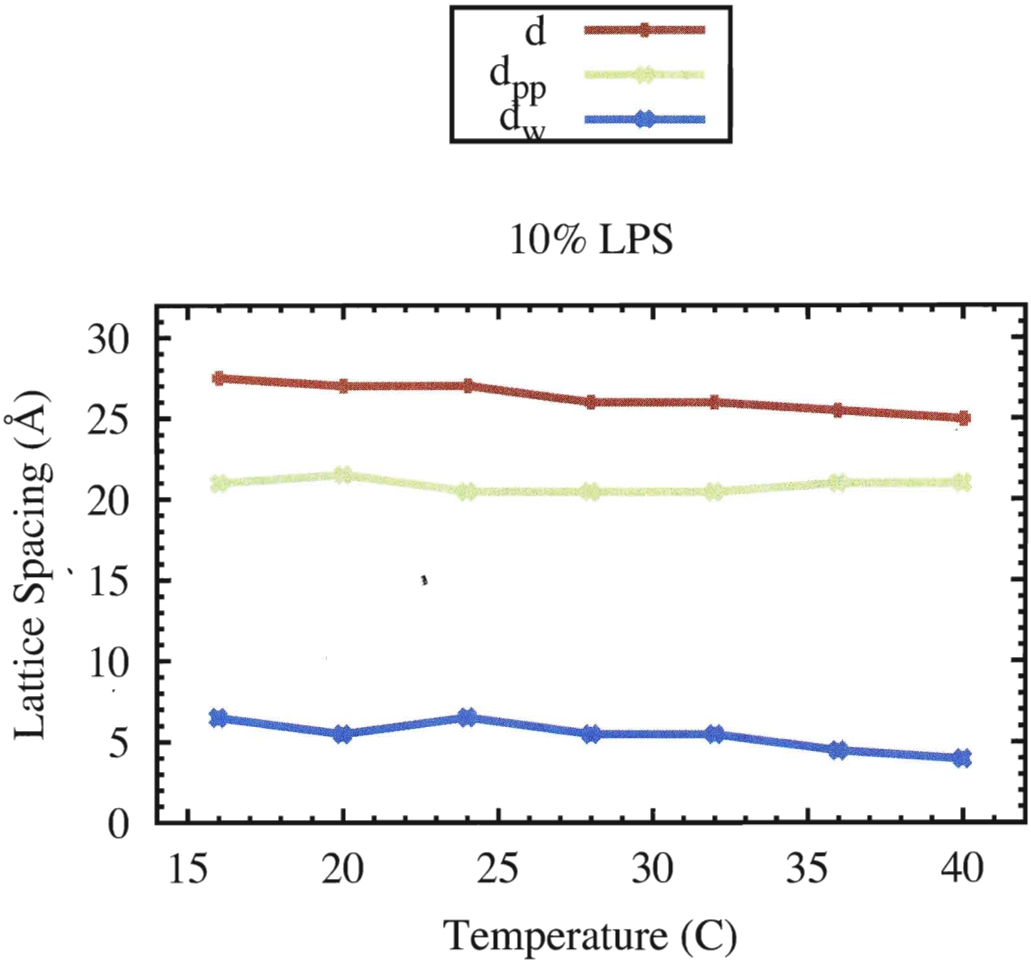

Figure 3.37: **Lattice spacing of POPC with 10% LPS.** The figure shows the change in the distance of the lamellar spacing from the center d, bilayer thickness from the center d_{pp} and water thickness d_w for POPC sample with 10% LPS concentration as a function of temperature.

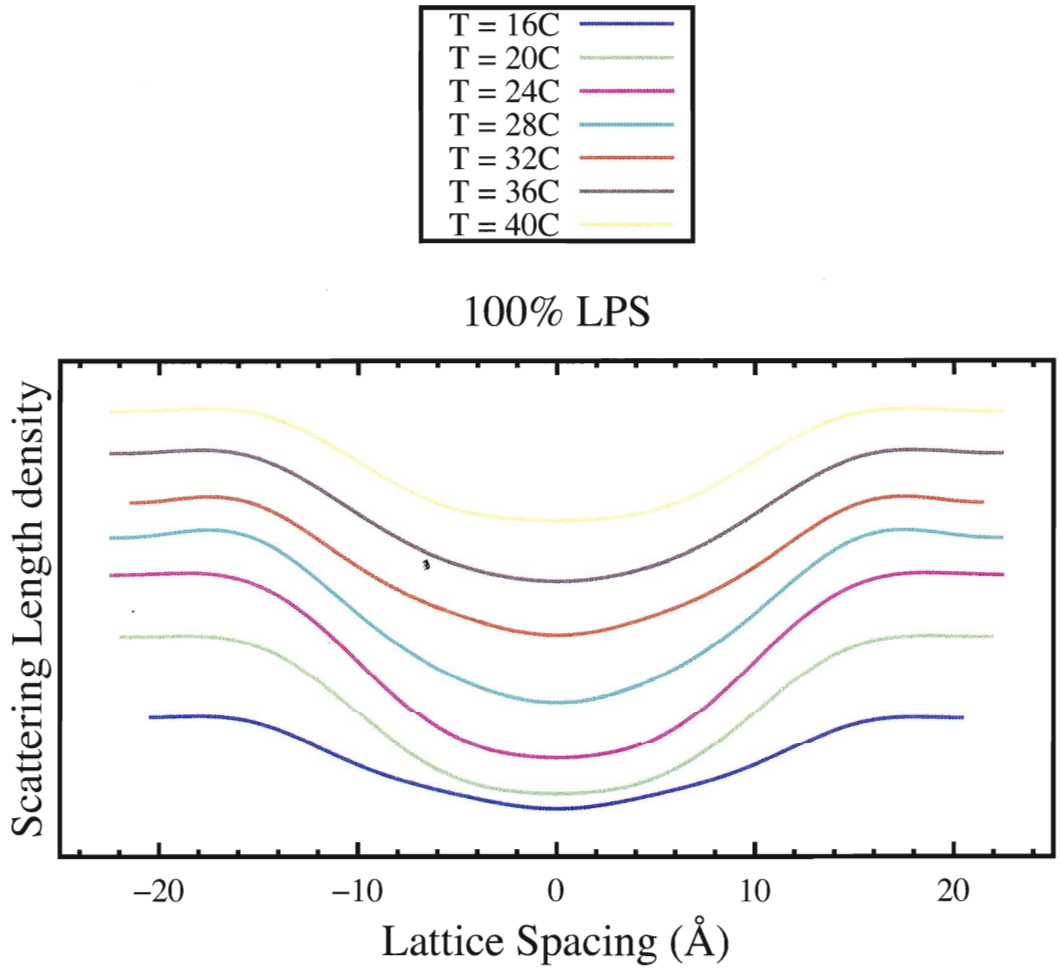

Figure 3.38: **Electron density profile of pure LPS.** Scattering length density profile of pure LPS sample as a function of lattice spacing of the bilayer with saturated salt solution of KNO_3.

Figure 3.39 shows the scattering length density of the minimum and maximum temperature and their 95% confidence limit of the pure LPS sample. The graph shows that the confidence limits of 16° C and 40° C are overlapping each other. As the result the electron density change of pure LPS sample within this range is not significant.

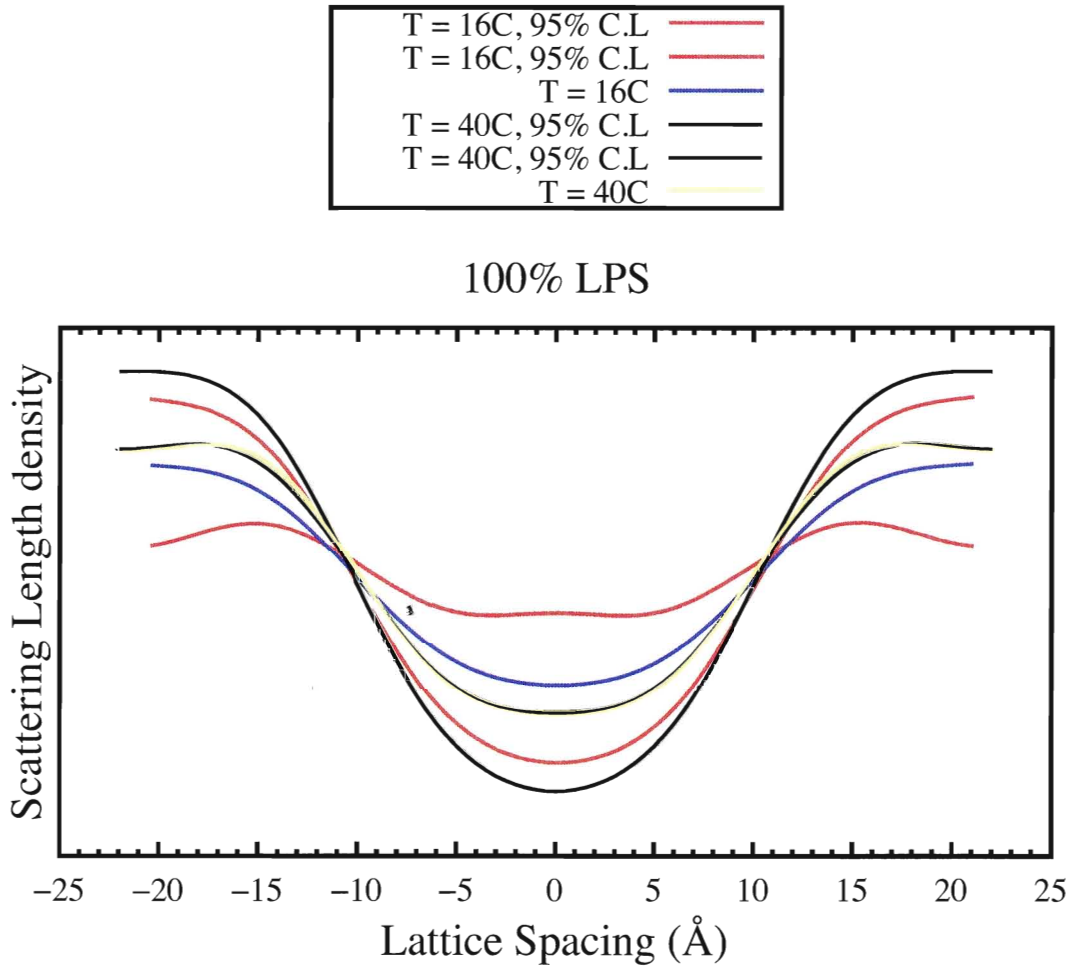

Figure 3.39: **C.L of electron density profile at pure LPS.** Scattering length density of minimum and maximum temperature of 16° C to 40° C with their 95% confidence limit for sample of pure LPS.

The change in lattice spacing of pure LPS sample is graphed in figure 3.40, within the temperature range of 16° C to 40° C, however the data at the temperature of 24° C was not available as a results of broadness of its electron density plot. The extra smoothness and the broadness of the electron density profile caused a fluctuation in change of lattice spacing distance, especially the lamellar spacing and bilayer thickness of the pure LPS sample in the temperature range.

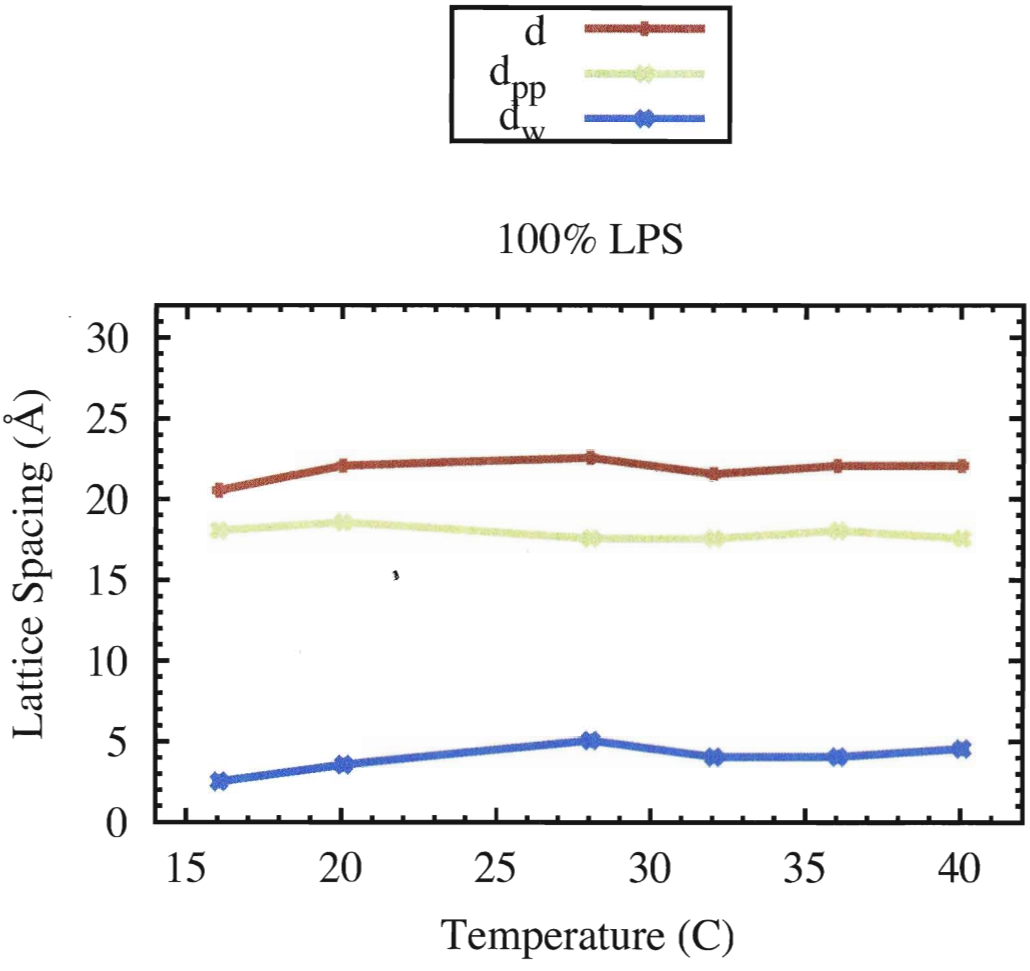

Figure 3.40: **Lattice spacing of pure LPS.** Change in lattice spacing as a function of temperature for pure LPS sample. Distance between center of bilayer to the edge of bilayer represented with d, while bilayer thickness or d_{pp} is the distance from center to the phosphate group in the bilayer and d_w is the thickness of water molecule.

Temp(°C)/ Sample	POPC 100% (Å)	LPS 1% (Å)	LPS 10% (Å)	LPS 100% (Å)
16°C	50.79	53.52	54.29	41.89
20°C	50.84	52.89	53.75	43.01
24°C	50.19	53.29	52.10	42.98
28°C	49.91	51.50	51.54	43.18
32°C	51.46	51.12	51.08	43.36
36°C	50.88	50.83	51.04	43.36
40°C	50.67	50. 31	50.63	43.27

Table 3.4: **Lamellar spacing of bilayer LPS**. Lamellar spacing at different concentration of LPS samples, with saturated salt solution of KNO_3.

Table 3.3.2 shows the lamellar spacing for pure POPC, 1% and 10% concentration of LPS and pure LPS sample with saturated salt solution of KNO_3. In the table the lamellar spacing is the distance across the bilayer.

3.3.3 Summary of LPS results

Figure 3.41 shows the comparison between the electron density profile of pure POPC sample, POPC with 1% and 10% LPS concentration and pure LPS sample. The top and bottom panel show the comparison at minimum and maximum temperatures corresponding to humidity level of 95.41 ± 0.96 and 89.03 ± 1.2 respectively. For a clear comparison the electron density of the 1%, 10% and 100% LPS sample were multiplied by a factor of 4, 8 and 16 respectively.

From the two panels it's easy to recognize that with increasing the concentration of LPS, the profiles become smoother and broader. Also the lamellar spacing of the pure LPS is significantly smaller than the lamellar spacing of the other samples. Meanwhile, there is no remarkable change in the lattice spacing of the other sample at the similar temperature. The lamellar spacing of the pure LPS is in order of 5 Å smaller than the pure POPC or POPC with 1% LPS. There is much loss of detail, as the resolution decreases and the disorder increases with more LPS concentration. Also, the electron density at the edges of the unit cell increases to such a point, that the phosphate peak cannot be recognized anymore.

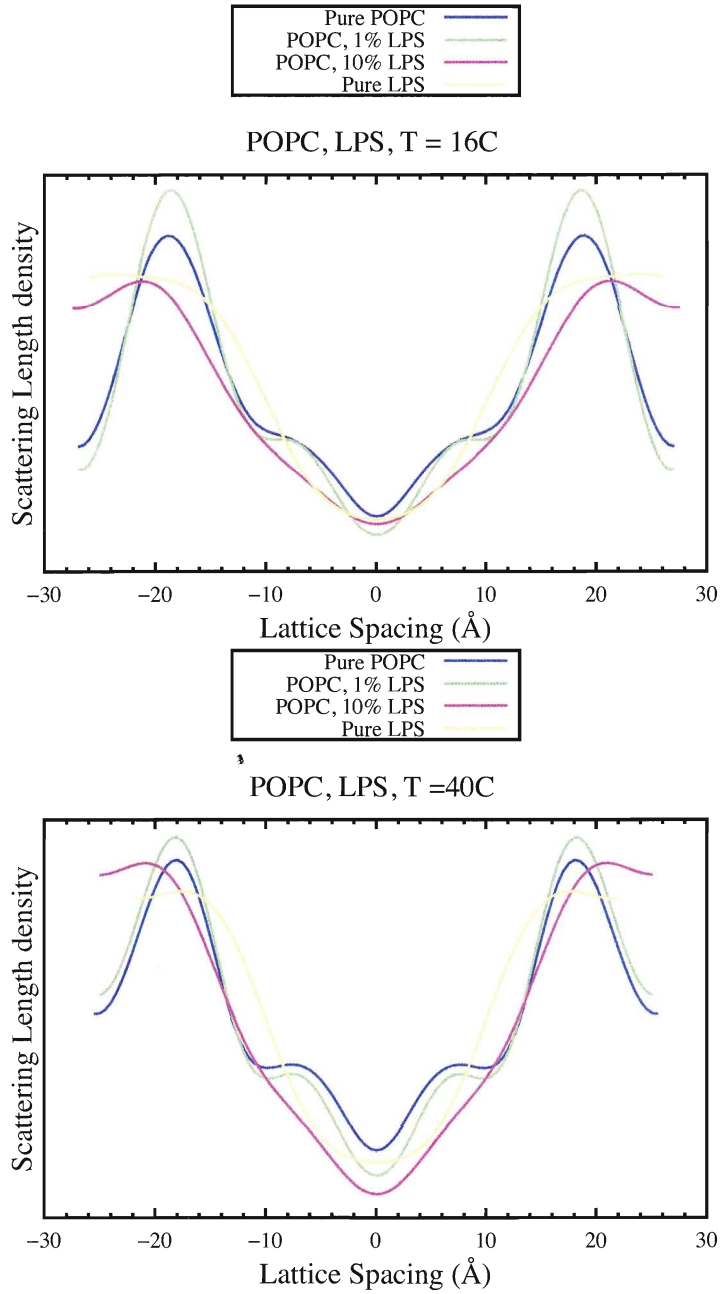

Figure 3.41: **Electron density profile of different LPS concentrations.** The top panel shows the electron density profile of pure POPC, POPC with 1% and 10% LPS concentrations and pure LPS sample at temperature of 16 °C, while the bottom panel show the same comparison at temperature of 40 °C. Samples with LPS concentration were multiplied by appropriate factor for comparability reasons.

Chapter 4

Conclusions

X-ray diffraction patterns of DMPC with 20% cholesterol, POPC samples at various hydration levels and different concentrations of LPS samples were measured across specific temperature ranges. The position and the amplitude of the lamellar diffraction peaks were used to specify the structure factors. The continuous Fourier transforms of the electron density profiles were constructed from the diffraction amplitudes measured at each temperature level. The structure factors phases were chosen in the way that the Fourier transform plots can pass through the order values. The electron density profiles of the bilayer were determined from a Fourier sum of the structure factors. The accuracy of the order diffracted measurements were obtained from the third order polynomial of line of best fit to each order, with a 95% confidence interval.

The significant effect of the temperature changes on the structure of the sample molecules were determined through 95% confidence limit at minimum and maximum temperature range for both the structure factors and electron density profile. Then the temperature effect on the lamellar spacing and decomposition of the spacing into the structural components of bilayer thickness and water thickness were verified. The lipid bilayers are centrosymmetric thus the measurements were expressed in terms of a monolayer spacing.

4.1 DMPC and cholesterol

The structure factor of DMPC with 20% cholesterol were measured because we wished to test the department x-ray machine with a known and well respected measurement from the literature. We expected that a significant fraction of cholesterol in DMPC would increase the ordering and allignment of the lipid bilayers, which results in stronger signal.

Indeed, within a temperature range of 18 °C to 28 °C using KNO_3 saturated salt solution

(representing the humidity levels of around 94% to 92% and lamellar spacing of 57.75 Å to 55.85 Å), there were nine strong Bragg peaks found in these ranges. The number of Bragg peaks and the position of these peaks corresponds to DMPC cholesterol solution in the L_{β} gel phase which is confirmed by research done by Hung et al [14]. The change in the Fourier transform plots were very smooth and continuous for all the temperatures.

The Fourier transform plots express more detail in the electron density profile at the higher temperature as a result of the more orders. The lattice spacing graphs confirm that by increasing the temperature, the lamellar spacing and the bilayer thickness is decreasing together while the water layer thickness remains the same.

The characteristics of the DMPC with 20% cholesterol were compared with previous research and held as a base reference for the other sets of the experiments. The gel phase of the sample confirms with the DMPC solution at 17% cholesterol concentration within the specified range and the number of the diffracted orders is similar with 17% cholesterol concentration at 30°C with the relative humidity of 91.8% [14]. Also the structure factor and electron density profile of the sample at 22°C were compared with 40% cholesterol in lecithin sample at 23°C [9].

4.2 POPC and LPS

For future membrane biophysics studies that look at the effects of antibiotics and other molecules on the membranes of gram-negative bacteria, we want to have a better model of those membranes, which include lipopolysaccharides. LPS is a large lipid molecule, and we expect that it will not form well alligned bilayers that are good for x-ray diffraction. If we incorporate LPS into a phospholipid that does form well aligned bilayers, we may have a better model system for study.

A comparison between the pure POPC sample, POPC with 1%, 10% LPS concentration, and pure LPS samples, shows a remarkable change in molecular structure with increasing the LPS concentration and smoothness of the profile.

The electron density profiles of POPC samples with R.H controlled by saturated salt solutions of K_2SO_4 ($\sim$ 97%-R.H), KNO_3 ($\sim$ 93%-R.H) and KCl($\sim$ 84%-R.H) were compared within the temperature range of 22 °C to 32 °C. The highest number of Bragg peaks, eight, which indicates

the best lipid allingment, came with KNO_3. A higher hydration, closer to 100% there were only 5 Bragg peaks, and at much dryer conditions there were only 6. In each case, the phosphate to phosphate bilayer thickness was easy to measure, and the internal structure of the hydrocarbon region, such as the location of the oleoyl double bond was clearly indicated [41, 42]. Clearly, POPC likes to form lamellar bilayers that are easy to characterize with x-ray diffraction at high resolution.

In the POPC sample with high humidty K_2SO_4 salt solution, the significant effect of change in temperature is shown in the electron density graphs. Although the changes are smooth within the temperature range but three dimensional plot shows that there is a kink at temperature 28 °C. In the POPC sample with KCl saturated salt the significant changes in Fourier transform and electron density profiles belong to higher structural orders. The Fourier transform plots within the temperature range changes smoothly and continuously.

In the POPC sample with KNO_3, the Fourier transform graph were plotted within the temperature range of 16 °C to 40 °C. The structure of the graph changes smoothly for the last three and the first four temperatures, with a kink at temperature of 24 °C. This would cause a significant difference in Fourier transform plots at temperature of 16 °C and 40 °C. However, it is not easy to see the significant of the change in the scattering length density profile for the temperature of 16 °C and 40 °C or 20 °C and 32 °C. Still, the plots clearly shows that the electron density profile at higher temperature has more detail and better resolution.

At the temperature range of 20 °C to 32 °C, the K_2SO_4 solution with the highest humidity level has the longest lamellar spacing. Within the temperature range, the lamellar spacing of POPC with saturated salt solution of K_2SO_4 and KCl are decreasing from 53.7 Å to 52.1 Å and from 51.8 Å to 50.9 Å respectively, while the lamellar spacing of POPC with KNO_3 solution is just fluctuating.

Within the temperature range, in POPC sample with K_2SO_4 salt solution, the bilayer thickness is constant, while the water thickness is decreasing as a results of drying the sample. The R.H in the sample cell is at 97%, which is very sensitive to temperature, and there is likely to be condensation on any cool spots like the cell windows. The bilayer thickness is decreasing in the sample with KCl saturated salt solution, while the water thickness is constant for this experiments. This is becuase increasing temperature adds thermal order to the hydrocarbon chains, while the R.H in the sample

cell remains more steady. In every case, there was no phase change due to temperature or hydration changes, and the sample was in the liquid crystalline L_α phase [11].

The POPC samples with 1% and 10% LPS concentration, and the pure LPS sample have 6, 4 and 3 diffraction orders respectively. As expected, although the rocking curves indicates that the LPS does forms well alligned bilayers, there is little correlated strucutre in the LPS bilayer. Typically, four diffraction orders are required for accurate Fourier reconstruction of the electron density profile [9], which may not be possible for much more than 10% LPS.

The change in three dimensional Fourier transform of the samples are very smooth and continuous for the temperature range of 16°C to 40°C. In 1% and 10% LPS concentration samples, the structural changes are significant at higher order values for scattering length density and Fourier transform graphs. However, in pure LPS sample, the typical profile of a phospholipid bilayer is lost, and there was little structural change in the electron density profile across the temperature range.

The electron density profile of the pure *Pseudomonas aeruginosa* sample shows that this molecule is a bilayer with a phosphate groups on the outside and two chains facing each other at the center of the bilayer, just like the DMPC and POPC samples. However, the smoothness and lack of details in the scattering length density profile of pure Pseudomonas aeruginosa sample implies that the large head group prevents the lipids from reaching the degree of stacking order achievable by phospholipids. Especially at the lower temperature, the core oligosaccharide and the O side chain of the LPS molecule can easily and freely mix with the water molecules and create a high electron density region. As a result the number of discernible order values reduces from 1% LPS concentration to pure LPS sample.

Increasing the temperature caused the lamellar spacing of 1% LPS concentration to decrease from 53.52 Å to 50.31 Å, and the lamellar spacing for 10% LPS concentration to decrease from 54.29 Å to 50.63 Å. The bilayer thickness of the POPC samples with LPS concentration were fluctuating while the water thickness were decreasing within the temperature range, which shows a loss of water while heating the sample.

In the pure LPS sample, it is difficult to assign a value to the bilayer thickness, because the position of the phosphate cannot be easilty determined. There is disorder, in terms of bilayer fluctuations, the O side chain, as well as hydrocarbon chain disorder, in the pure LPS samples to

say with certainty what part of the electron density curve is represented by what chemical group.

However the lamellar spacing of about 43 Å and three diffracted order values confirm that the pure LPS solution is at L_α gel phase [7].

The lamellar spacing of the pure POPC sample, POPC with 1% and 10% LPS solutions are all decreasing with increasing the temperature within the range of 16 °C to 40 °C with KNO_3 saturated salt solution. Comparing these three solutions, increasing the LPS concentration, cause the lamellar spacing to increase. Which means probably the LPS concentration formed separates domains of Bragg peaks, representing two different unit cells. Also there is a phase change in the range of pure POPC to pure LPS concentration. This could be another reason for huge change in lamellar spacing of pure LPS solution.

The phosphate peaks are identifiable in the electron density profiles, which means we can monitor the membrane structure as conditions change, such as temperature, hydration, or in the future, adding antibiotics and other molecules. With as much as 10% LPS, a significant fraction of the membrane area is now covered by saccharide oligomers, which may change how other molecules interact with lipid bilayers in way that can be studied. This new sample of POPC and 1% to 10% LPS is a good new model membrane that can be used for future biophysics studies.

Appendix A

First Appendix

A.1 C.L of Structure Factor profile

Details on third order polynomial fit of the structure factors are shown in the following figures. The structure factor for third lamellar peak $h = 3$, with the best polynomial fit and 95% confidence limit are graphed. Each of the aqua dots represent the structure factor at a specific temperature. The figures show that all the experimental values of structure factors at third order values are within the 95% confidence limit.

A.1.1 DMPC and POPC

A.1.2 LPS

A.2 Three dimensional profile of structure factors

The following three dimensional graphs show the changes in Fourier Transform plots as a function of temperature, reciprocal lattice.

A.2.1 DMPC and POPC

A.2.2 LPS

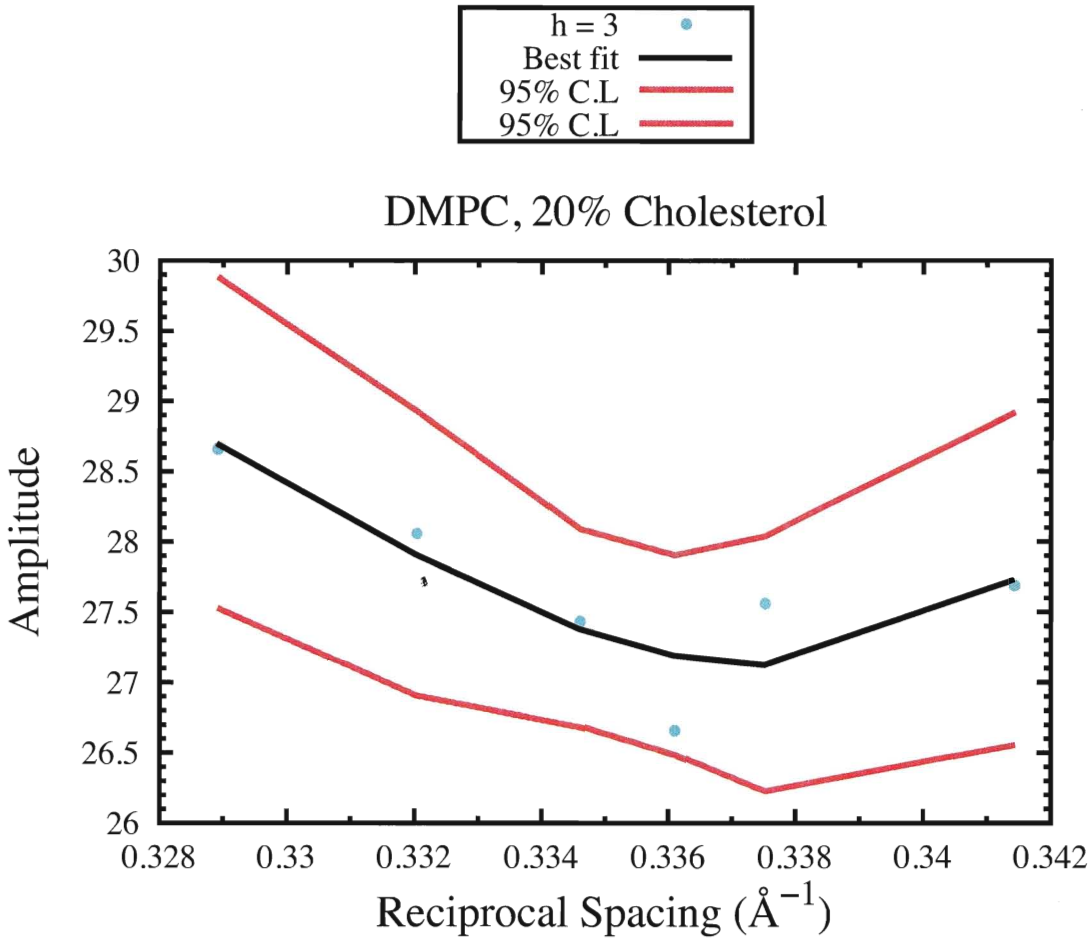

Figure A.1: **Order value of DMPC with 20% cholesterol.** The level of confidence analysis of the structure factor for order value of $h = 3$. Third order polynomial curve and %95 confidence limit shows in the picture. The experiment is done by changing the temperature in the range of 18°C and 28°C degree.

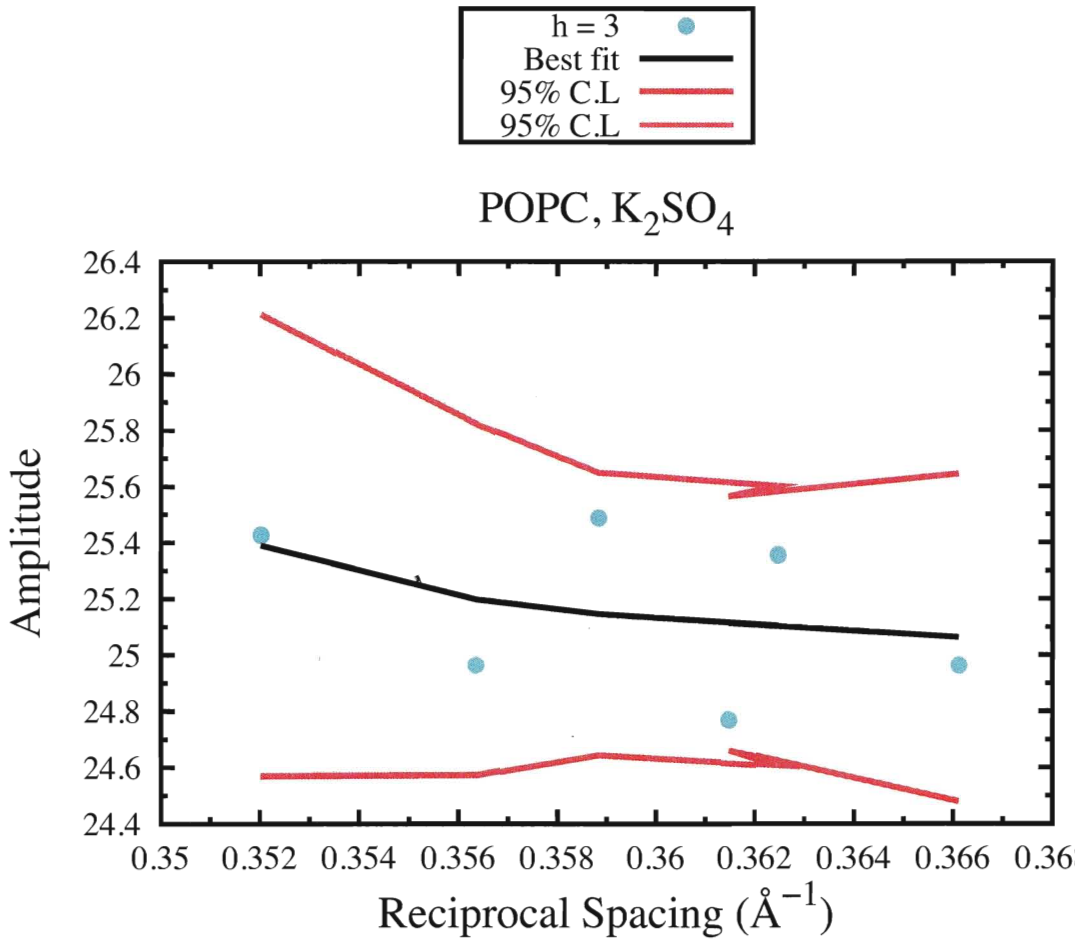

Figure A.2: **Order value of POPC with K_2SO_4** Structure factors of third order value for POPC sample with K_2SO_4 saturated salt . Each blue dots is a third lamellar peak at a specific temperature. The black line is the line of best fit and the red lines show the 95% confidence limit of the structure factor

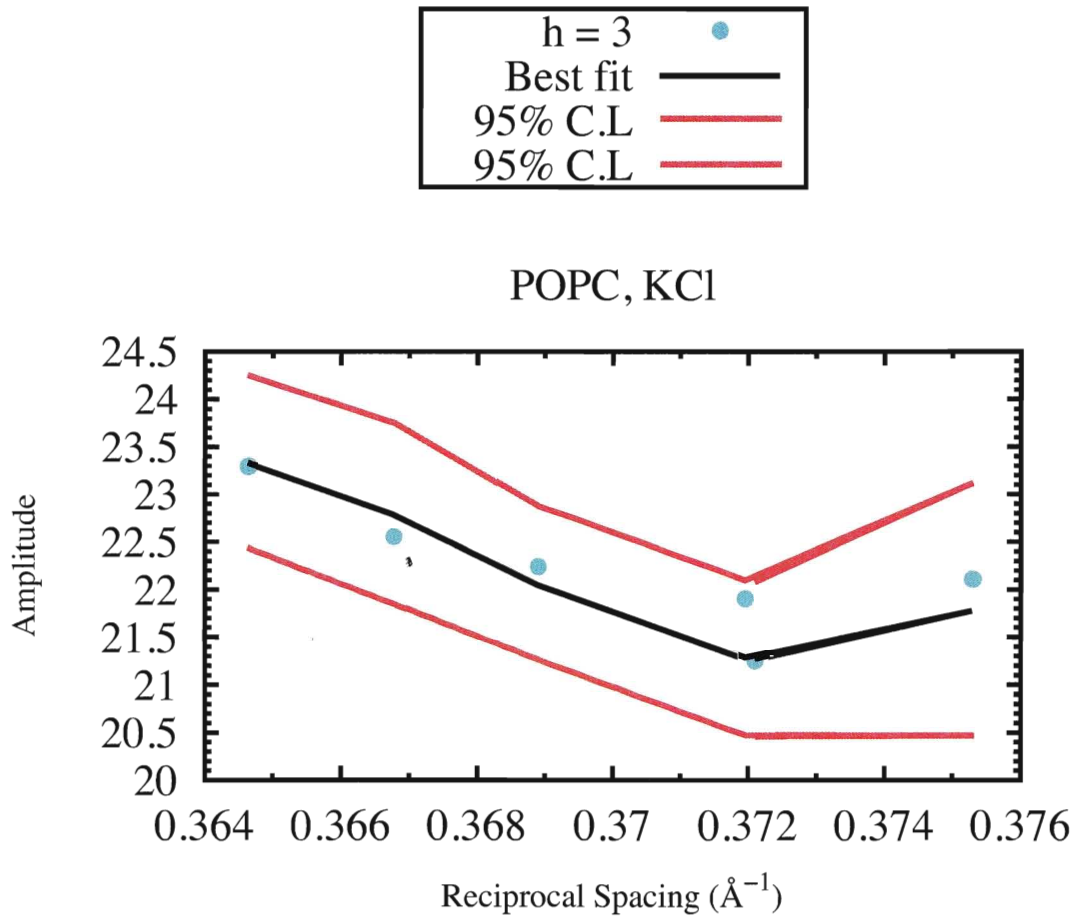

Figure A.3: **Order value of POPC with KCl.** The third order structure factor of POPC with KCl salt. The experimental data are shown with jade blue dots, polynomial fit is shown in black and 95% confidence limits are shown in red.

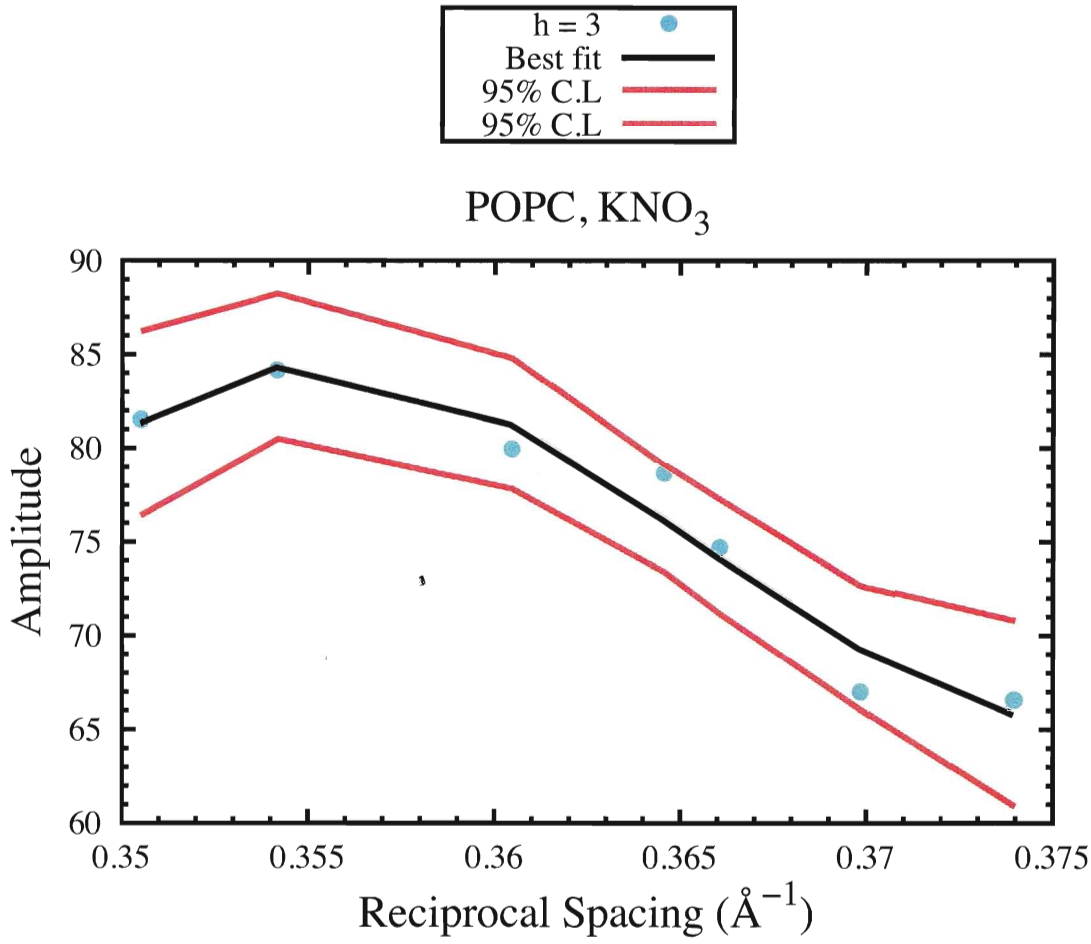

Figure A.4: **Structure factor of POPC with KNO_3.** Seven structure factors corresponding to equal interval in temperature range of 16° C to 40° C for POPC with KNO_3 solution. The structure factors, line of best fit and 95% confidence limit is shown for third order value.

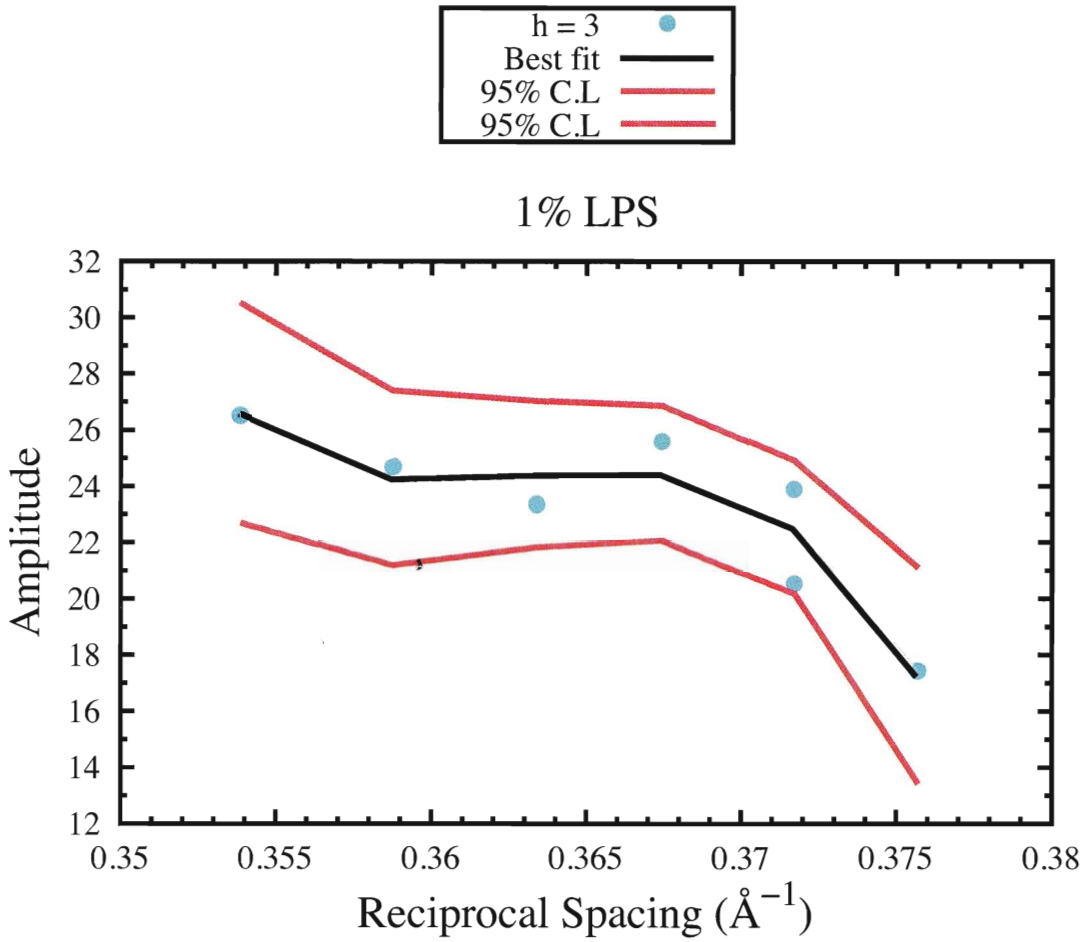

Figure A.5: **Order value of POPC with 1% LPS.** Structure factor profile for h=3. Line of the best fit and the 95% confidence limit shows the accuracy of the experimental data plotted with aqua color.

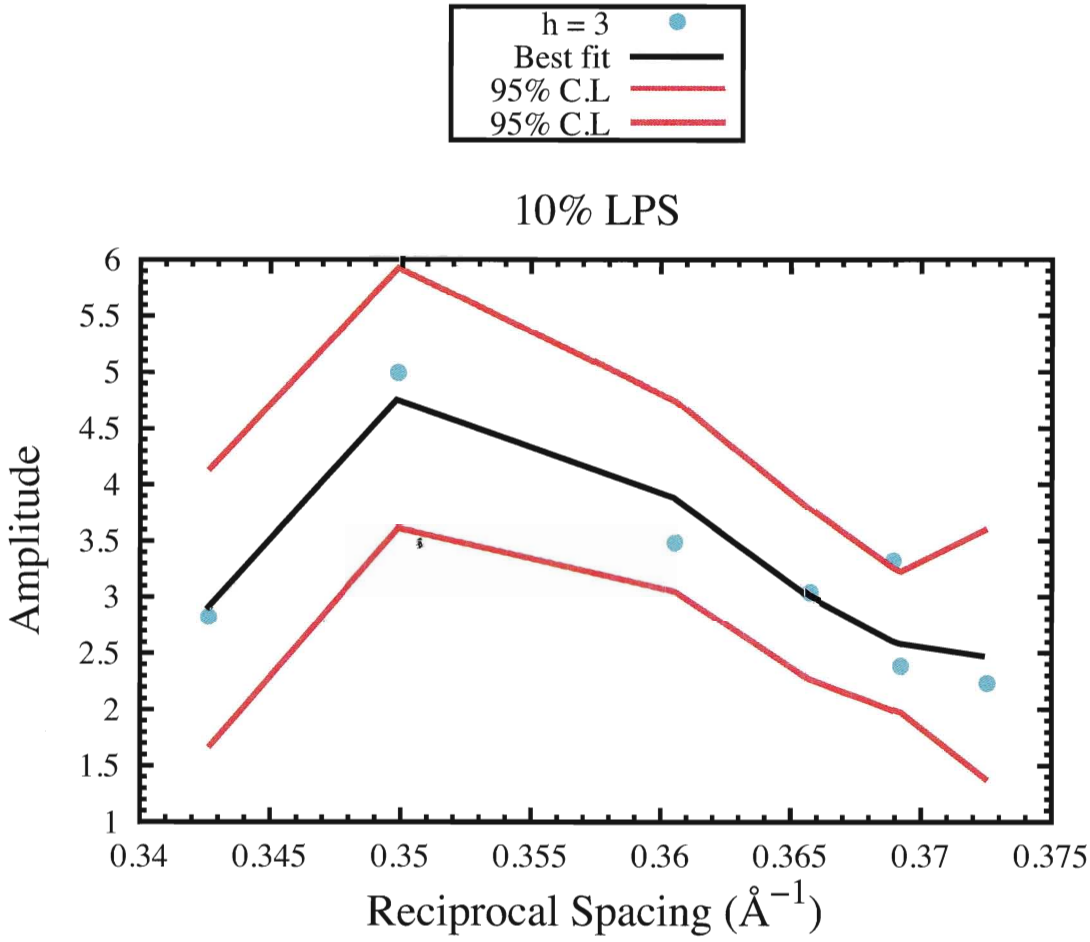

Figure A.6: **Order value of POPC with 10% LPS.** Structure factors at order value of h=3, with 95% confidence limit and line of the best fit.

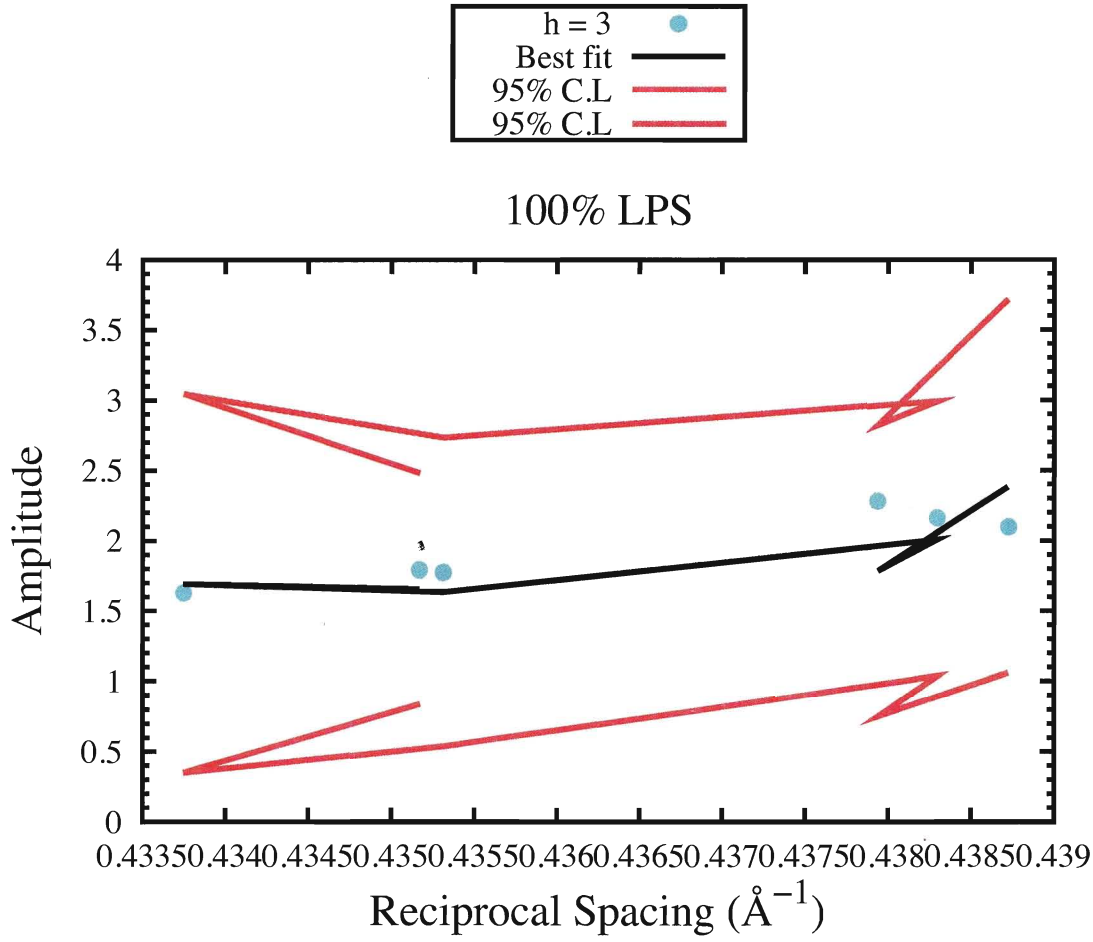

Figure A.7: **Order value of pure LPS.** Structure factor at third oder value. 95% confidence limit and line of the best fit are also plotted.

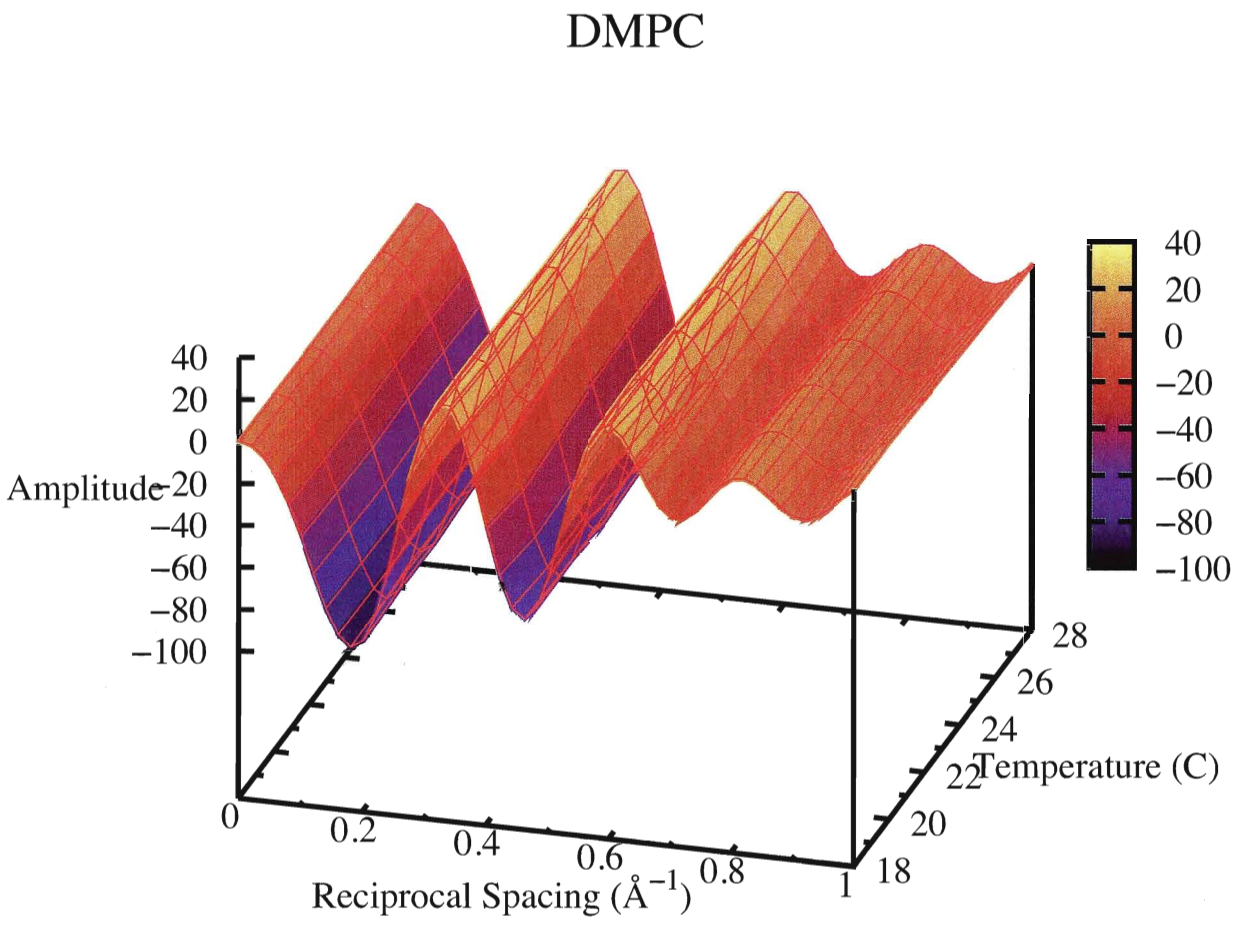

Figure A.8: **Three dimensional plot of DMPC with** 20% **cholesterol.** The three dimensional Fourier transform plot of DMPC with 20% cholesterol. The temperature range is between 18° C to 28° C degree.

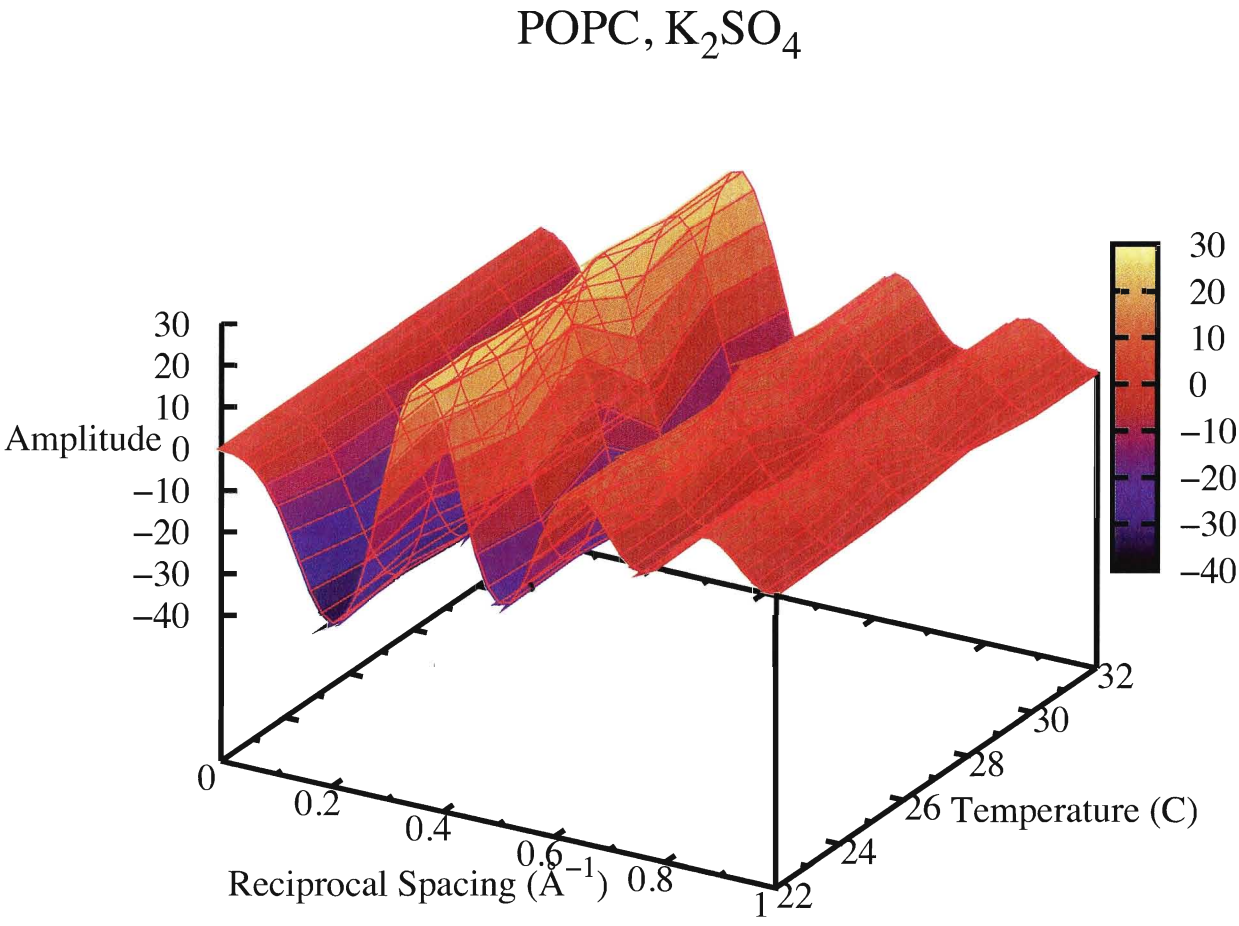

Figure A.9: **Three dimensional plot of POPC with K_2SO_4** Three dimensional Fourier transform graph of POPC with K_2SO_4 saturated salt as a function of temperature, amplitude and reciprocal lattice

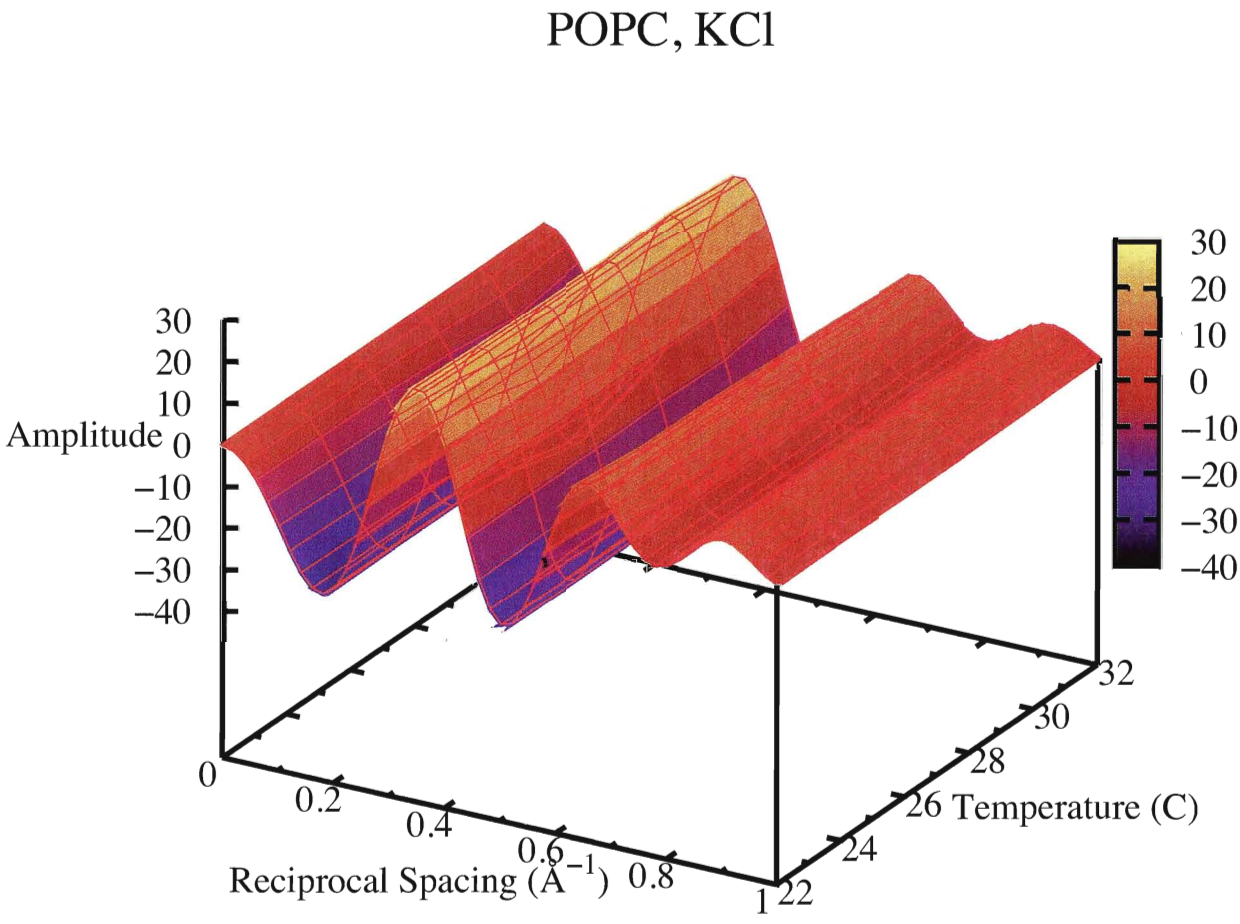

Figure A.10: **Three dimensional plot of POPC with KCl.** Fourier transform plots at three dimension for POPC sample with saturated salt solution of KCl.

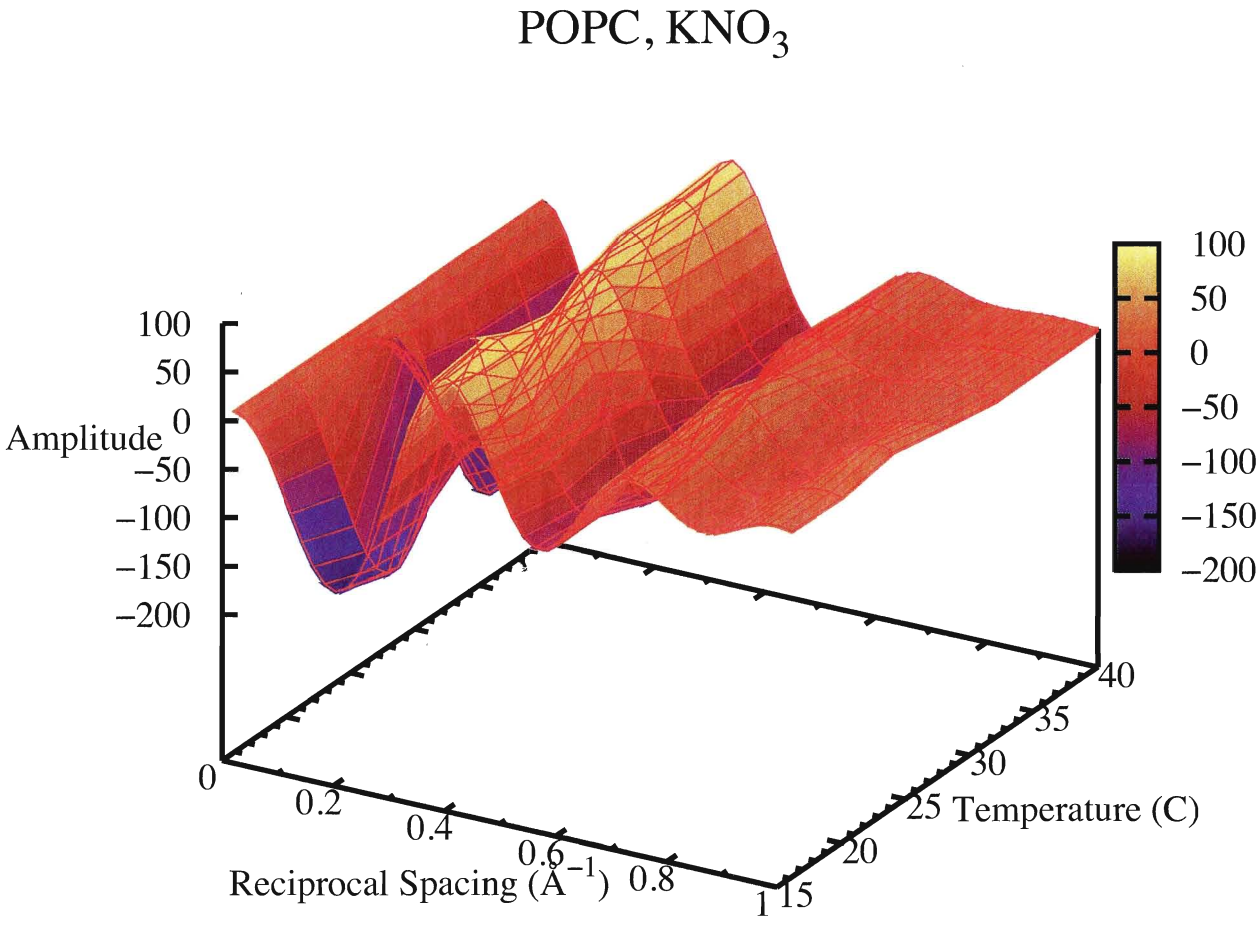

Figure A.11: **Three dimensional plot of POPC with KNO_3.** Three dimensional graph of Fourier transform of POPC sample with KNO_3 salt solution.

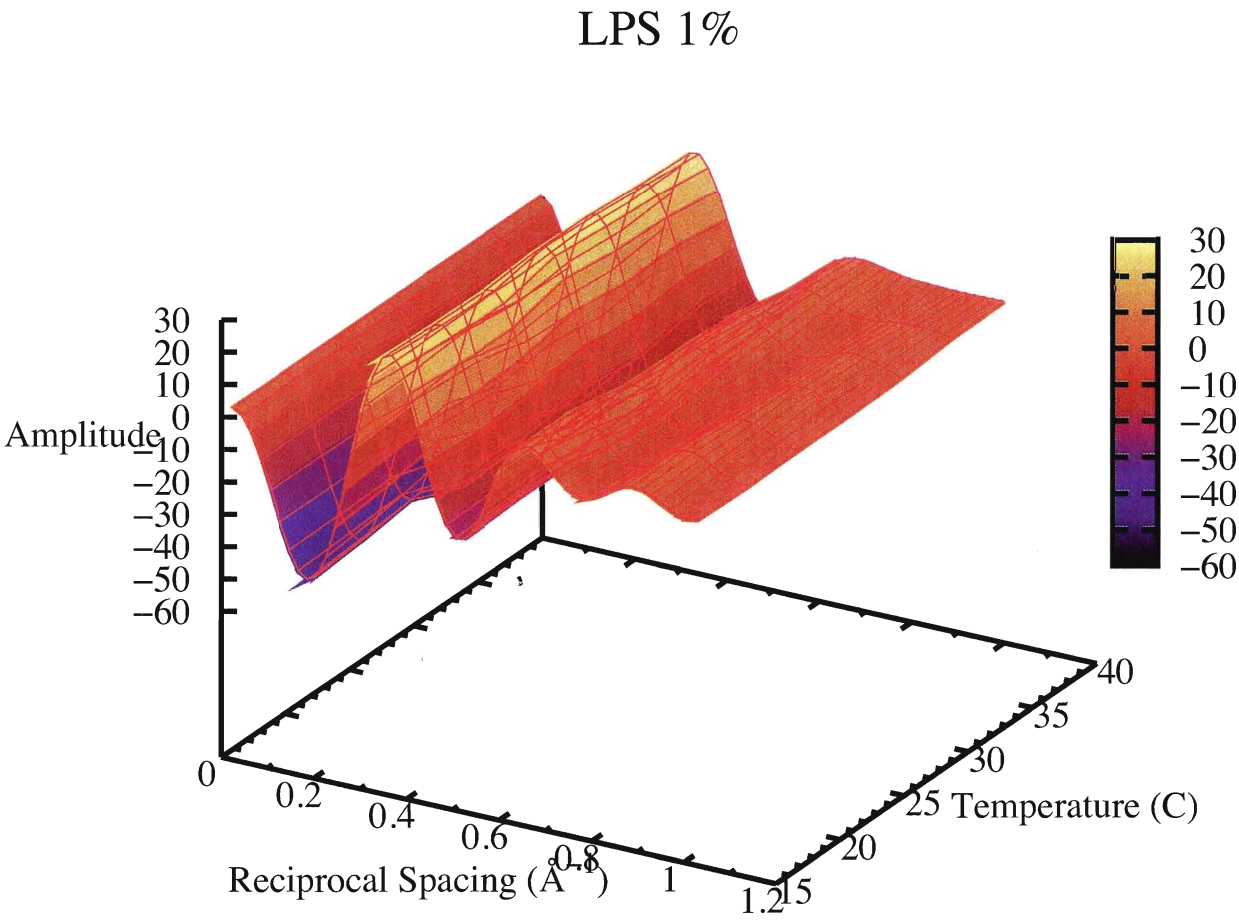

Figure A.12: **Three dimensional plot of POPC with 1% LPS.** A three dimensional Fourier transform graph at temperature range of 16° C to 40° C for concentration of 1% LPS in POPC sample.

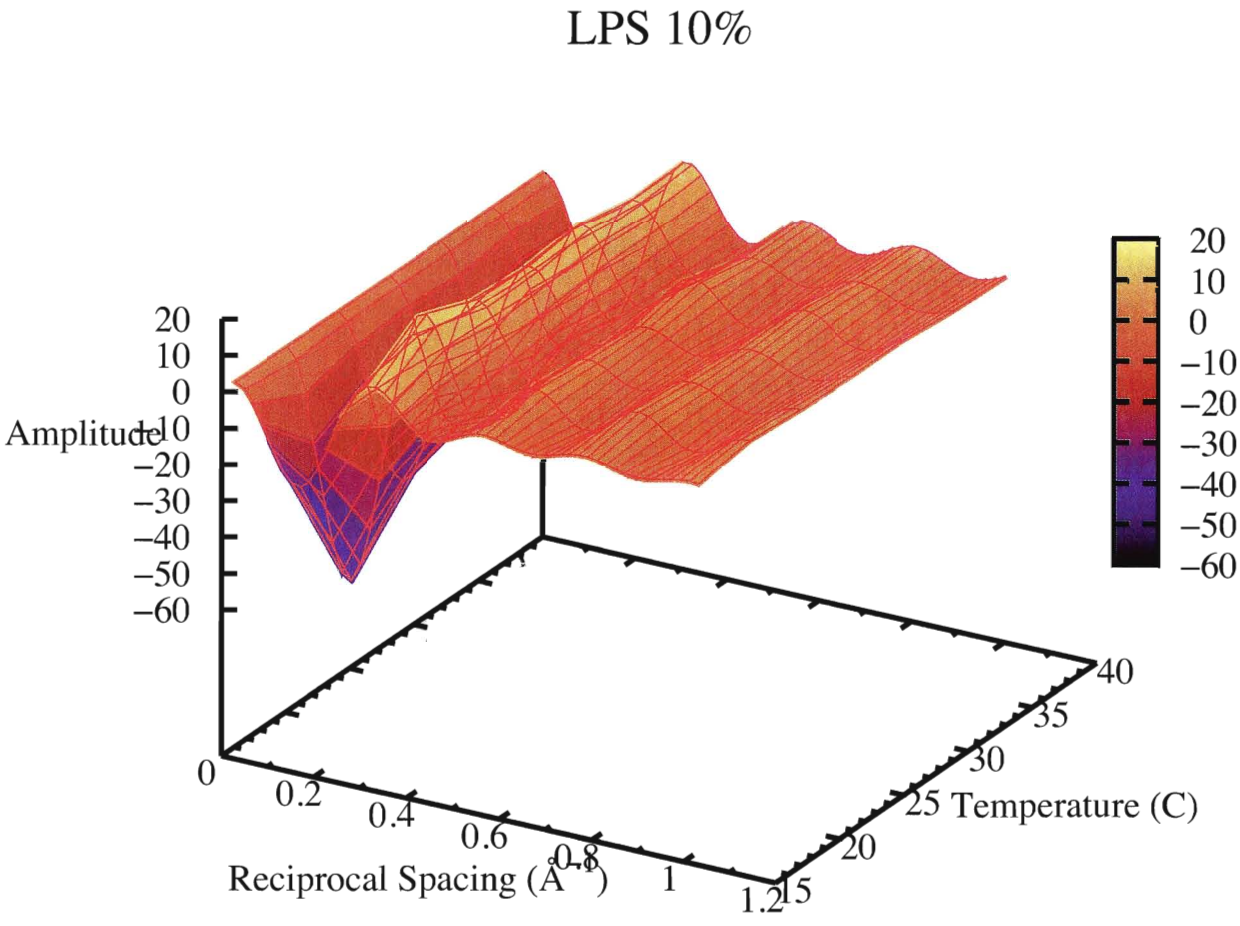

Figure A.13: **Three dimensional plot of POPC with 10% LPS.** Fourier transform graphs of 10% LPS concentration in three dimension at temperature range of 16° C to 40° C

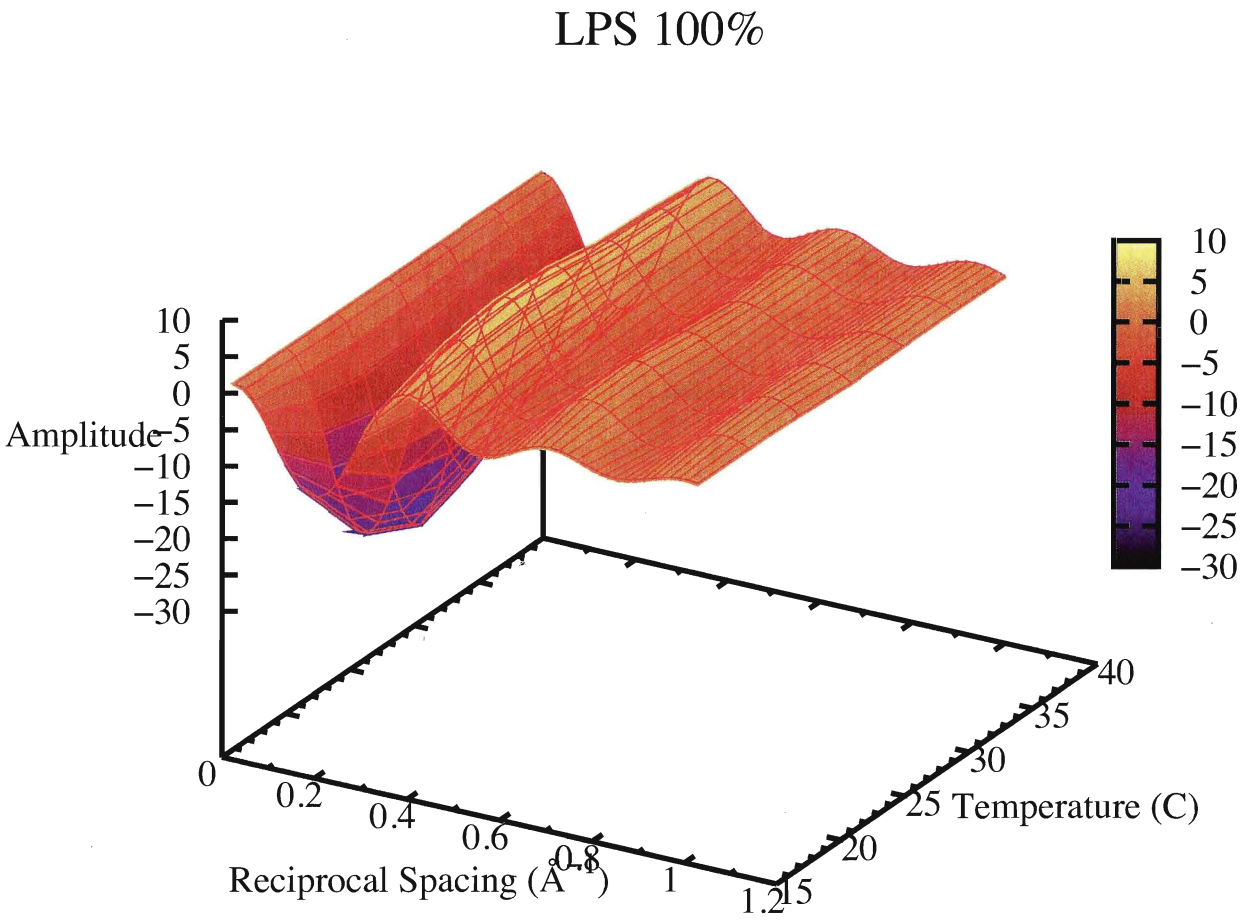

Figure A.14: **Three dimensional plot of pure LPS.** Three dimensional Fourier transform plots for pure LPS sample at temperature range of 16° C to 40° C

Bibliography

[1] N.W. Ashcroft and N.D. Mermin. *Solid state physics.* Singapore, 1976.

[2] B. Beutler and E.T. Rietschel. Innate immune sensing and its roots: the story of endotoxin. *Nature Reviews Immunology*, 3(2):169–176 2003.

[3] E. Bingen, E. Denamur, B. Picard, P. Goullet, N. Lambert-Zechovsky, P. Foucaud, J. Navarro, and J. Elion. Molecular epidemiological analysis ofPseudomonas aeruginosa strains causing failure of antibiotic therapy in cystic fibrosis patients. *European Journal of Clinical Microbiology & Infectious Diseases*, 11(5):432–437, 1992

[4] H. Brade. *Endotoxin in health and disease.* Marcel Dekker, 1999.

[5] M. Caroff and D. Karibian. Structure of bacterial lipopolysaccharides. *Carbohydrate research*, 338(23):2431–2447, 2003.

[6] HL Currie, J. Lightfoot, and JS Lam. Prevalence of gca, a gene involved in synthesis of A-band common antigen polysaccharide in Pseudomonas aeruginosa. *Clinical and Vaccine Immunology*, 2(5):554–562, 1995.

[7] L. Ding, L. Yang, T.M. Weiss, A.J. Waring, R.I. Lehrer, and H.W. Huang. Interaction of antimicrobial peptides with lipopolysaccharids. *Biochemistry(Washington)*, 42(42):12251–12259, 2003.

[8] MN Dudley. Overview of gram-negative sepsis. *American Journal of Health-System Pharmacy*, 47(11_Suppl):3–6, 1990.

[9] NP Franks and WR Lieb. The structure of lipid bilayers and the effects of general anaesthetics. An x-ray and neutron diffraction study. *J Mol Biol*, 133(4):469–500, 1979.

[10] P. Garidel, M. Rappolt, A.B. Schromm, . . Howe, K. Lohner, J. Andrä, M.H.J. Koch, and K. Brandenburg. Divalent cations affect ch in mobility and aggregate structure of lipopolysaccharide from Salmonella minnesota reflec ed in a decrease of its biological activity. *BBA-Biomembranes*, 1715(2):122–131, 2005.

[11] K. Gawrisch, H.C. Gaede, M. Mihailescu, a id S.H. White. Hydration of POPC bilayers studied by 1 H-PFG-MAS-NOESY and neutron di fraction. *European Biophysics Journal*, 36(4):281–291, 2007.

[12] L. Greenspan. Humidity fixed points of inary saturated aqueous solutions. *J. Res. Nat. Bureau Stds.*, 81A(1), 1977.

[13] J. Hellman, J.D. Roberts, M.M. Tehan, J.E Allaire, and H.S. Warren. Bacterial peptidoglycan-associated lipoprotein is released into the bloodstream in gram-negative sepsis and causes inflammation and death in mice. *Journal of Biological Chemistry*, 277(16):14274–14280, 2002.

[14] W.C. Hung, M.T. Lee, F.Y. Chen, and H.W. Huang. The condensing effect of cholesterol in lipid bilayers. *Biophysical Journal*, 92(11):3960–3967, 2007.

[15] Wei-Chin Hung and Ming-Tao Lee. The Interaction of Melittin with E. Coli Membrane: the Role of Cardiolipin. *The Chinese Journal of Physics*, 44(2):137–150, 2006.

[16] Manfred Kastowsky, Thomas Gutberlet, a id Hans Bradaczek. Comparison of x-ray powder-diffraction data of various bacterial lipopo ysaccharide structures with theoretical model conformations. *European Journal of Biochemi try*, 217:771–779, 1993.

[17] M. Kielhofner, RL Atmar, RJ Hamill, and DM Musher. Life-threatening Pseudomonas aeruginosa infections in patients with human in munodeficiency virus infection. *Clinical infectious diseases: an official publication of the Infe tious Diseases Society of America*, 14(2):403, 1992.

[18] Y.A. Knirel. Polysaccharide antigens of Ps eudomonas aeruginosa. *Critical Reviews in Microbiology*, 17(4):273–304, 1990.

[19] M.F.C Ladd and R.A Palmer. *Structure de ermination by x-ray crystallography*. Plenum Press, 1977.

[20] JS Lam, LL Graham, J. Lightfoot, T. Da gupta, and TJ Beveridge. Ultrastructural examination of the lipopolysaccharides of Pseudomonas aeruginosa strains and their isogenic rough mutants by freeze-substitution. *Journal of bacteriology*, 174(22):7159–7167, 1992.

[21] P.V. LIU, H. MATSUMOTO, H. KUSAMA, and TOM BERGAN. Survey of heat-stable, major somatic antigens of Pseudomonas aeruginosa. *International Journal of Systematic and Evolutionary Microbiology*, 33(2):256, 1983

[22] PV Liu and S. Wang. Three new major somatic antigens of Pseudomonas aeruginosa. *Journal of Clinical Microbiology*, 28(5):922–925, 1990.

[23] V. Luzzati and F. Husson. The Structure of the Liquid-Crystalline Phases of Lipid-Water Systems. *The Journal of Cell Biology*, 12:207–219, 1962.

[24] M.T. Madigan, J.M. Martinko, J. Parker, et al. *Brock biology of microorganisms*. Prentice Hall Upper Saddle River, NJ, 2000.

[25] K.E. Mdluli, P.R. Witte, T. Kline, A.W. Barb, A.L. Erwin, B.E. Mansfield, A.L. McClerren, M.C. Pirrung, L.N. Tumey, P. Warrener, et al. Molecular validation of lpxc as an antibacterial drug target in pseudomonas aeruginosa. *Antimicrobial agents and Chemotherapy*, 50(6):2178–2184, 2006.

[26] M. Millesimo, G. Intinis, M.G. Chirill, T. Musso, and D. Savoia. Pseudomonas aeruginosa clinical isolates: serotypes, resistance phenotypes and plasmid profiles. *European journal of epidemiology*, 12(2):123–129, 1996.

[27] RN Moore, L.L. Burrows, R.V. Urbanic, and J.S. Lam. Functional conservation of the polysaccharide biosynthetic protein WbpM and its homologues in Pseudomonas aeruginosa and other medically significant bacteria, 2000.

[28] H. Nikaido. Molecular basis of bacterial outer membrane permeability revisited. *Microbiology and molecular biology reviews*, 67(4):593–656, 2003.

[29] Pathobiology of lipopolysaccharide. Maye ix, p.r. *Journal of Toxicology and Environmental Health, Part A*, 51(5):415–435, 1997.

[30] B. Olson, RA Weinstein, C. Nathan, W. Chamberlin, and SA Kabins. Epidemiology of endemic Pseudomonas aeruginosa: why infection control efforts have failed. *The Journal of infectious diseases*, 150(6):808, 1984.

[31] C.R.H. Raetz and C. Whitfield. LIPOPOLYSACCHARIDE ENDOTOXINS. *Annual review of biochemistry*, 71(1):635–700, 2002.

[32] C.K. Raymond, E.H. Sims, A. Kas, D.H. Spencer, T.V. Kutyavin, R.G. Ivey, Y. Zhou, R. Kaul, J.B. Clendenning, and M.V. Olson. Genetic variation at the O-antigen biosynthetic locus in Pseudomonas aeruginosa. *Journal of bacteriology*, 184(13):3614–3622, 2002.

[33] M. Rivera, LE Bryan, RE Hancock, and EJ McGroarty. Heterogeneity of lipopolysaccharides from Pseudomonas aeruginosa: analysis of lipopolysaccharide chain length. *Journal of Bacteriology*, 170(2):512–521, 1988.

[34] CA Schnaitman and JD Klena. Genetics of lipopolysaccharide biosynthesis in enteric bacteria. *Microbiology and Molecular Biology Reviews*, 57(3):655–682, 1993.

[35] E.S. Stanislavsky and J.S. Lam. Pseudomonas aeruginosa antigens as potential vaccines. *FEMS microbiology reviews*, 21(3):243–277, 1997.

[36] M. Stürzbecher. Klebs, Edwin. In *Encyclopedia of Life Sciences*. John Wiley & Sons, Ltd., 1977.

[37] B.E Warren. *X-ray crystallography*. Dover publications, Inc, 1969.

[38] R.C. Weast and Chemical Rubber Company. *CRC handbook of chemistry and physics*. CRC press Cleveland, Ohio, 1988.

[39] Web:. www.melcore.com.

[40] Web:. *www.newport.com*.

[41] Michael C. Wiener and Stephen H. White. Fluid bilayer structure determination by the combined use of x-ray and neutron diffraction. I. Fluid bilayer models and the limits of resolution. *Biophys. J.*, 59:162–173, January 1991.

[42] Michael C. Wiener and Stephen H. White. Fluid bilayer structure determination by the combined use of x-ray and neutron diffraction. II. "Composition-space" refinement method. *Biophys. J.*, 59:174–185, January 1991.

[43] S. YOKOTA, S. KAYA, S. SAWADA, T. KAWAMURA, Y. ARAKI, and E. ITO. Characterization of a polysaccharide component of lipopolysaccharide from Pseudomonas aeruginosa IID 1008 (ATCC 27584) as D-rhamnan. *European Journal of Biochemistry*, 167(2):203–209, 1987.

[44] G. Zaccaï, J. K. Blasie, and B. P. Schoenborn. Neutron Diffraction Studies on the Location of Water in Lecithin Bilayer Model Membranes. *Proc. Natl. Acad. Sci. USA*, 72:376–380, 1975.